

**Ultimate Strength of Clamped Steel-Elastomer Sandwich
Panels under Combined In-plane Compression and Lateral
Pressure**

Feng Zhou

Dissertation submitted to the faculty of the Virginia Polytechnic Institute and State
University in partial fulfillment of the requirements for the degree of

Doctor of Philosophy

In

Aerospace Engineering

Dr. Owen F. Hughes, Chair

Dr. Rakesh K. Kapania

Dr. Raymond H. Plaut

Dr. Alan J. Brown

Dr. Wayne L. Neu

February 4, 2008

Blacksburg, Virginia

Key words: Sandwich Panels, Steel-Elastomer, Ultimate Strength,
In-plane Compression, Lateral Pressure

Copyright 2008, Feng Zhou

Abstract

Ultimate Strength of Clamped Steel-Elastomer Sandwich Panels under Combined In-plane Compression and Lateral Pressure

Feng Zhou

An efficient interaction formula and a semi-analytical method are developed for calculating the ultimate strength of steel-elastomer sandwich panels under combined in-plane compression and lateral pressure.

By using the Galerkin method and extending the semi-analytical method to clamped sandwich panels, the governing equations of sandwich panels have been solved by the Galerkin method. The material nonlinearity is treated by iteration and a three-dimensional mesh. For the load case of pure lateral pressure, the ultimate strength from the semi-analytical method is similar to that from hinge line theory and finite element analysis (FEA). However, the semi-analytical method requires about as much computation as FEA, and it is therefore not suitable for design.

Finite element modeling and nonlinear analysis are performed to calculate the ultimate strength of sandwich panels under combined load. The results agree with experimental results. This verifies the accuracy of the current finite element model. The verified finite element model is used to obtain the results for a large set of sandwich panels with various dimensions and load combinations. The FEA results for pure lateral pressure load cases are used to derive a correction factor for the hinge line formula. Statistical analysis confirms that the generalized hinge line formula gives accurate values of ultimate strength of sandwich panels under pure lateral pressure.

Except for the pressure-only FEA data points, the other FEA data points are corrected so as not to count the in-plane load carried by the elastomer core. Based on the corrected FEA data points, a general expression is developed for an interaction equation. The resulting equation has a bias of -0.003 and a standard deviation of 0.029. Since the radius of the interaction curve is close to 1, this standard deviation is of the order of 3%, which shows that the ultimate strength given by the equation is very close to the FEA results. The interaction equation is so simple that the ultimate strength of clamped sandwich panels under combined in-plane compression and lateral pressure can be easily calculated.

Acknowledgements

I wish to thank the people who made this dissertation possible:

My advisor, Dr. Owen Hughes, your support, guidance, and patience, during the development of this project are greatly appreciated. Your knowledge, expertise, and professionalism helped immensely in the completion of this research. It is such an honor to have the opportunity to work under your supervision.

The members of my committee, Dr. Rakesh K. Kapania, Dr. Raymond H. Plaut, Dr. Alan J. Brown and Dr. Wayne L. Neu, who gave me the valuable suggestions and ideas of this dissertation, which helped my understanding and broadened my vision. Prof. Liviu Librescu, one of the heroes in the April 16, 2007, Tragedy at Virginia Tech, gave me great help for my dissertation.

I also thank all my friends for the great time we shared in Blacksburg.

Finally, I would like to express my deepest appreciation to my parents who showed me the endless support and love.

Table of Contents

ABSTRACT	II
ACKNOWLEDGEMENTS	IV
TABLE OF CONTENTS	V
LIST OF TABLES.....	VIII
LIST OF FIGURES.....	IX
NOMENCLATURE	XIII
CHAPTER 1 INTRODUCTION OF SANDWICH PANELS	1
1.1 INTRODUCTION	1
1.2 BENEFITS OF SANDWICH PANELS.....	2
1.3 PREVIOUS WORK DONE BY OTHERS	4
1.4 OBJECTIVE OF PRESENT STUDY	6
1.5 SUMMARY	7
CHAPTER 2 HINGE LINE THEORY AND EXPERIMENTS	10
2.1 HINGE LINE THEORY	10
2.1.1 <i>Introduction to Hinge Line Theory</i>	10
2.1.2 <i>Formulas of Hinge Line Theory for Bare Plates</i>	13
2.1.3 <i>Comparison and Selection of a Formula</i>	16
2.1.4 <i>Plastic Moment for a Sandwich Panel</i>	18
2.1.5 <i>Limitations</i>	20
2.2 EXPERIMENTS	20
2.2.1 <i>Test Specimens</i>	21
2.2.2 <i>Three Special Features</i>	21
2.2.3 <i>Results</i>	23
2.2.4 <i>Discussion of Failure Stress Seeming to Exceed Yield Stress</i>	25
CHAPTER 3 SEMI-ANALYTICAL SOLUTION FOR THE ULTIMATE STRENGTH OF CLAMPED SANDWICH PANELS.....	28
3.1 GOVERNING EQUATIONS	28
3.2 INCREMENTAL APPROACH	30
3.3 SOLUTION FOR MATERIAL NONLINEARITY	34

3.4 VERIFICATION.....	36
3.5 DEFLECTION FUNCTION AND SOLUTION PROCEDURE.....	37
3.5.1 <i>Deflection Function</i>	37
3.5.2 <i>Solution Procedure</i>	38
3.6 RESULTS	41
CHAPTER 4 NONLINEAR FINITE ELEMENT ANALYSIS	44
4.1 FINITE ELEMENT MODELING OF THE EXPERIMENTAL PANELS.....	44
4.1.1 <i>Number of Elements</i>	46
4.1.2 <i>Boundary Conditions</i>	47
4.1.3 <i>Loads</i>	48
4.2 RESULTS AND COMPARISON WITH EXPERIMENTS	49
4.2.1 <i>Definition of Failure under In-plane Compression as 0.5% Strain</i>	49
4.2.2 <i>Comparison of Yield Expansion Patterns under Pure Lateral Pressure</i>	52
4.3 DEFINITION OF FAILURE UNDER PURE LATERAL PRESSURE.....	57
4.4 COMPARISON OF ULTIMATE PRESSURE.....	59
CHAPTER 5 CORRECTION FACTOR	60
5.1 INTRODUCTION; OVERALL METHOD.....	60
5.1.1 <i>Determination of $(\sigma_x)_{ult}$</i>	61
5.1.2 <i>Determination of p_{ult}</i>	61
5.2 PROPERTIES OF FEA MODELS.....	62
5.3 GENERALIZING THE HINGE LINE COLLAPSE PRESSURE EQUATION FOR A STEEL-ELASTOMER SANDWICH PANEL	64
5.4 MODIFICATION OF THE HINGE LINE COLLAPSE PRESSURE.....	66
5.4.1 <i>The Part of the Correction Factor Accounting for \bar{t}_c and \bar{t}_f: $g(\bar{t}_f, \bar{t}_c)$</i>	68
5.4.2 <i>The Part of the Correction Factor Accounting for α: $h(\alpha)$</i>	76
5.5 VERIFICATION OF THE CORRECTION FACTOR	79
CHAPTER 6 METHOD FOR OBTAINING AN EXPLICIT EQUATION FOR THE INTERACTIVE COLLAPSE OF A STEEL-ELASTOMER SANDWICH PANEL	81
6.1 SAMPLES OF INTERACTIVE ULTIMATE STRENGTH DATA POINTS.....	82
6.2 FINDING AN INTERACTION EQUATION	84
6.3 OBTAINING AN EXPRESSION FOR THE COEFFICIENT C	95
6.4 VERIFICATION.....	103
6.5 SOME OBSERVATIONS ABOUT THE INTERACTION FORMULA.....	105
CHAPTER 7 SUMMARY AND CONCLUSIONS	108

REFERENCES110

VITA112

List of Tables

Table 3.1 The dimensions of nine sandwich panels.	42
Table 3.2 Comparison of results of semi-analytical method and hinge line theory .	43
Table 4.1 Boundary conditions of the FEA model	47
Table 5.1 General properties of 36 FEA models	64
Table 5.2 Ratios of $p_{ult,FE} / p_{ult,HL}$	67
Table 6.1 Values of C for different sandwich panels	95

List of Figures

Figure 1.1 Specimen of sandwich panel	1
Figure 1.2 Sandwich structure	2
Figure 1.3 Conventional structure.....	2
Figure 1.4 Computational model of a clamped sandwich panel under in-plane compression and lateral pressure	6
Figure 2.1 Hinge line in a panel.....	11
Figure 2.2 Deformation mechanism of hinge line theory for a clamped plate	12
Figure 2.3 Formation of the plastic bending moment for a single layer plate	13
Figure 2.4 Deformation mechanism of hinge line theory by Sabotka (1989)	16
Figure 2.5 Ultimate strength calculated by Equation (2.6).....	17
Figure 2.6 Ultimate strength calculated by Equation (2.7).....	17
Figure 2.7 Difference between the results of Equation (2.6) and Equation (2.7)	18
Figure 2.8 Formation of the plastic bending moment for a sandwich panel.....	19
Figure 2.9 Plan view of test frame	22
Figure 2.10 Double-panel system	23
Figure 2.11 Progression of out of plane deflected shape	24
Figure 2.12 Failure points obtained from experiments	25
Figure 3.1 Division of mesh regions for a face plate of a sandwich panel	35
Figure 3.2 Load versus deflection curve of a simply supported square panel under lateral pressure load	36
Figure 3.3 Mode shapes of the deflection functions	38
Figure 3.4 Solution procedure.....	39
Figure 3.5 Ultimate strength calculated by hinge line theory and semi-analytical method.....	42
Figure 4.1 Finite element type: SOLID 45	45
Figure 4.2 Stress versus strain curves for steel and elastomer.....	45

Figure 4.3 Finite element model	46
Figure 4.4 Profile of the sandwich panel element mesh	47
Figure 4.5 Boundary conditions of the FEA model	48
Figure 4.6 0.5% strain method	50
Figure 4.7 Non-dimensionalized in-plane load versus in-plane deflection	50
Figure 4.8 Comparison of FEA and test results	51
Figure 4.9 First occurrence of yield at mid-thickness of the top face plate	53
Figure 4.10 First occurrence of yield at mid-thickness of the bottom face plate	53
Figure 4.11 Yield pattern almost at failure at mid-thickness of the top face plate ...	54
Figure 4.12 Yield pattern almost at failure at mid-thickness of the bottom face plate	54
Figure 4.13 First occurrence of yield at mid-thickness of the top face plate	55
Figure 4.14 First occurrence of yield at mid-thickness of the bottom face plate	55
Figure 4.15 Yield pattern almost at failure at mid-thickness of the top face plate ...	56
Figure 4.16 Yield pattern almost at failure at mid-thickness of the bottom face plate	56
Figure 4.17 Non-dimensionalized lateral pressure versus lateral deflection	57
Figure 4.18 Plastic strain distribution on a sandwich panel under later pressure	58
Figure 4.19 FEA interaction curve, including failure load under pure lateral pressure	59
Figure 5.1 Interaction Diagram	61
Figure 5.2 FEA Interaction Diagram ($a = 1800 \text{ mm}$ $b = 1200 \text{ mm}$ $t_f = 5 \text{ mm}$) ...	65
Figure 5.3 g_1 for $\bar{t}_c = 25$	69
Figure 5.4 g_2 for $\bar{t}_c = 37.5$	70
Figure 5.5 g_3 for $\bar{t}_c = 50$	70
Figure 5.6 c_1 versus \bar{t}_c	71
Figure 5.7 c_2 versus \bar{t}_c	72
Figure 5.8 c_1 and $c_1(\bar{t}_c)$ versus \bar{t}_c	73
Figure 5.9 c_2 and $c_2(\bar{t}_c)$ versus \bar{t}_c	73

Figure 5.10 FEA Interaction Diagram ($a = 1800$ mm $b = 1200$ mm $t_f = 5$ mm)....	74
Figure 5.11 $g(\bar{t}_f, \bar{t}_c)$ and $p_{ult,FE} / p_{ult,HL}$ versus \bar{t}_f and \bar{t}_c	75
Figure 5.12 FEA Interaction Diagram ($t_f = 7$ mm $t_c = 60$ mm).....	76
Figure 5.13 $\frac{P_{ult,FE}}{P_{ult,HL} \cdot g(\bar{t}_c, \bar{t}_f)}$ versus α	77
Figure 5.14 $\frac{P_{ult,FE}}{P_{ult,HL} \cdot g(\bar{t}_c, \bar{t}_f)}$ and $h(\alpha)$ versus α	78
Figure 5.15 Distribution of the error of the correction factor	80
Figure 5.16 Updated FEA Interaction Diagram ($t_f = 7$ mm $t_c = 60$ mm)	80
Figure 6.1 Interaction curves of sandwich panels with different face plate thickness	82
Figure 6.2 Interaction curves of sandwich panels with different core thickness	83
Figure 6.3 Interaction curves of sandwich panels with different aspect ratios	83
Figure 6.4 Curve shapes of Equation (6.2) $X^2 - CXY + Y = 1$	85
Figure 6.5 Curve shapes of Equation (6.3) $X^2 - CX^2Y + Y = 1$	86
Figure 6.6 Curve shapes of Equation (6.4) $X^2 - CX^2Y + Y^2 = 1$	86
Figure 6.7 Curve shapes of Equation (6.5) $X^2 - CX^2Y^2 + Y = 1$	87
Figure 6.8 Curve shapes of Equation (6.6) $X^2 - CX^2Y^2 + Y^2 = 1$	87
Figure 6.9 Interaction Diagram of sandwich panels with $t_c = 30$ mm, $\alpha = 0.5$	89
Figure 6.10 Interaction Diagram of sandwich panels with $t_c = 45$ mm, $\alpha = 0.5$...	89
Figure 6.11 Interaction Diagram of sandwich panels with $t_c = 60$ mm, $\alpha = 0.5$...	90
Figure 6.12 Interaction Diagram of sandwich panels with $t_c = 30$ mm, $\alpha = 1$	90
Figure 6.13 Interaction Diagram of sandwich panels with $t_c = 45$ mm, $\alpha = 1$	91
Figure 6.14 Interaction Diagram of sandwich panels with $t_c = 60$ mm, $\alpha = 1$	91
Figure 6.15 Interaction Diagram of sandwich panels with $t_c = 30$ mm, $\alpha = 1.5$	92
Figure 6.16 Interaction Diagram of sandwich panels with $t_c = 45$ mm, $\alpha = 1.5$	92
Figure 6.17 Interaction Diagram of sandwich panels with $t_c = 60$ mm, $\alpha = 1.5$...	93

Figure 6.18 Interaction Diagram of sandwich panels with $t_c = 30\text{mm}$, $\alpha = 3$	93
Figure 6.19 Interaction Diagram of sandwich panels with $t_c = 45\text{mm}$, $\alpha = 3$	94
Figure 6.20 Interaction Diagram of sandwich panels with $t_c = 60\text{mm}$, $\alpha = 3$	94
Figure 6.21 C versus \bar{t}_c for $\alpha = 0.5$	96
Figure 6.22 C versus \bar{t}_c for $\alpha = 1$	97
Figure 6.23 C versus \bar{t}_c for $\alpha = 1.5$	97
Figure 6.24 C versus \bar{t}_c for $\alpha = 3$	98
Figure 6.25 C versus α for $\bar{t}_c = 25$	99
Figure 6.26 C versus α for $\bar{t}_c = 37.5$	99
Figure 6.27 C versus α for $\bar{t}_c = 50$	100
Figure 6.28 C versus α and normalized \bar{t}_c	101
Figure 6.29 Interaction surface	102
Figure 6.30 Probabilities of the errors of the interaction formula	103
Figure 6.31 Standard normal distribution of the errors of the interaction formula.	104
Figure 6.32 Curve shapes of function $X^2 - CX^2Y^2 + Y = 1$ when $C = 1.01$	106
Figure 6.33 Curve shapes of function $X^2 - CX^2Y^2 + Y = 1$ when $C = 1$	107

Nomenclature

Roman

a	= length of the panel in the x direction
A	= length of the panel long dimension (Hinge line theory)
A_{ij}, A_{ij}^*	= stiffness quantities associated with the face plates and their inverse counterparts, respectively
b	= length of the panel in the y direction
B	= length of the panel short dimension (Hinge line theory)
C	= coefficient of the interaction formula
D_{ij}, F_{ij}	= stiffness quantities associated with the face plates
E, E_c	= elastic moduli of the face plate and core
F_{TOT}	= total force applied as in-plane compression
G_c	= transverse shear modulus of the core
h	= distance between the global mid-surface and the mid-thickness of face plates
K^2	= transverse shear correction factor associated with the core (=5/6)
$[K_B]$	= bending stiffness matrix
$[K_M]$	= stiffness matrix associated with membrane action
$[K_S]$	= stiffness matrix associated with transverse shear
m, n	= serial number of mode shapes in the x, y directions
M, N	= maximum number of mode shapes in the x, y directions
M_p	= plastic bending moment
M_x^l, M_x^u	= stress couples of the lower and upper face plates in the x direction (per unit length)
M_y^l, M_y^u	= stress couples of the lower and upper face plates in the y direction (per unit length)

N_x^l, N_x^u	= stress resultants (load per unit width) of the lower and upper face plates in the x direction
N_y^l, N_y^u	= stress resultants (load per unit width) of the lower and upper face plates in the y direction
P	= lateral pressure load
$P_{ult,FE}$	= finite element collapse pressure
P_{HL}	= hinge line collapse pressure
P_{SM}	= collapse pressure calculated by semi-analytical method
$P_{ult,temp}$	= $P_{ult,HL} \cdot g(\bar{t}_f, \bar{t}_c)$
P_{ult}	= collapse lateral pressure load if acted alone
$[P_0]$	= stiffness matrix due to the initial stress
$\{\Delta P\}$	= vector of external incremental load (length MN)
t_f, t_c	= thickness of the face plate and core
R_p	= strength ratio for lateral pressure
R_σ	= strength ratio for in-plane compression
V_x^l, V_x^u	= tangential displacements of the mid-surface of the lower and upper face plates in the x direction
V_y^l, V_y^u	= tangential displacements of the mid-surface of the lower and upper face plates in the y direction
w, w_0	= added deflection due to applied loads and stress-free initial deflection
$\{\Delta w\}$	= vector of unknown coefficients

Greek

α	= aspect ratio of the panel (= a/b)
δ	= $4K^2G_c/t_c$
δ_{mid}	= displacement of the midpoint of the panel (hinge line theory)
η_x, η_y	= $(V_x^l - V_x^u)/2, (V_y^l - V_y^u)/2$
θ	= out-of-plane rotation angle of the plate (hinge line theory)
ν	= Poisson's ratio of the face plates
ν_c	= Poisson's ratio of the core
ξ_x, ξ_y	= $(V_x^l + V_x^u)/2, (V_y^l + V_y^u)/2$
σ_c	= stress in the core
σ_{fail}	= increased in-plane compressive stress at failure
σ_x	= in-plane compressive stress
$(\sigma_x)_{ult}$	= collapse in-plane load if acted alone
σ_y	= yield stress of the face plates
ϕ	= Airy stress function
λ	= $\frac{b^2}{2a}[-1 + \sqrt{1 + 3\frac{a^2}{b^2}}]$ (hinge line theory)

Chapter 1

Introduction of Sandwich Panels

1.1 Introduction

A sandwich panel consists of two face plates and a core between them. In this research, the face plates of the sandwich panels are made of steel and the core is made of an elastomer. The elastomer is itself a natural adhesive and when it solidifies it forms a very strong bond to the steel face plates, as shown in Figure 1. Delamination has never occurred over the ten years that this type of sandwich panel has been in service. The core acts as a web and provides continuous support to the face plates. Therefore local plate buckling is avoided and closely spaced stiffeners are not required.



Figure 1.1 Specimen of sandwich panel

Figures 1.2 and 1.3 are respectively a typical sandwich structure and a conventional stiffened structure to withstand the same design loads. The difference between these two structures is obvious. It is feasible that the flexural stiffness and strength of a sandwich panel can meet particular structural requirements by selecting appropriate thicknesses for the sandwich elements so as to be structurally equivalent to a stiffened steel plate.

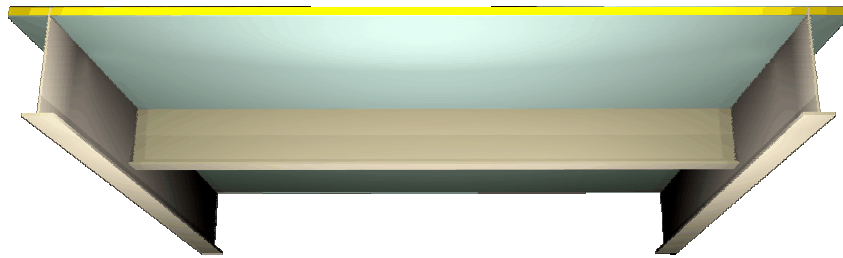


Figure 1.2 Sandwich structure

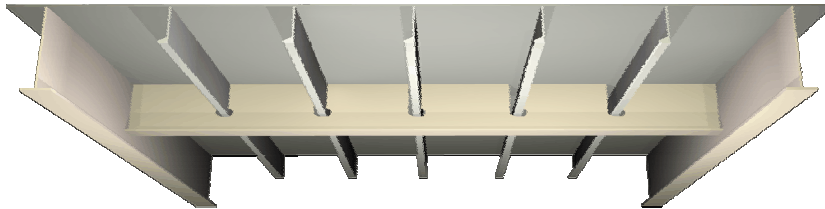


Figure 1.3 Conventional structure

1.2 Benefits of Sandwich Panels

As presented by Denis Welch (2005), sandwich panels offer many benefits.

1. Simple structure

Because closely spaced stiffeners are not required, the complexity of sandwich structures is less. The manufacturing procedure is improved by reducing the welding work, and therefore both time and materials are saved. At the same time, there is more internal space and both external surfaces are smooth.

2. Improved performance

Because the elastomer core dissipates strain energy over a large area, the load concentrations that lead to the formation and propagation of cracks are reduced. Compared to conventional structures, sandwich structures are more robust against daily in-service loads and hence have a longer working life.

With the physical properties of the elastomer core, sandwich structures provide significant damping of structural vibration and noise. Sandwich structures can be used to replace heavy concrete structures, which use mass for damping vibration.

The elastomer core has excellent insulation properties. It can contain a fire and prevent it from spreading to adjacent compartments without producing smoke or toxic gases. Full-scale deck panel and bulkhead tests conducted in laboratories under International Maritime Organization (IMO) A60 specified conditions have shown that after exposure to a 945°C fire for 60 minutes, the temperature increase on the unexposed surface of a sandwich structure was $+5^{\circ}\text{C}$ with insulation (on exposed side) and $+38^{\circ}\text{C}$ without insulation. The comparable temperature changes for a steel stiffened plate are $+192^{\circ}\text{C}$ and $+710^{\circ}\text{C}$ respectively.

Blast tests conducted by the US Navy Research Center in Carderock, Maryland, and by Hitachi Zosen for the Japanese Defense Agency, show that sandwich panels have superior performance in limiting the damage caused by explosions. Tests carried out by QinetiQ demonstrate that sandwich panels stop projectiles at shorter strike ranges and higher attack angles than steel plates.

1.3 Previous Work Done by Others

Until now there has been no direct (explicit, closed form) formula for the ultimate strength of clamped steel-elastomer sandwich panels under combined in-plane compression and lateral pressure. There are, however, some related research and experiments that provide a starting point and some useful results.

Hinge line theory was originally developed for the design of concrete slabs (Drucker, 1958). Based on this theory, Save, Massonnet and Saxce (1997) imagined a roof-like deformation mechanism of plates under lateral pressure (see Figure 2.2). They applied the Principle of Virtual Work to obtain the lateral pressure which causes collapse of the plate. Sobotka (1989) derived a different formula for the collapse pressure from a similar roof-shaped deformation but with four yield fans in the corners (see Figure 2.4). These formulas are presented in Section 2.1.2.

Padhi, Sheno, Moy and Hawkins (1998) presented a method to study the ultimate collapse of laminated composite plates with clamped edges, subjected to lateral pressure. They used several failure criteria to predict the failure mechanisms. They studied the effect of aspect ratio on the strength and stiffness of laminated composite plates. A progressive failure methodology was obtained. Based on this methodology, they calculated the ultimate collapse load of composite plates under lateral pressure by a numerical approach.

Paik, Thayamballi, Lee and Kang (2001) presented a semi-analytical method for the ultimate strength of elastic-plastic large deflection analysis of simply supported, isotropic unstiffened steel or aluminum plates under combined in-plane and out-of-plane loads. They solved the geometrical nonlinearity by the Galerkin method and treated the material nonlinearity by iteration and a three-dimensional mesh.

By using Hamilton's variational principle, Librescu, Hause and Camarda (1997) developed a comprehensive geometrically non-linear theory of initially imperfect doubly

curved sandwich shells. Their theory includes the special cases of buckling and post-buckling of flat and circular cylindrical sandwich shells compressed by uniaxial compression and lateral pressure loads. There are five basic assumptions of their theory: (1) the material of the face plates and core is orthotropic; (2) the face plates and core are incompressible in the transverse normal direction; (3) the panel is symmetric with respect to the global mid-surface; (4) the face plates are thin and therefore the Love-Kirchhoff hypothesis is adopted; (5) the bonding between the face plates and core is perfect (delamination never happens)

Based on the theory of Librescu et al. (1997) and assuming the face plates and core are isotropic and the core is relatively soft (carrying only transverse shear stresses), Kim and Hughes (2005) presented a closed-form analytical solution for the ultimate strength of simply supported sandwich panels with metal face plates and an elastic isotropic core under combined in-plane compression and lateral pressure. They solved the geometrically non-linear governing differential equations by the Galerkin method and obtained results for load cases in which the in-plane load is dominant. They validated their results by nonlinear finite element analysis.

Little (2007) conducted experimental tests on three identical clamped steel-elastomer sandwich panels under combined uniaxial in-plane compression and uniform lateral pressure. A double-panel testing system was adopted in which the lateral pressure load was produced by pumping water into the space between two parallel panels. He measured three “ultimate strength” combinations of in-plane load and lateral pressure which caused collapse of the sandwich panels.

1.4 Objective of Present Study

Since steel-elastomer sandwich panels have many benefits as presented in Section 1.2, there have been applications in such areas as ship repair and conversion, oil and gas drilling platforms, and civil engineering structures such as bridges, stadium risers and flooring systems.

The most important loads applied on a sandwich panel in a ship are in-plane compression and lateral pressure. Under this combination of loads, the boundary condition of a sandwich panel is most closely approximated as clamped on all four edges. Figure 1.4 is the simplified computational model of a clamped sandwich panel under the load combination of in-plane compression and lateral pressure.

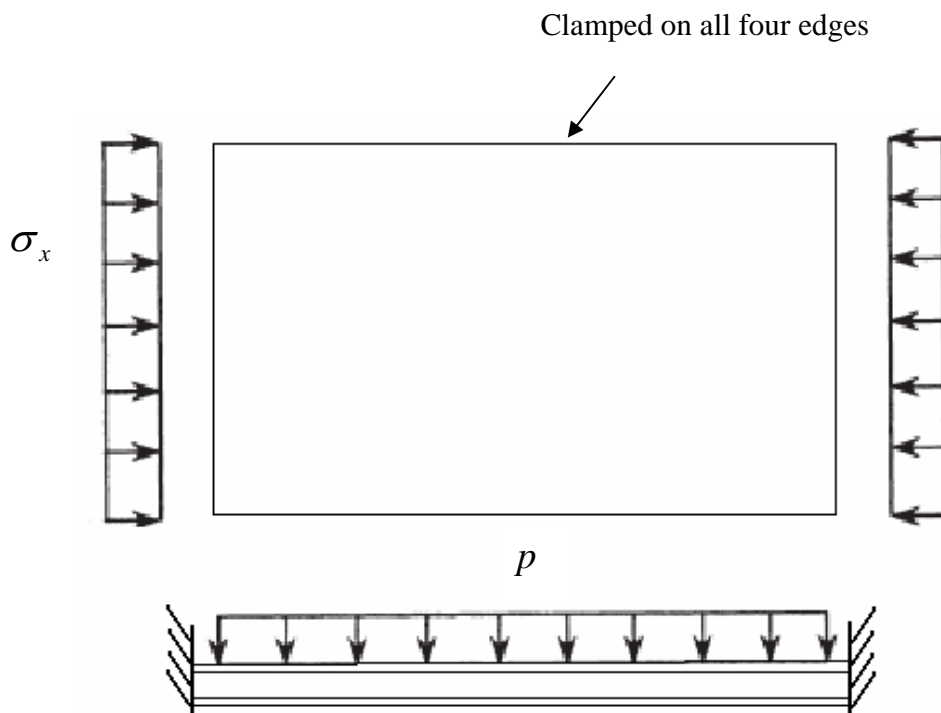


Figure 1.4 Computational model of a clamped sandwich panel under in-plane compression and lateral pressure

For the structural design of such panels, it is important to have a simple, rapid and yet accurate and efficient method for predicting their ultimate strength against typical loads. The main purpose of the research in this dissertation is to develop two potential methods for calculating the ultimate strength:

- 1) a semi-analytical method similar to that of Paik et al. (2001), but applied to the more difficult case of a sandwich panel (instead of a bare plate) and clamped boundaries (instead of simply supported).
- 2) a simple explicit (closed-form) expression, obtained by starting with hinge-line theory and extending it to allow for the sandwich properties (face thickness and core thickness), based on 180 data points obtained from nonlinear finite element analysis and verified by the experiments of Little (2007).

It will be shown that the semi-analytical method involves too much computation to be useful for design. In contrast, the simple explicit formula has sufficient accuracy to be ideally suited for the design of such panels.

1.5 Summary

The work presented in the following chapters can be summarized as follows:

Chapter 2 consists of two parts. The first part presents the hinge line theory. This theory can only calculate the ultimate strength of plates loaded by pure lateral pressure. In Chapter 5 it will be generalized to allow for the sandwich properties: face thickness and core thickness. The second part describes and gives the results of the full-scale experiments of Little (2007). These are the first and only experimental measurements of the ultimate strength of clamped steel-elastomer sandwich panels under combined in-plane compression and lateral pressure. They provide the verification of the nonlinear

finite element model in Chapter 4, which is used in Chapter 5 to generate data for a wide range of panels.

For the case of pure in-plane compression, the collapse stress (both experimental and finite element) exceeded the yield stress by about 5-10% because in both cases the elastomer core is carrying this portion of the load. This is not the purpose of the core, and designers would be reluctant to include this small extraneous “extra strength” in their design calculations. Therefore in Chapter 6 the small load carried by the core is subtracted, which makes the collapse stress equal to the yield stress.

Chapter 3 presents the semi-analytical method for the ultimate strength of clamped sandwich panels under combined in-plane compression and lateral pressure. The geometrical nonlinearity is solved by the Galerkin method. The material nonlinearity is treated by iteration and a three-dimensional mesh. Some results of this method are presented and compared to the results of hinge line theory. The method requires about the same amount of computation as nonlinear finite element analysis.

Chapter 4 introduces the finite element modeling and nonlinear analysis to calculate the ultimate strength of sandwich panels under combined load. The modeling is the same as used by Little (2007) and the results agree with his finite element results and with his experimental results. This verifies the accuracy of the current finite element model, from which further results are obtained in Chapter 5.

Chapter 5 identifies a comprehensive set of 180 finite element ultimate strength analyses, involving 3 face plate thicknesses t_f , 3 core thicknesses t_c , 4 panel aspect ratios α and 5 load combinations. For the case of pure lateral pressure (36 data points), these results are used to derive a correction factor which generalizes the hinge-line collapse pressure to allow for the sandwich properties: t_f, t_c and α .

Chapter 6 derives the final interaction formula for the ultimate strength of sandwich panels of usual proportions under any combination of loads. The formula is

expressed in terms of “strength ratios” R_p and R_σ , in which the numerators are the actual (interactive) collapse loads (pressure p and in-plane compressive stress σ_x) and the denominators are the collapse values of p and σ_x if those loads were acting alone, namely the corrected hinge-line collapse pressure p_{ult} and the yield stress σ_Y . The formula is:

$$R_p^2 - CR_p^2 R_\sigma^2 + R_\sigma^2 = 1$$

in which C is a function of t_c and α . The formula is plotted in Figure 6.20 for $C = 0.9$ (corresponding to $\alpha = 3$). When compared to the 180 data points, the formula has a standard deviation of 0.029, and since the radius of the interactive collapse curve is never very far from 1 (see Figure 6.20), this standard deviation corresponds to a percentage error of only 3%. Therefore the formula is not only simple but also has the accuracy required for the design of steel-elastomer sandwich panels of standard properties.

Chapter 2

Hinge Line Theory and Experiments

2.1 Hinge Line Theory

2.1.1 Introduction to Hinge Line Theory

Hinge line theory was originally developed for the design of concrete slabs (Drucker, 1958). It can provide explicit formulas to calculate the ultimate strength of steel plates under pure lateral pressure. Although the results of hinge line theory are approximate, it is still employed by many people due to its simple explicit formulas, especially for the early design stage.

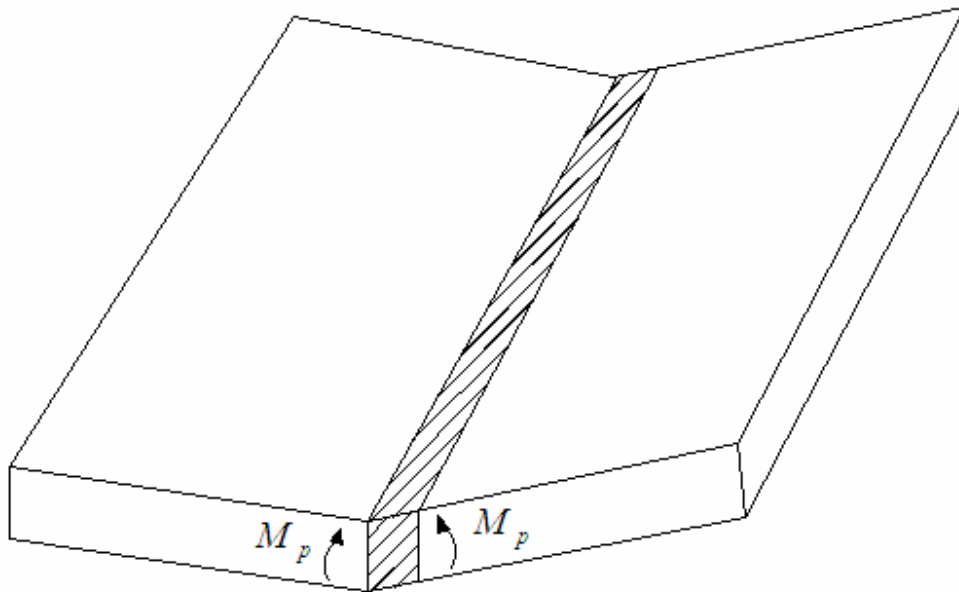


Figure 2.1 Hinge line in a panel

As can be seen in Figure 2.1, a panel is deformed due to lateral pressure. The stress-strain relation is assumed as perfect rigid-plastic, and the loaded panel forms a through-thickness fully yielded zone (a plastic hinge line) which is represented by the narrow strip in Figure 2.1. By this hinge line, the panel is divided into individual parts that can rotate along the lines as shown in Figure 2.2.

All lines are hinge lines, including the four boundaries

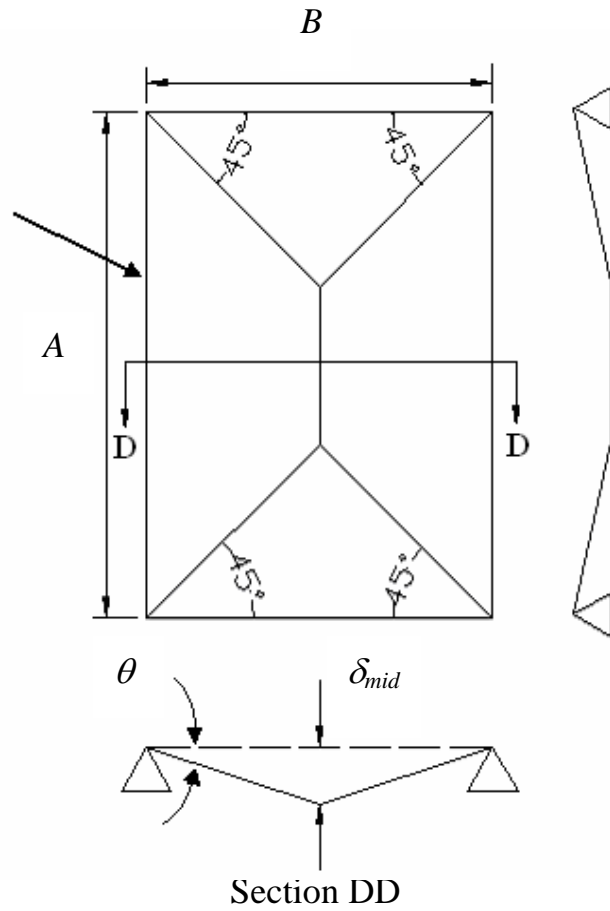


Figure 2.2 Deformation mechanism of hinge line theory for a clamped plate

Because the stress reaches the yield stress σ_Y , there is a plastic bending moment M_p per unit length along each hinge line. As shown in Figure 2.3, the plastic bending moment of a single layer plate can be calculated as:

$$M_p = \sigma_Y \cdot \frac{t^2}{4} \quad (2.1)$$

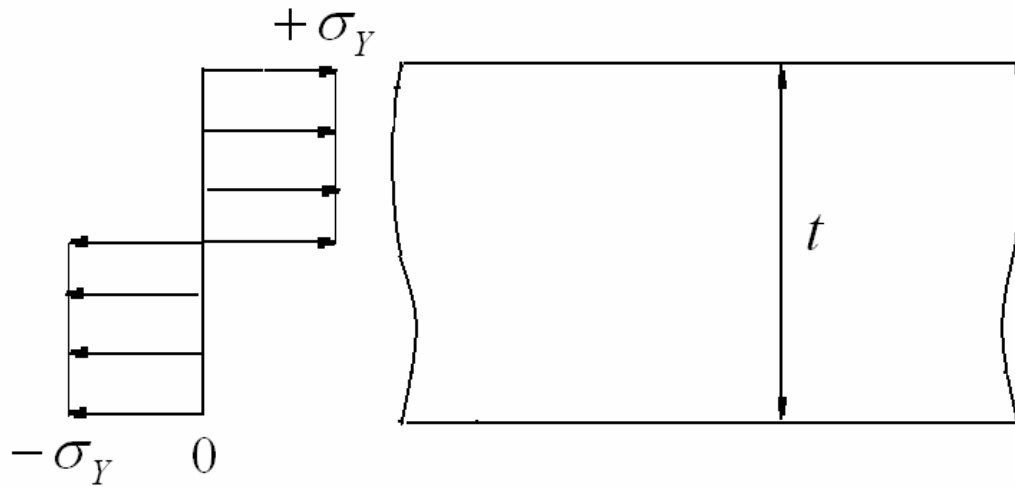


Figure 2.3 Formation of the plastic bending moment for a single layer plate

2.1.2 Formulas of Hinge Line Theory for Bare Plates

Based on hinge line theory, there are two representative formulas which can be used to calculate the ultimate pressure for bare plates. The first of them was developed by Save (1997).

A deformation mechanism formed of straight yield lines (hinge lines) is imagined as shown in Figure 2.2, where A is the panel long dimension, and B is the panel short dimension.

Some physical values can be defined as:

δ_{mid} : The displacement of the midpoint of the panel

θ : The out-of-plane rotation angle of the plate along section DD

p_{HL} : The lateral pressure which causes the collapse of a panel

It can be seen from Figure 2.2 that the deformed panel consists of two right triangles and two trapezoids. Each trapezoid can then be divided into two small isosceles triangles and one rectangle.

The external virtual work needed to form a set of two small isosceles triangles is equal to that which is needed for a big right triangle. Therefore the roof-like shape can be divided into four right triangles and two rectangles.

It is easy to show that $\frac{\delta_{mid}}{3}$ is the displacement of the centroid of a right triangle and $\frac{\delta_{mid}}{2}$ is the centroid displacement for a rectangle.

The external virtual work EVW done by p_{HL} can now be calculated:

$$EVW = p_{HL} \cdot \frac{\delta_{mid}}{3} \cdot \frac{B^2}{4} \cdot 4 + p_{HL} \cdot \frac{\delta_{mid}}{2} \cdot (A - B) \cdot \frac{B}{2} \cdot 2 = \frac{p_{HL} \cdot \delta_{mid}}{3} (3AB - B^2) \quad (2.2)$$

By assuming that the out-of-plane rotation angle is small, it can be calculated as:

$$\theta = \frac{\delta_{mid}}{B/2} = \frac{2\delta_{mid}}{B} \quad (2.3)$$

The four 45 degree hinge lines can each be treated as if they consisted of two component hinge lines, each of length $\frac{B}{2}$: one parallel to the width of the panel, and the other parallel to the length of the panel. Thus there are eight component hinge lines. When viewed from the side, each component has the same rotation angle θ as in section DD of Figure 2.2. The rotation angle of the mid hinge line is 2θ .

Then the internal virtual work IVW is calculated as:

$$IVW = M_p \theta \left(\frac{B}{2}\right) \cdot 8 + M_p \theta (2A + 2B) + M_p (2\theta)(A - B) = 8M_p \delta \left(\frac{A}{B} + 1\right) \quad (2.4)$$

The first term corresponds to the eight component (projected) hinge lines; the second term corresponds to the four clamped edge hinge lines; the third term corresponds to the central hinge line.

By the principle of virtual work, the external virtual work is equal to the internal virtual work:

$$EVW = IVW \Rightarrow \frac{P_{HL} \cdot \delta_{mid}}{3} (3AB - B) = 8M_p \delta_{mid} \left(\frac{A}{B} + 1\right) \quad (2.5)$$

The displacement δ_{mid} can be cancelled and p_{HL} is solved as:

$$p_{HL} = \frac{M_p [24(\frac{A}{B} + 1)]}{B^2 (1.5 \cdot \frac{A}{B} - 0.5)} \quad (2.6)$$

The other formula of hinge line theory was developed by Sabotka (1989). The derivation of his formula started from a similar roof-shaped deformation but with four yield fans in the corners as shown in Figure 2.4.

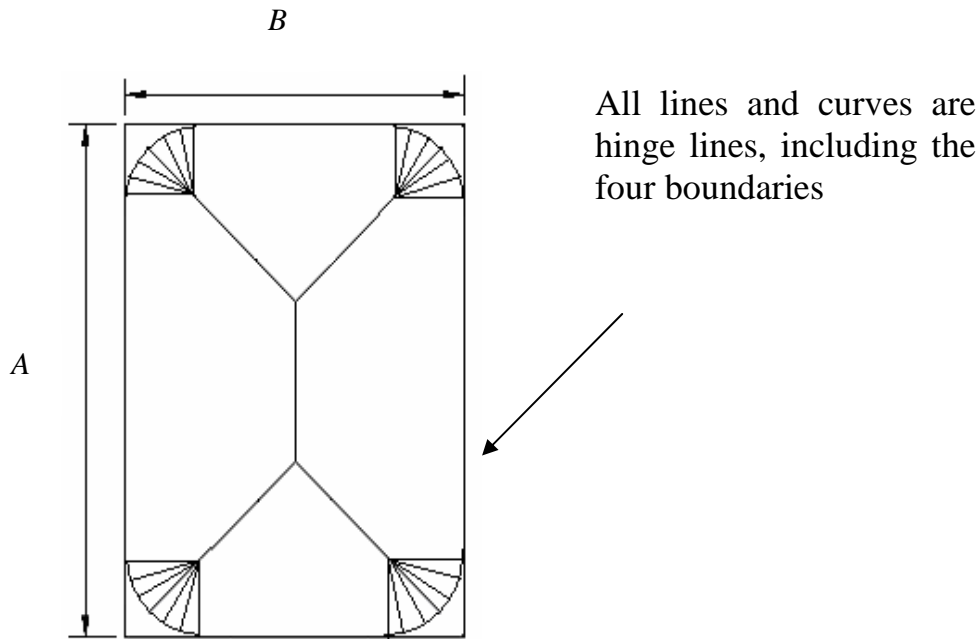


Figure 2.4 Deformation mechanism of hinge line theory by Sabotka (1989)

With the absence of the four yield fans, he finally gave the formula as:

$$p_{HL} = \frac{24M_p (2A + \frac{B^2}{\chi})}{B^2 (3A - 2\chi)}, \quad \chi = \frac{B^2}{2A} [-1 + \sqrt{1 + 3\frac{A^2}{B^2}}] \quad (2.7)$$

2.1.3 Comparison and Selection of a Formula

The two formulas introduced above are different and so it is necessary to compare their results and choose one of them for further applications. Since the calculation of M_p is the same for both formulas, M_p is replaced by 1. Therefore only A and B remain as variables. Figures 2.5 and 2.6 are the 3D plots for the results generated by the two formulas. As can be seen, the two surfaces are quite similar to each other. The difference between these two formulas can be obtained by subtracting Equation (2.7) from Equation (2.6).

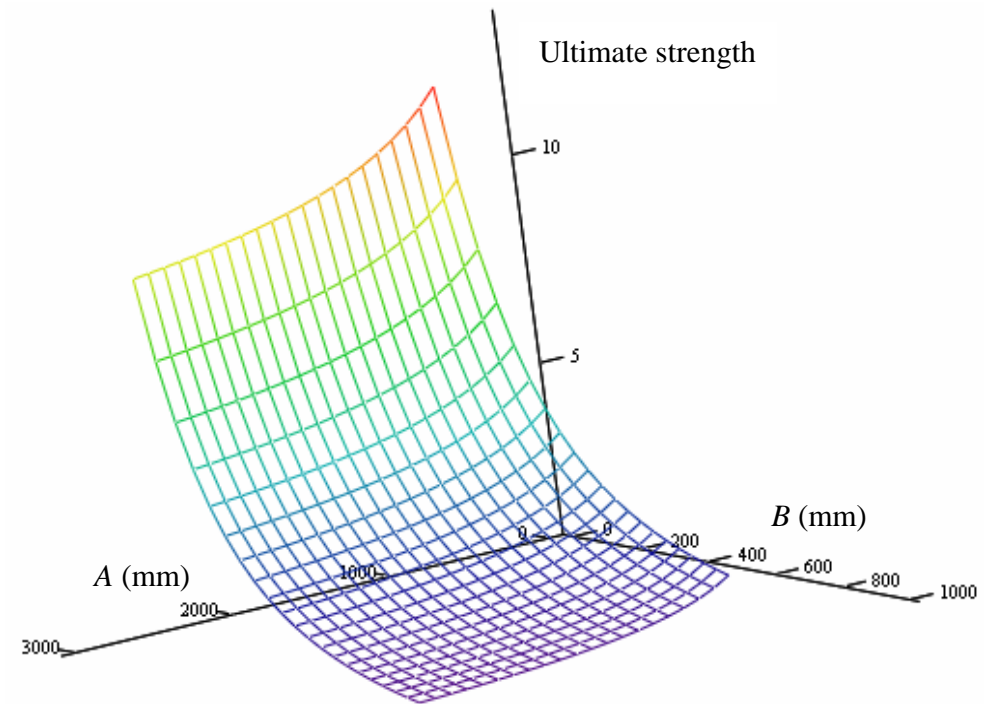


Figure 2.5 Ultimate strength calculated by Equation (2.6)

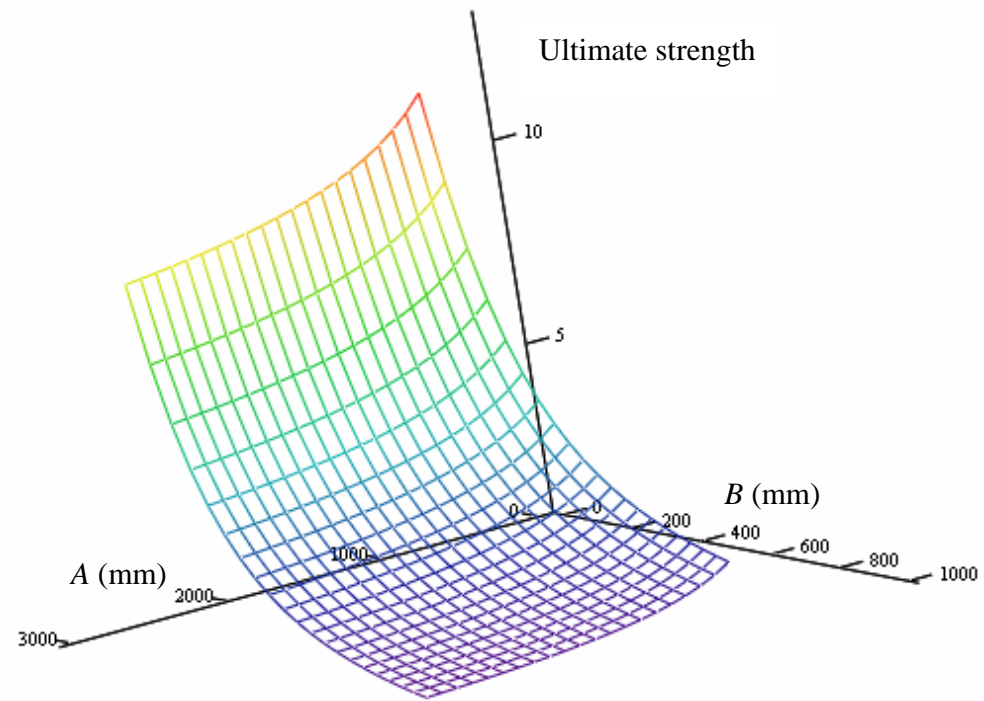


Figure 2.6 Ultimate strength calculated by Equation (2.7)

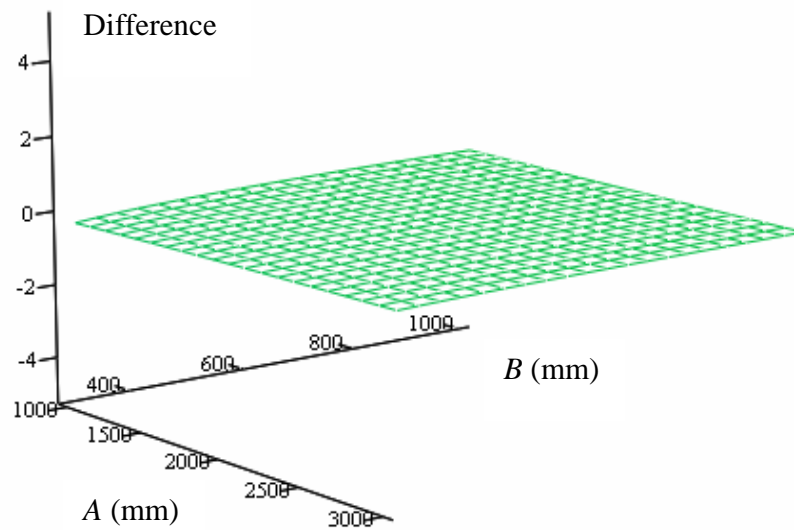


Figure 2.7 Difference between the results of Equation (2.6) and Equation (2.7)

As can be seen in Figure 2.7, the difference is so small as to be negligible. Since Equation (2.6) is simpler than Equation (2.7), the former is chosen to calculate the ultimate strength of clamped panels under lateral pressure. The resulting p_{HL} will be employed to calculate reference values in the following part of this dissertation.

2.1.4 Plastic Moment for a Sandwich Panel

For sandwich panels, the situation is different. The core of a sandwich panel is relatively soft and therefore only carries transverse shear. The yield stress is only generated in the face plates.

The formation of the plastic bending moment is plotted in Figure 2.8, where

t_f : the thickness of the steel face plates

t_c : the thickness of the core

σ_y : the yield stress of the steel face plates

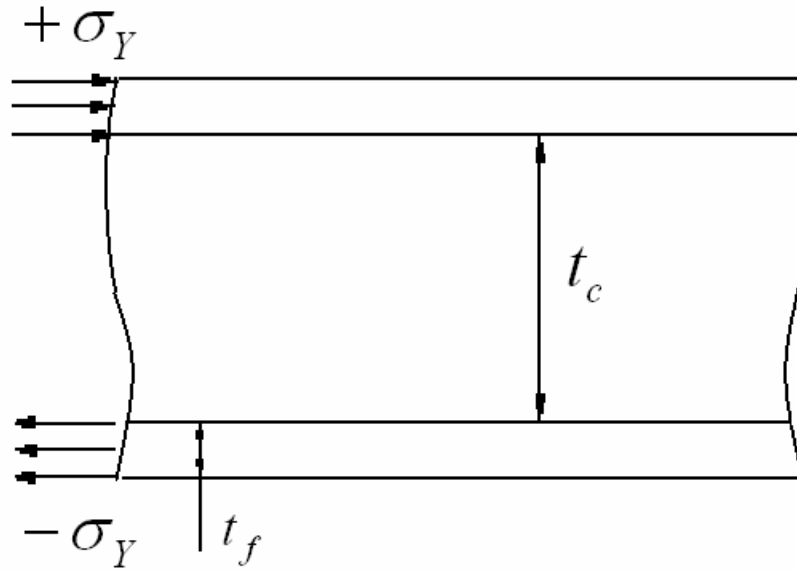


Figure 2.8 Formation of the plastic bending moment for a sandwich panel

The neutral surface is the global mid-surface of the sandwich panel. The distance between the surfaces of the mid-thickness of face plates is $t_f + t_c$. Therefore M_p can be calculated as:

$$M_p = \sigma_Y \cdot t_f (t_f + t_c) \quad (2.8)$$

By substituting Equation (2.8) into Equation (2.6), the ultimate strength of a sandwich panel is

$$p_{HL} = \frac{[24(\frac{A}{B} + 1)]}{b^2(1.5 \cdot \frac{A}{B} - 0.5)} \cdot \sigma_Y \cdot t_f (t_f + t_c) \quad (2.9)$$

2.1.5 Limitations

Although hinge line theory is a rapid and easy method to predict the ultimate strength of sandwich panels, there are two limitations:

1. The hinge line theory can only calculate ultimate strength for pure lateral pressure load. If in-plane compression is present, it cannot be used.

2. For metal-faced and elastomer-cored sandwich panels, the geometry is different, and so the collapse pressure p_{HL} will be different. Therefore it will be necessary to correct the hinge line theory formula of Equation (2.9). This will be done in Chapter 5.

2.2 Experiments

There are several ways to calculate the ultimate strength of sandwich panels, such as approximate analytical methods (e.g. hinge line theory), finite element analysis, and experimental measurements. The most reliable method is to conduct full-scale experiments, since this involves fewer assumptions and simplifications. The main limitation of experiments is the considerable expense, and until recently there were no experimental measurements of the ultimate strength of clamped steel-elastomer sandwich panels. Such experiments have now been performed, and are reported by Little (2007). Now that these are available, they can be used to validate finite element analysis (FEA), other analytical methods and simplified ultimate strength formulas. Once validated, the latter can be used to calculate the ultimate strength for a variety of panel geometries and load combinations, as needed in panel design. The experiments by Little (2007) will now be described.

2.2.1 Test Specimens

Three identical panels were tested. The basic dimensions and material properties are listed below:

1. Dimensions

Length: 1800 mm

Width: 1200 mm

Core thickness: 32 mm

Face thickness (each): 5 mm

2. Material properties

Material of face plates: steel

Yield stress: 355 MPa

Young's modulus: 199290 N/mm²

Poisson's ratio: 0.3

Material of core: elastomer

Young's modulus: 862 N/mm²

Poisson's ratio: 0.36

2.2.2 Three Special Features

1. Clamped boundary condition

The boundary condition of the sandwich panels is clamped. As shown in Figure 2.9, the actual plan dimensions of the tested sandwich panels are 240mm longer and 270 mm

wider than the nominal dimensions, in order for the panels to be clamped into the test frame.

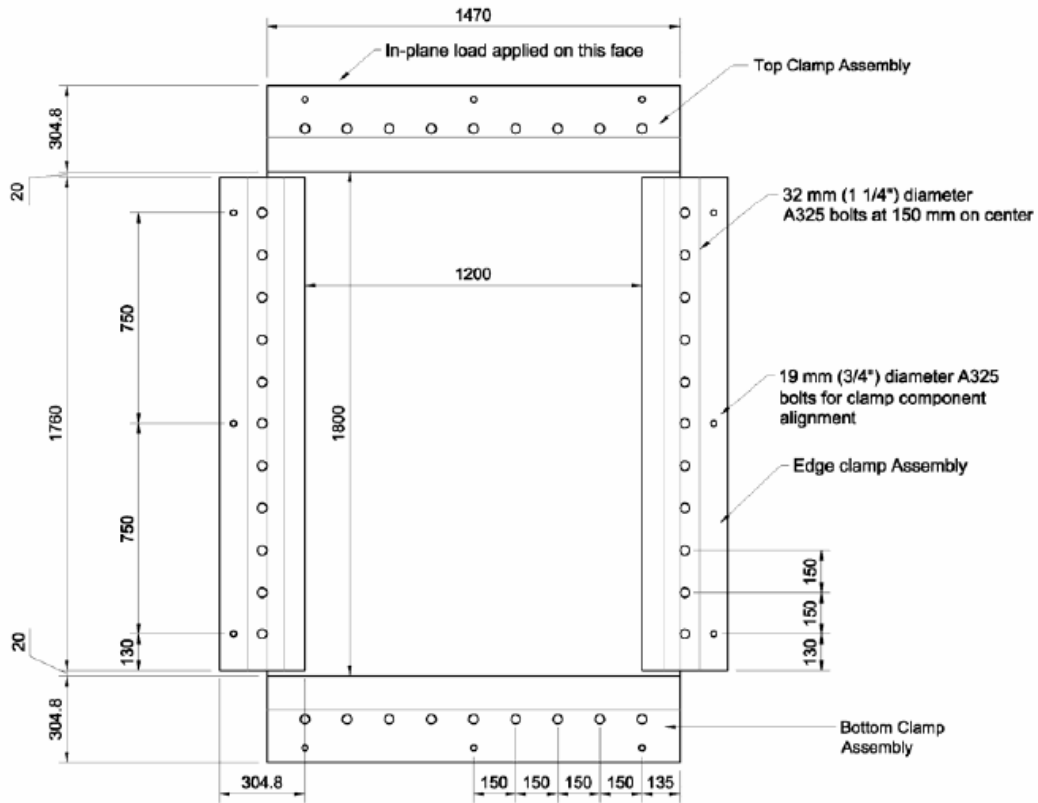


Figure 2.9 Plan view of test frame

2. Double-panel system

An important issue is how to apply the lateral pressure over the panel surface. As shown in Figure 2.10, a double-panel testing system was adopted instead of a single panel system. In this system two identical panels were mounted face to face. The lateral pressure load was imposed by pumping water into the space between the two panels and controlling the inside pressure as desired.



Figure 2.10 Double-panel system

3. Two load steps

The load applied on the sandwich panels was a combination of lateral pressure and in-plane compression. For the experiments, the load was applied in two steps. Lateral pressure was first applied to some fixed value and kept constant. Then the in-plane load was increased until the panel failed.

2.2.3 Results

1. Deflected shape

Three sandwich panels were loaded to an ultimate in-plane compressive ultimate strength under constant lateral pressures of 207, 415 and 690 kPa. Figure 2.11 shows the progressive out-of-plane deflection for the third panel. Results for the other two panels were similar. As will be shown in Chapter 3, the deflected shape of the panel just prior to collapse can be represented by the superposition of a one half-sine-wave shape and a three half-sine-waves shape. This representation of the deflected shape is exploited for the semi-analytical method which is presented in Chapter 3.

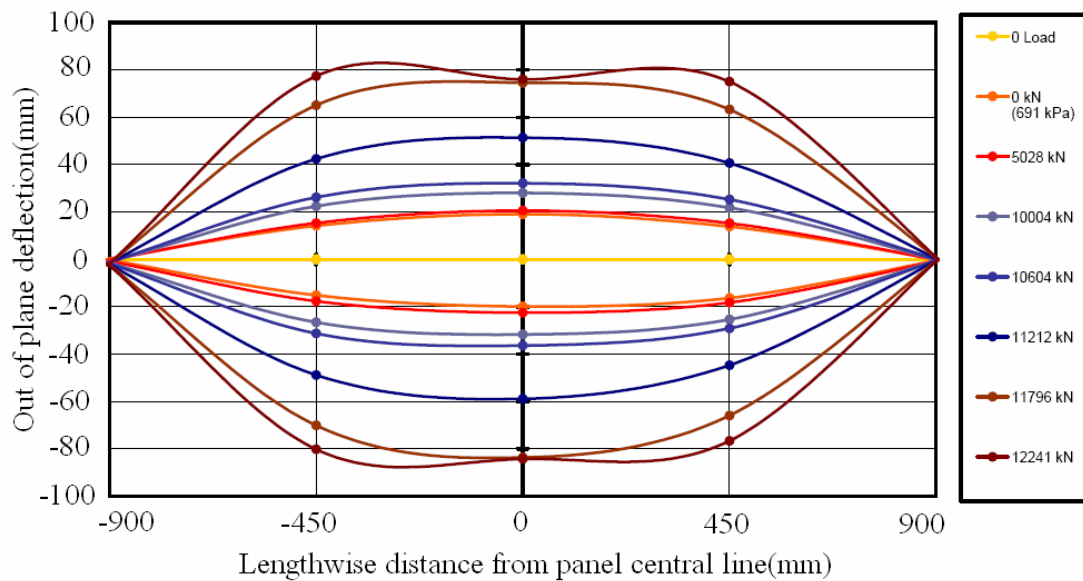


Figure 2.11 Progression of out of plane deflected shape

2. Failure points

For each of the three specimens, the combination of lateral pressure and in-plane compression which caused collapse is plotted in Figure 2.12. The lateral pressure is non-dimensionalized by p_{HL} , the collapse pressure calculated by hinge line theory as given by Equation (2.9). The in-plane load is non-dimensionalized by σ_y (355MPa), the yield stress of the steel face plates. In Chapter 4 these full-scale experimental values are used to validate the finite element model

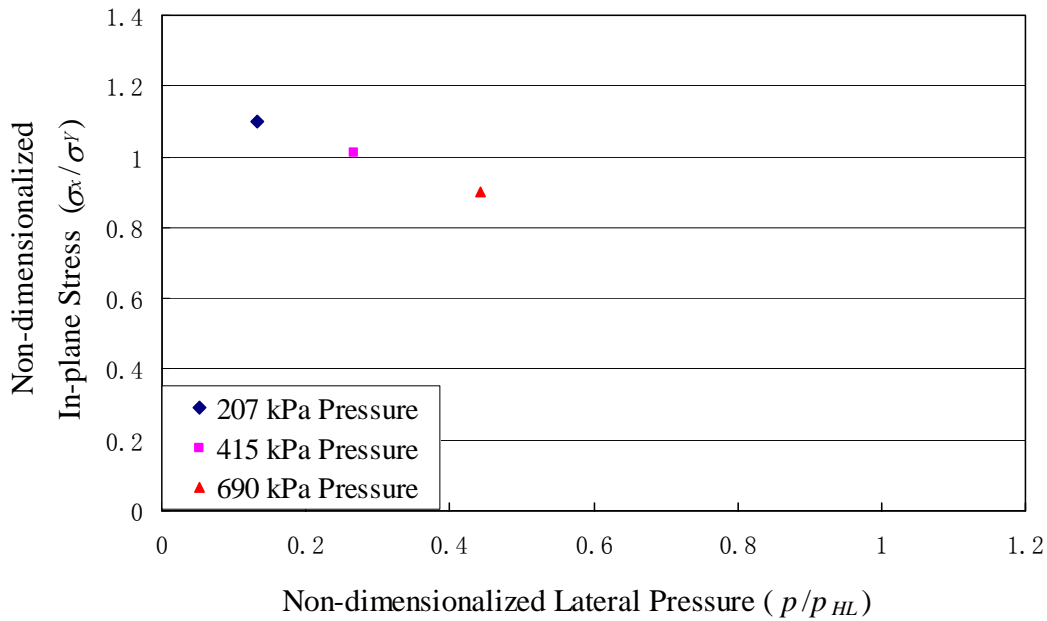


Figure 2.12 Failure points obtained from experiments

2.2.4 Discussion of Failure Stress Seeming to Exceed Yield Stress

The experiments have confirmed that there is no delamination or buckling of the face plates. The elastomer is itself an adhesive, and in the fabrication of the sandwich panels the elastomer forms a very strong bond with the face plates, thus preventing delamination. Also, the elastomer core is sufficiently rigid to prevent local buckling of the face plates. For these reasons, when the load is pure in-plane compression, both face plates reach the “squash load”; i.e. they reach a fully yielded condition.

As can be seen in Figure 2.12, for $p = 207$ kPa the ultimate in-plane compressive stress exceeds the yield stress by about 10%. It will be shown in Section 4.2.1 that the panel is deemed to have failed when the strain reaches 0.005. The elastomer does not “yield”; when the panel reaches failure (i.e. when the strain in the face plates is 0.005),

the modulus of the elastomer core is still the original value: $E_c = 862$ MPa. The strain in the core is always the same as in the steel. Therefore the stress in the core is $\sigma_c = \varepsilon \times E_c = 0.005 \times 862 = 4.31$ MPa. The total force will be stress \times area. The thickness of the core is 32 mm and the combined thickness of the two face plates is 10 mm. Therefore the total force is

$$F_{TOT} = \sigma_Y \times 2t_f \times b + \sigma_c \times t_c \times b = 355 \times 10b + 4.31 \times 32b = 3688b$$

where b is the width of the panel.

In calculating the failure stress, Little took this total force and divided by (only) the face plate area. This seems reasonable since carrying (any of) the in-plane load is not considered part of the role of the core. However, the result is to give a slightly increased value of the applied external stress at failure:

$$\frac{\sigma_{fail}}{\sigma_Y} = \frac{F_{TOT} / (2t_f \times b)}{\sigma_Y} = \frac{3688b / 10b}{355} = 1.04$$

This increase also occurs in Little's FEA results because he used the ANSYS option of applying an imposed displacement on the nodes at the loaded edge, including the elastomer nodes. (This is the reverse of the usual procedure, which is to impose nodal forces.) With this procedure the program calculates the reaction forces at all these nodes, including the elastomer nodes. Little then divided the total reaction force by the area of (only) the face plates. Therefore the failure stress is again slightly too large, and for pure in-plane compression it is slightly above σ_Y .

For the sake of comparison, this study used the same method as Little for all of the FEA calculations (Chapters 4 and 5). However, before using the FEA results in Chapter 6 to obtain the interaction formula, the in-plane failure stresses are proportionately reduced such that for pure in-plane compression they are equal to σ_Y .

The other portion of the exceedance of σ_Y is probably due to “strain hardening”: i.e. for large values of strain the height of the stress-strain curve steadily increases above the nominal yield value σ_Y (here 355 MPa). This is another reason why the experimental failure stress in Figure 2.12 exceeds σ_Y . It does not occur in the FEA results because the steel was taken to be elastic, perfectly plastic.

Chapter 3

Semi-Analytical Solution for the Ultimate Strength of Clamped Sandwich Panels

3.1 Governing Equations

By using Hamilton's variational principle, Librescu et al (1997) derived a comprehensive geometrically non-linear theory of initially imperfect doubly curved sandwich shells. There are five basic assumptions of this theory:

- (1) the material of core and faces is orthotropic
- (2) the core and faces are incompressible in the transverse normal direction
- (3) the panel is symmetric with respect to the global mid-surface
- (4) the faces are thin (i.e., the Love-Kirchhoff hypothesis can be adopted)
- (5) the bonding between face and core is perfect (no delamination)

If the faces and core are isotropic and the core is soft (carrying only transverse shear stresses), the compatibility equation is:

$$\begin{aligned}
 & A_{22}^* \frac{\partial^4 \phi}{\partial x^4} + A_{11}^* \frac{\partial^4 \phi}{\partial y^4} + (A_{66}^* + 2A_{12}^*) \frac{\partial^4 \phi}{\partial x^2 \partial y^2} \\
 & - 2 \left(\frac{\partial^2 w}{\partial x \partial y} \right)^2 + 2 \frac{\partial^2 w}{\partial x^2} \frac{\partial^2 w}{\partial y^2} + 2 \frac{\partial^2 w_0}{\partial x^2} \frac{\partial^2 w}{\partial y^2} + 2 \frac{\partial^2 w}{\partial x^2} \frac{\partial^2 w_0}{\partial y^2} - 4 \frac{\partial^2 w}{\partial x \partial y} \frac{\partial^2 w_0}{\partial x \partial y} = 0
 \end{aligned} \tag{3.1}$$

and the equilibrium equations are:

$$A_{11} \frac{\partial^2 \eta_x}{\partial x^2} + A_{66} \frac{\partial^2 \eta_x}{\partial y^2} + (A_{12} + A_{66}) \frac{\partial^2 \eta_y}{\partial x \partial y} - \delta (\eta_x + h \frac{\partial w}{\partial x}) = 0 \tag{3.2.a}$$

$$A_{22} \frac{\partial^2 \eta_y}{\partial y^2} + A_{66} \frac{\partial^2 \eta_y}{\partial x^2} + (A_{12} + A_{66}) \frac{\partial^2 \eta_x}{\partial x \partial y} - \delta (\eta_x + h \frac{\partial w}{\partial y}) = 0 \tag{3.2.b}$$

$$\frac{\partial^2 \phi}{\partial x^2} \left(\frac{\partial^2 w}{\partial y^2} + \frac{\partial^2 w_0}{\partial y^2} \right) - 2 \frac{\partial^2 \phi}{\partial x \partial y} \left(\frac{\partial^2 w}{\partial x \partial y} + \frac{\partial^2 w_0}{\partial x \partial y} \right) + \frac{\partial^2 \phi}{\partial y^2} \left(\frac{\partial^2 w}{\partial x^2} + \frac{\partial^2 w_0}{\partial x^2} \right) \tag{3.2.c}$$

$$- F_{11} \frac{\partial^4 w}{\partial x^4} - 2(F_{12} + 2F_{66}) \frac{\partial^4 w}{\partial x^2 \partial y^2} - F_{22} \frac{\partial^4 w}{\partial y^4} + \delta h \left(\frac{\partial \eta_x}{\partial x} + h \frac{\partial^2 w}{\partial x^2} \right) + \delta h \left(\frac{\partial \eta_y}{\partial y} + h \frac{\partial^2 w}{\partial y^2} \right) + p = 0$$

The constitutive equations are

$$N_x^l = A_{11}(\varepsilon_x^l + \nu \varepsilon_y^l) / 2, \quad N_y^l = A_{11}(\varepsilon_y^l + \nu \varepsilon_x^l) / 2, \quad N_{xy}^l = A_{66} \gamma_{xy}^l / 2 \tag{3.3.a-c}$$

$$N_x^u = A_{11}(\varepsilon_x^u + \nu \varepsilon_y^u) / 2, \quad N_y^u = A_{11}(\varepsilon_y^u + \nu \varepsilon_x^u) / 2, \quad N_{xy}^u = A_{66} \gamma_{xy}^u / 2 \tag{3.3.d-f}$$

$$M_x^l = F_{11}(\kappa_x^l + \nu \kappa_y^l) / 2, \quad M_{xy}^l = F_{66} \gamma_{xy}^l / 2 \tag{3.3.g-h}$$

$$M_x^u = F_{11}(\kappa_x^u + \nu \kappa_y^u) / 2, \quad M_{xy}^u = F_{66} \gamma_{xy}^u / 2 \tag{3.3.i-j}$$

where $A_{11} = A_{22} = 2Et_f / (1 - \nu^2)$, $A_{12} = \nu A_{11}$, $A_{66} = A_{11}(1 - \nu) / 2$,

$$A_{11}^* = A_{22}^* = 2 / (1 - \nu^2) A_{11}, \quad A_{12}^* = -2\nu / (1 - \nu^2) A_{11}, \quad A_{66}^* = 1 / A_{66}$$

$$F_{11} = F_{22} = D_{11} - h^2 A_{11} = Et_f^3 / 6(1 - \nu^2)$$

$$D_{11} = Et_f (3t_c^2 + 6t_c t_f + 4t_f^2) / 6(1 - \nu^2)$$

$$F_{12} = \nu F_{11}, \quad F_{66} = F_{11}(1 - \nu) / 2, \quad \delta = 4K^2 G_c / t_c, \quad h = (t_c + t_f) / 2,$$

$$\begin{aligned}\varepsilon_x^l &= \frac{\partial \xi_x}{\partial x} + \frac{\partial \eta_x}{\partial x} + \frac{1}{2} \left(\frac{\partial w}{\partial x} \right)^2 + \frac{\partial w}{\partial x} \frac{\partial w_0}{\partial x}, & \varepsilon_y^l &= \frac{\partial \xi_y}{\partial y} + \frac{\partial \eta_y}{\partial y} + \frac{1}{2} \left(\frac{\partial w}{\partial y} \right)^2 + \frac{\partial w}{\partial y} \frac{\partial w_0}{\partial y}, \\ \varepsilon_x^u &= \frac{\partial \xi_x}{\partial x} - \frac{\partial \eta_x}{\partial x} + \frac{1}{2} \left(\frac{\partial w}{\partial x} \right)^2 + \frac{\partial w}{\partial x} \frac{\partial w_0}{\partial x}, & \varepsilon_y^u &= \frac{\partial \xi_y}{\partial y} - \frac{\partial \eta_y}{\partial y} + \frac{1}{2} \left(\frac{\partial w}{\partial y} \right)^2 + \frac{\partial w}{\partial y} \frac{\partial w_0}{\partial y}, \\ \gamma_{xy}^l &= \frac{\partial \xi_x}{\partial y} + \frac{\partial \xi_y}{\partial x} + \frac{\partial \eta_x}{\partial y} + \frac{\partial \eta_y}{\partial x} + \frac{\partial w}{\partial x} \frac{\partial w}{\partial y} + \frac{\partial w_0}{\partial x} \frac{\partial w}{\partial y} + \frac{\partial w}{\partial x} \frac{\partial w_0}{\partial y}, \\ \gamma_{xy}^u &= \frac{\partial \xi_x}{\partial y} + \frac{\partial \xi_y}{\partial x} - \frac{\partial \eta_x}{\partial y} - \frac{\partial \eta_y}{\partial x} + \frac{\partial w}{\partial x} \frac{\partial w}{\partial y} + \frac{\partial w_0}{\partial x} \frac{\partial w}{\partial y} + \frac{\partial w}{\partial x} \frac{\partial w_0}{\partial y}, \\ \kappa_x^l &= -\frac{\partial^2 w}{\partial x^2}, & \kappa_y^l &= -\frac{\partial^2 w}{\partial y^2}, & \kappa_x^u &= -\frac{\partial^2 w}{\partial x^2}, & \kappa_y^u &= -\frac{\partial^2 w}{\partial y^2}.\end{aligned}$$

3.2 Incremental Approach

In order to simulate a clamped edge condition, the assumed added and initial deflection functions are:

$$w = \sum_{m=1}^M \sum_{n=1}^N w_{mn} \left[\cos \frac{2(m-1)\pi x}{a} - \cos \frac{2m\pi x}{a} \right] \cdot \left[\cos \frac{2(n-1)\pi y}{b} - \cos \frac{2n\pi y}{b} \right] \quad (3.4)$$

$$w_0 = \sum_{m=1}^M \sum_{n=1}^N w_{0mn} \left[\cos \frac{2(m-1)\pi x}{a} - \cos \frac{2m\pi x}{a} \right] \cdot \left[\cos \frac{2(n-1)\pi y}{b} - \cos \frac{2n\pi y}{b} \right] \quad (3.5)$$

These functions are for the general case of M and N terms in the in the x and y directions. Section 3.5 will give the values of M and N that have been assumed in the present model, and will present plots of these functions.

By assuming the external load is applied incrementally, the deflection function at the end of the $(i-1)$ th incremental load step is:

$$w_{i-1} = \sum_{m=1}^M \sum_{n=1}^N w_{i-1,mm} \left[\cos \frac{2(m-1)\pi x}{a} - \cos \frac{2m\pi x}{a} \right] \cdot \left[\cos \frac{2(n-1)\pi y}{b} - \cos \frac{2n\pi y}{b} \right] \quad (3.6)$$

The deflection function at the end of the i th incremental load step is:

$$w_i = w_{i-1} + \Delta w \quad (3.7)$$

where Δw is the increment of the deflection function and can be written as:

$$\Delta w = \sum_{m=1}^M \sum_{n=1}^N \Delta w_{mn} \left[\cos \frac{2(m-1)\pi x}{a} - \cos \frac{2m\pi x}{a} \right] \cdot \left[\cos \frac{2(n-1)\pi y}{b} - \cos \frac{2n\pi y}{b} \right] \quad (3.8)$$

At the end of the $(i-1)$ th incremental load step, Equation (3.1) and (3.2.a-c) can be rewritten as:

$$\begin{aligned} & A_{22}^* \frac{\partial^4 \phi_{i-1}}{\partial x^4} + A_{11}^* \frac{\partial^4 \phi_{i-1}}{\partial y^4} + (A_{66}^* + 2A_{12}^*) \frac{\partial^4 \phi_{i-1}}{\partial x^2 \partial y^2} \\ & - 2 \left(\frac{\partial^2 w_{i-1}}{\partial x \partial y} \right)^2 + 2 \frac{\partial^2 w_{i-1}}{\partial x^2} \frac{\partial^2 w_{i-1}}{\partial y^2} + 2 \frac{\partial^2 w_0}{\partial x^2} \frac{\partial^2 w_{i-1}}{\partial y^2} + 2 \frac{\partial^2 w_{i-1}}{\partial x^2} \frac{\partial^2 w_0}{\partial y^2} - 4 \frac{\partial^2 w_{i-1}}{\partial x \partial y} \frac{\partial^2 w_0}{\partial x \partial y} = 0 \end{aligned} \quad (3.9)$$

$$A_{11} \frac{\partial^2 \eta_{x,i-1}}{\partial x^2} + A_{66} \frac{\partial^2 \eta_{x,i-1}}{\partial y^2} + (A_{12} + A_{66}) \frac{\partial^2 \eta_{y,i-1}}{\partial x \partial y} - \delta (\eta_{x,i-1} + h \frac{\partial w_{i-1}}{\partial x}) = 0 \quad (3.10.a)$$

$$A_{22} \frac{\partial^2 \eta_{y,i-1}}{\partial y^2} + A_{66} \frac{\partial^2 \eta_{y,i-1}}{\partial x^2} + (A_{12} + A_{66}) \frac{\partial^2 \eta_{x,i-1}}{\partial x \partial y} - \delta (\eta_{x,i-1} + h \frac{\partial w_{i-1}}{\partial y}) = 0 \quad (3.10.b)$$

$$\begin{aligned} & \frac{\partial^2 \phi_{i-1}}{\partial x^2} \left(\frac{\partial^2 w_{i-1}}{\partial y^2} + \frac{\partial^2 w_0}{\partial y^2} \right) - 2 \frac{\partial^2 \phi_{i-1}}{\partial x \partial y} \left(\frac{\partial^2 w_{i-1}}{\partial x \partial y} + \frac{\partial^2 w_0}{\partial x \partial y} \right) + \frac{\partial^2 \phi_{i-1}}{\partial y^2} \left(\frac{\partial^2 w_{i-1}}{\partial x^2} + \frac{\partial^2 w_0}{\partial x^2} \right) \\ & - F_{11} \frac{\partial^4 w_{i-1}}{\partial x^4} - 2(F_{12} + 2F_{66}) \frac{\partial^4 w_{i-1}}{\partial x^2 \partial y^2} - F_{22} \frac{\partial^4 w_{i-1}}{\partial y^4} + \delta h \left(\frac{\partial \eta_{x,i-1}}{\partial x} + h \frac{\partial^2 w_{i-1}}{\partial x^2} \right) \\ & + \delta h \left(\frac{\partial \eta_{y,i-1}}{\partial y} + h \frac{\partial^2 w_{i-1}}{\partial y^2} \right) + p_{i-1} = 0 \end{aligned} \quad (3.10.c)$$

Equation (3.6) is substituted in Equations (3.9), (3.10.a), and (3.10.b) to solve for the functions ϕ_{i-1} , $\eta_{x,i-1}$, and $\eta_{y,i-1}$.

At the end of the i th incremental load step, Equations (3.1) and (3.2.a-c) can be rewritten as:

$$A_{22}^* \frac{\partial^4 \phi_i}{\partial x^4} + A_{11}^* \frac{\partial^4 \phi_i}{\partial y^4} + (A_{66}^* + 2A_{12}^*) \frac{\partial^4 \phi_i}{\partial x^2 \partial y^2} - 2 \left(\frac{\partial^2 w_i}{\partial x \partial y} \right)^2 + 2 \frac{\partial^2 w_i}{\partial x^2} \frac{\partial^2 w_i}{\partial y^2} + 2 \frac{\partial^2 w_0}{\partial x^2} \frac{\partial^2 w_i}{\partial y^2} + 2 \frac{\partial^2 w_i}{\partial x^2} \frac{\partial^2 w_0}{\partial y^2} - 4 \frac{\partial^2 w_i}{\partial x \partial y} \frac{\partial^2 w_0}{\partial x \partial y} = 0 \quad (3.11)$$

$$A_{11} \frac{\partial^2 \eta_{x,i}}{\partial x^2} + A_{66} \frac{\partial^2 \eta_{x,i}}{\partial y^2} + (A_{12} + A_{66}) \frac{\partial^2 \eta_{y,i}}{\partial x \partial y} - \delta(\eta_{x,i} + h \frac{\partial w_i}{\partial x}) = 0 \quad (3.12.a)$$

$$A_{22} \frac{\partial^2 \eta_{y,i}}{\partial y^2} + A_{66} \frac{\partial^2 \eta_{y,i}}{\partial x^2} + (A_{12} + A_{66}) \frac{\partial^2 \eta_{x,i}}{\partial x \partial y} - \delta(\eta_{x,i} + h \frac{\partial w_i}{\partial y}) = 0 \quad (3.12.b)$$

$$\begin{aligned} & \frac{\partial^2 \phi_i}{\partial x^2} \left(\frac{\partial^2 w_i}{\partial y^2} + \frac{\partial^2 w_0}{\partial y^2} \right) - 2 \frac{\partial^2 \phi_i}{\partial x \partial y} \left(\frac{\partial^2 w_i}{\partial x \partial y} + \frac{\partial^2 w_0}{\partial x \partial y} \right) + \frac{\partial^2 \phi_i}{\partial y^2} \left(\frac{\partial^2 w_i}{\partial x^2} + \frac{\partial^2 w_0}{\partial x^2} \right) \\ & - F_{11} \frac{\partial^4 w_i}{\partial x^4} - 2(F_{12} + 2F_{66}) \frac{\partial^4 w_i}{\partial x^2 \partial y^2} - F_{22} \frac{\partial^4 w_i}{\partial y^4} + \delta h \left(\frac{\partial \eta_{x,i}}{\partial x} + h \frac{\partial^2 w_i}{\partial x^2} \right) \\ & + \delta h \left(\frac{\partial \eta_{y,i}}{\partial y} + h \frac{\partial^2 w_i}{\partial y^2} \right) + p_i = 0 \end{aligned} \quad (3.12.c)$$

Equations (3.9) and (3.10.a-c) are respectively subtracted from Equations (3.11) and (3.12.a-c), thus giving the incremental governing equations:

$$A_{22}^* \frac{\partial^4 \Delta \phi}{\partial x^4} + A_{11}^* \frac{\partial^4 \Delta \phi}{\partial y^4} + (A_{66}^* + 2A_{12}^*) \frac{\partial^4 \Delta \phi}{\partial x^2 \partial y^2} - 4 \frac{\partial^2 (w_{i-1} + w_0)}{\partial x \partial y} \frac{\partial^2 \Delta w}{\partial x \partial y} + 2 \frac{\partial^2 (w_{i-1} + w_0)}{\partial x^2} \frac{\partial^2 \Delta w}{\partial y^2} + 2 \frac{\partial^2 (w_{i-1} + w_0)}{\partial y^2} \frac{\partial^2 \Delta w}{\partial x^2} = 0 \quad (3.13)$$

$$A_{11} \frac{\partial^2 \Delta \eta_x}{\partial x^2} + A_{66} \frac{\partial^2 \Delta \eta_x}{\partial y^2} + (A_{12} + A_{66}) \frac{\partial^2 \Delta \eta_y}{\partial x \partial y} - \delta(\Delta \eta_x + h \frac{\partial \Delta w}{\partial x}) = 0 \quad (3.14.a)$$

$$A_{22} \frac{\partial^2 \Delta \eta_y}{\partial y^2} + A_{66} \frac{\partial^2 \Delta \eta_y}{\partial x^2} + (A_{12} + A_{66}) \frac{\partial^2 \Delta \eta_x}{\partial x \partial y} - \delta(\Delta \eta_x + h \frac{\partial \Delta w}{\partial y}) = 0 \quad (3.14.b)$$

$$\begin{aligned} & F_{11} \frac{\partial^4 \Delta w}{\partial x^4} + 2(F_{12} + 2F_{66}) \frac{\partial^4 \Delta w}{\partial x^2 \partial y^2} + F_{22} \frac{\partial^4 \Delta w}{\partial y^4} - \delta h \left(\frac{\partial \Delta \eta_x}{\partial x} + h \frac{\partial^2 \Delta w}{\partial x^2} \right) - \delta h \left(\frac{\partial \Delta \eta_y}{\partial y} + h \frac{\partial^2 \Delta w}{\partial y^2} \right) \\ & - \frac{\partial^2 \phi_{i-1}}{\partial x^2} \frac{\partial^2 \Delta w}{\partial y^2} + 2 \frac{\partial^2 \phi_{i-1}}{\partial x \partial y} \frac{\partial^2 \Delta w}{\partial x \partial y} - \frac{\partial^2 \phi_{i-1}}{\partial y^2} \frac{\partial^2 \Delta w}{\partial x^2} - \frac{\partial^2 \Delta \phi}{\partial x^2} \frac{\partial^2 (w_{i-1} + w_0)}{\partial y^2} \\ & + 2 \frac{\partial^2 \Delta \phi}{\partial x \partial y} \frac{\partial^2 (w_{i-1} + w_0)}{\partial x \partial y} - \frac{\partial^2 \Delta \phi}{\partial y^2} \frac{\partial^2 (w_{i-1} + w_0)}{\partial x^2} - \Delta p = 0 \end{aligned} \quad (3.14.c)$$

Equation (3.6) is substituted in Equation (3.13), (3.14.a), and (3.14.b) to solve for the incremental functions $\Delta \phi$, $\Delta \eta_x$, and $\Delta \eta_y$. As required by the Galerkin Method, Equation (3.14.c) must be multiplied by the deflection function and integrated over the volume of the face plates and set to zero :

$$\iiint \Delta \Phi \cdot \left[\cos \frac{2(r-1)\pi x}{a} - \cos \frac{2r\pi x}{a} \right] \left[\cos \frac{2(s-1)\pi y}{b} - \cos \frac{2s\pi y}{b} \right] dvol = 0 \quad (3.15)$$

where $\Delta \Phi$ is the LHS of Equation (3.14.c)

The result of Equation (3.15) is a set of linear equations which can be organized in matrix form as:

$$([P_0] + [K_B] + [K_M] + [K_S]) \{\Delta w\} = \{\Delta P\} \quad (3.16)$$

where

$[P_0]$ is the stiffness matrix due to the initial stress (all matrices are of dimension $MN \times MN$)

$[K_B]$ is the bending stiffness matrix

$[K_M]$ is the stiffness matrix associated with membrane action

$[K_S]$ is the stiffness matrix associated with transverse shear

$\{\Delta w\}$ is the vector of unknown coefficients (length MN)

$\{\Delta P\}$ is the vector of external incremental load (length MN)

Kim and Hughes (2005) applied the Galerkin method to solve Librescu's governing equations of sandwich panels, but not in the form of Equation (3.16). Paik et al. (2001) presented a solution for bare steel plates similar to Equation (3.16). The only difference between Equation (3.16) and Paik's equation is that $[K_S]$ is introduced here due to the transverse shear carried by the core.

3.3 Solution for Material Nonlinearity

The unknown $\{\Delta w\}$ in Equation (3.16) can be simply solved by methods for linear systems, and the latest deflection function is obtained from Equation (3.7). The stress distribution in the face plates can then be calculated by Equation (3.3).

To check the progress of yielding, each of the face plates is divided into mesh regions in three dimensions as plotted in Figure 3.1.

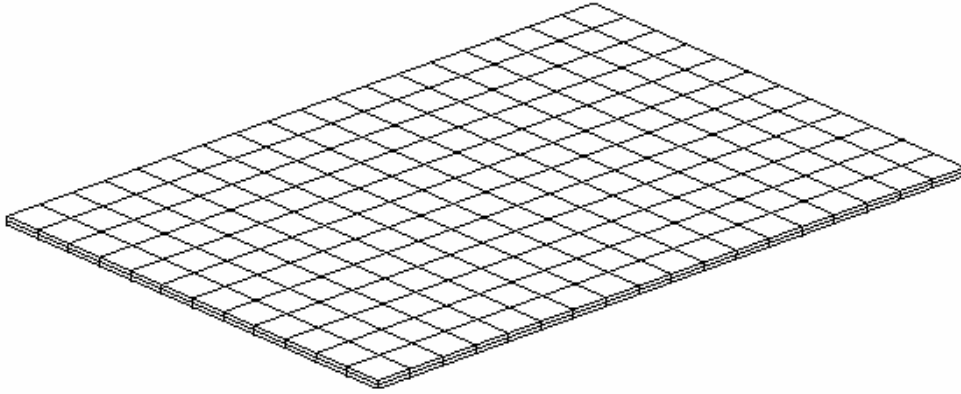


Figure 3.1 Division of mesh regions for a face plate of a sandwich panel

The von Mises criterion is employed to check yielding as:

$$\sigma_x^2 - \sigma_x \sigma_y + \sigma_y^2 + 3\tau^2 \geq \sigma_Y^2 \quad (3.17)$$

If one of the elements of the mesh is yielded, the integration of $[K_B]$ and $[K_S]$ in Equation (3.16) will not include this element. For $[K_M]$ in Equation (3.16), all the elements that have the same x or y coordinates with the yielded element will not be included in the integration.

With increasing external load, the stiffness matrix is decreased due to the expansion of the yielded region. Once the determinant of the stiffness matrix is equal to (or smaller than) zero, the ultimate strength of the sandwich panel is reached.

Since the material nonlinearity is solved iteratively, the overall method is classified as a semi-analytical method.

3.4 Verification

Paik et al (2001) applied the semi-analytical method to calculate the ultimate strength of simply supported isotropic steel square plates. Before presenting the results for clamped sandwich panels, it is necessary to calculate one of their cases and compare with their results. The selected case is for pure lateral pressure and the following geometric dimensions and material properties: $a = b = 1000$ mm, $t = 14.3$ mm, $E = 205800$ MPa, and $\sigma_y = 264.6$ MPa.

The steel panel is simply supported, therefore the panel deflection functions are assumed as:

$$w = w_{11} \sin \frac{\pi x}{a} \sin \frac{\pi y}{b} \quad (3.18)$$

$$w_0 = w_{011} \sin \frac{\pi x}{a} \sin \frac{\pi y}{b} \quad (3.19)$$

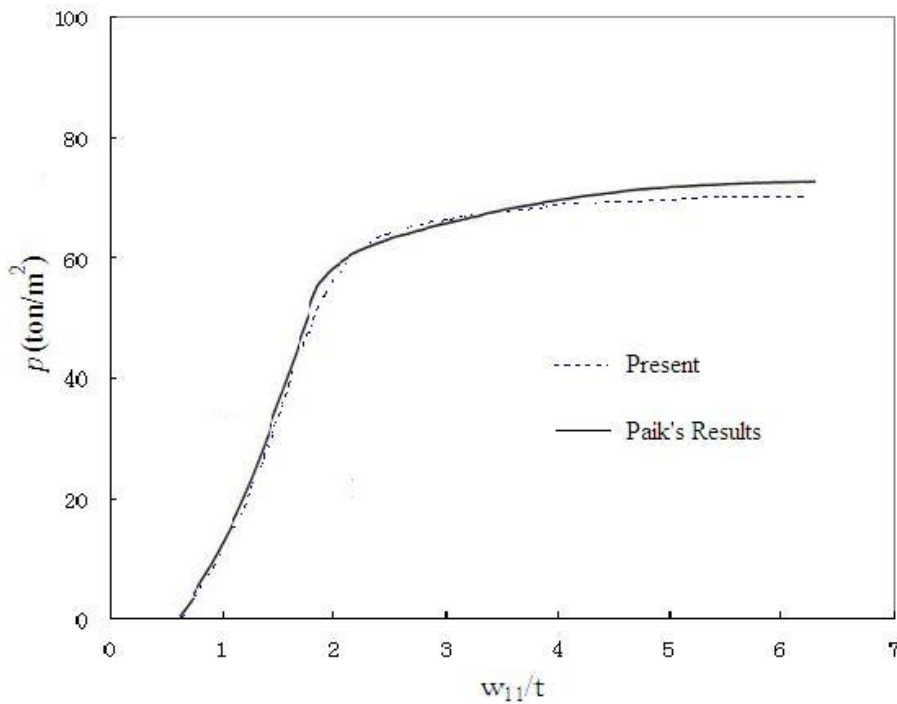


Figure 3.2 Load versus deflection curve of a simply supported square panel under lateral pressure load

The amplitude of initial deflection w_{011} is equal to 8.96 mm. The load versus deflection curve is plotted in Figure 3.2 (here $1 \text{ ton/m}^2 = 8.9 \times 10^{-3} \text{ MPa}$). As shown in Figure 3.2, the results are almost the same as Paik (2001). Having verified the basic method, it will be now used to calculate the ultimate strength of sandwich panels.

3.5 Deflection Function and Solution Procedure

3.5.1 Deflection Function

As presented in Section 2.2.3, two terms (one half wave and three half waves) are needed to represent the deformed shape of sandwich panels under in-plane compression and lateral pressure. Therefore in Equations (3.4), (3.5), etc., $M = 2$ and $N = 2$. The added and initial deflection functions now become:

$$\begin{aligned}
 w = & w_{11} \left[1 - \cos \frac{2\pi x}{a} \right] \left[1 - \cos \frac{2\pi y}{b} \right] + w_{12} \left[1 - \cos \frac{2\pi x}{a} \right] \left[\cos \frac{2\pi y}{b} - \cos \frac{4\pi y}{b} \right] \\
 & + w_{21} \left[\cos \frac{2\pi x}{a} - \cos \frac{4\pi x}{a} \right] \left[1 - \cos \frac{2\pi y}{b} \right] + w_{22} \left[\cos \frac{2\pi x}{a} - \cos \frac{4\pi x}{a} \right] \left[\cos \frac{2\pi y}{b} - \cos \frac{4\pi y}{b} \right]
 \end{aligned} \tag{3.19}$$

$$\begin{aligned}
 w_0 = & w_{011} \left[1 - \cos \frac{2\pi x}{a} \right] \left[1 - \cos \frac{2\pi y}{b} \right] + w_{012} \left[1 - \cos \frac{2\pi x}{a} \right] \left[\cos \frac{2\pi y}{b} - \cos \frac{4\pi y}{b} \right] \\
 & + w_{021} \left[\cos \frac{2\pi x}{a} - \cos \frac{4\pi x}{a} \right] \left[1 - \cos \frac{2\pi y}{b} \right] + w_{022} \left[\cos \frac{2\pi x}{a} - \cos \frac{4\pi x}{a} \right] \left[\cos \frac{2\pi y}{b} - \cos \frac{4\pi y}{b} \right]
 \end{aligned} \tag{3.20}$$

The mode shapes of the deflection functions are plotted in Figure 3.3, which consists of $1 - \cos \frac{2\pi x}{a}$ (one half wave mode), $\cos \frac{2\pi x}{a} - \cos \frac{4\pi x}{a}$ (three half waves mode), and $2.1[1 - \cos \frac{2\pi x}{a}] + 0.45[\cos \frac{2\pi x}{a} - \cos \frac{4\pi x}{a}]$ (a combination of these two mode shapes).

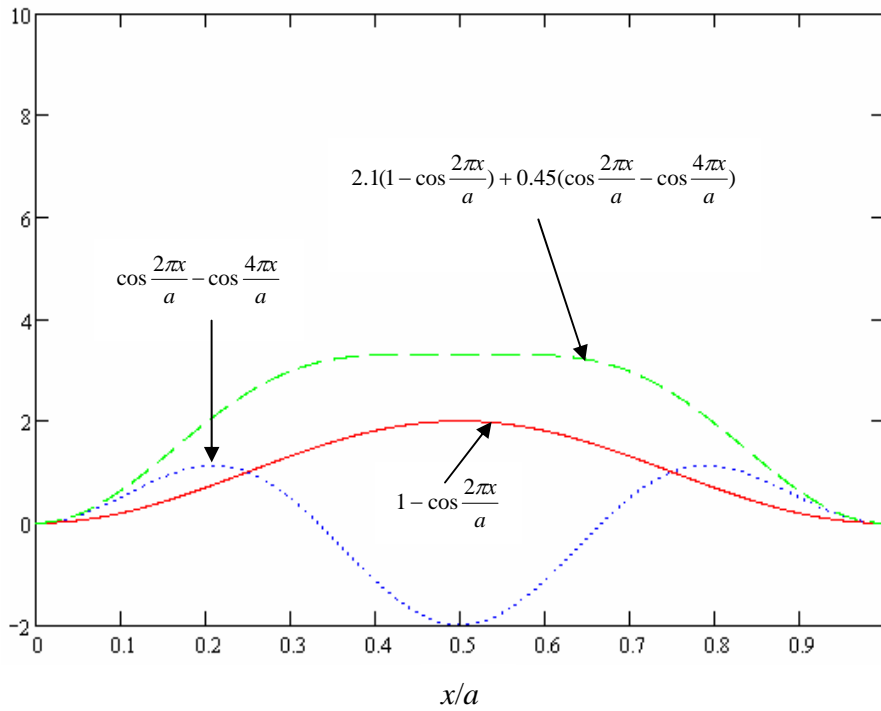


Figure 3.3 Mode shapes of the deflection functions

3.5.2 Solution Procedure

The solution procedure of the semi-analytical method is shown in Figure 3.4.

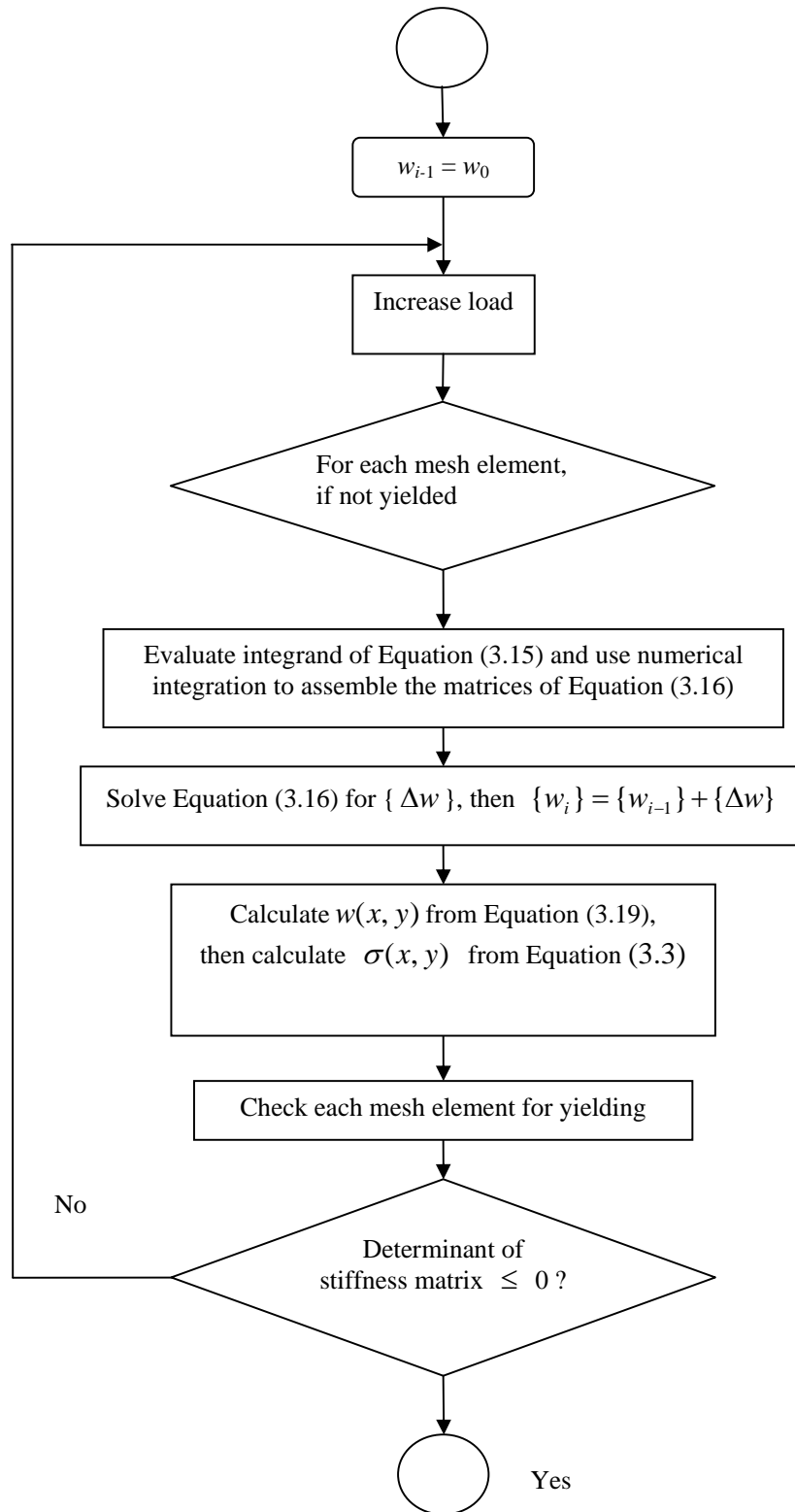


Figure 3.4 Solution procedure

Although the solution procedure is straightforward, the computation time is excessive. Most of the time is incurred in evaluating the integrand of Equation (3.15), and performing numerical integration, both of which have to be done separately for each element.

In these calculations $\Delta\Phi$ (LHS of Equation (3.14.c)) is divided into four parts:

$$\Delta\Phi = \Delta\Phi_{KB} + \Delta\Phi_{KM} + \Delta\Phi_{KS} + \Delta\Phi_{P0} \quad (3.21)$$

Each of the four parts consists of four groups: Δw_{11} , Δw_{12} , Δw_{21} and Δw_{22} , e.g.

$$\Delta\Phi_{KB} = B_1\Delta w_{11} + B_2\Delta w_{12} + B_3\Delta w_{21} + B_4\Delta w_{22} \quad (3.22)$$

Because there are four mode shapes as shown in Equation (3.19), integration is performed four times for each group ($r = 1, 2$ and $s = 1, 2$). After the integration, each part of $\Delta\Phi$ becomes a product of a coefficient matrix and a vector. For example, for the K_B matrix,

$$\begin{aligned} & \iiint \Delta\Phi_{KB} \cdot \left[\cos \frac{2(r-1)\pi x}{a} - \cos \frac{2r\pi x}{a} \right] \left[\cos \frac{2(s-1)\pi y}{b} - \cos \frac{2s\pi y}{b} \right] dvol \\ &= \begin{bmatrix} KB_{11} & KB_{12} & KB_{13} & KB_{14} \\ KB_{21} & KB_{22} & KB_{23} & KB_{24} \\ KB_{31} & KB_{32} & KB_{33} & KB_{34} \\ KB_{41} & KB_{42} & KB_{43} & KB_{44} \end{bmatrix} \begin{Bmatrix} \Delta w_{11} \\ \Delta w_{12} \\ \Delta w_{21} \\ \Delta w_{22} \end{Bmatrix} = [K_B] \{\Delta w\} \end{aligned} \quad (3.23)$$

Therefore for each mesh element, the number of integrations is $4 \times 4 \times 4 = 64$. For a typical mesh for a sandwich panel with dimension of $1800\text{mm} \times 1200\text{mm}$, the number of elements is about $20 \times 15 \times 4 = 1200$. The external load is divided into 100 load steps

by a constant small increment. For the beginning load steps, because there are no yielded mesh elements, the integration is performed for the whole panel and the number of integrations for each load step is $64 \times 1200 = 76800$. When the load becomes bigger and the number of yielded elements increases, the number of integrations decreases because yielded mesh elements are excluded from integration. When all the mesh elements are yielded, the number of integrations is zero and the solution procedure is finished. So the rough average number of integrations for each load step is $76800/2 = 38400$. Then the number of integrations in the whole solution procedure is $38400 \times 100 = 3,840,000$.

This huge number of integrations consumes most of the time of the solution and therefore an excessive amount of computation is required (e.g. 4 hours for a pressure-only load case, CPU 2.93 GHz).

3.6 Results

The results of ultimate strength of nine different sandwich panels under pure lateral pressure are calculated by the semi-analytical method. The yielding stress of the face plates of all the nine sandwich panels is 355 MPa. The dimensions of them are listed in Table 3.1. The results are plotted in Figure 3.5 along with the results obtained by hinge line theory. The surface is the results obtained by hinge line theory and the dots are the results calculated by semi-analytical method.

Panel Number	t_f (mm)	t_c (mm)	a (mm)	b (mm)
1	3	30	1800	1200
2	3	45	1800	1200
3	3	60	1800	1200
4	5	30	1800	1200
5	5	45	1800	1200
6	5	60	1800	1200
7	7	30	1800	1200
8	7	45	1800	1200
9	7	60	1800	1200

Table 3.1 The dimensions of nine sandwich panels.

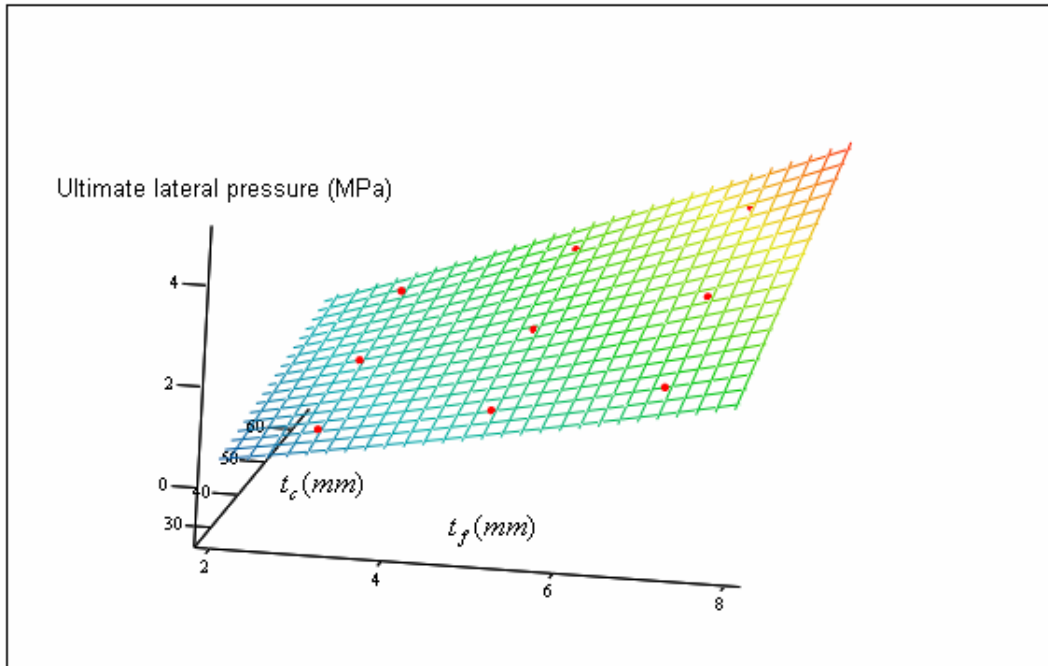


Figure 3.5 Ultimate strength calculated by hinge line theory and semi-analytical method

Panel Number	1	2	3	4	5	6	7	8	9
p_{HL}	0.837	1.217	1.597	1.479	2.113	2.747	2.189	3.077	3.964
p_{SM}	0.9	1.3	1.7	1.52	2.15	2.76	2.22	3.04	3.85
e	0.07	0.064	0.061	0.027	0.017	0.004	0.014	-0.012	-0.03

Table 3.2 Comparison of results of semi-analytical method and hinge line theory

The results of the nine sandwich panels are listed in Table 3.2. The normalized difference e between the results of the two methods is also listed, where p_{HL} is the lateral pressure which causes the collapse of a panel calculated by hinge line theory, p_{SM} is the lateral pressure which causes the collapse of a panel calculated by the semi-analytical method, and e is $\frac{p_{SM} - p_{HL}}{p_{SM}}$.

As can be seen from Figure 3.5 and Table 3.2, the difference of the results between these two methods is quite small.

The results of the semi-analytical method are reasonable. However, it requires an excessive amount of computation as shown in Section 3.5.2. Since the original purpose of this research is to obtain a fast and easy way for designers to calculate the ultimate strength of sandwich panels, the semi-analytical method was not pursued any further. In Chapter 4 the results of this method will be compared with those of the finite element method.

Chapter 4

Nonlinear Finite Element Analysis

This chapter explains the finite element modeling that was used to obtain all of the results. Nonlinear finite element analysis is a complex process which can give erroneous results if not done properly. Therefore it is very important to validate the modeling and analysis techniques, and in this chapter the full-scale experimental results of Little (2007) are used to provide such validation.

4.1 Finite Element Modeling of the Experimental Panels

The properties of the experimental panels were given in Section 2.2.1. This section gives the properties of the finite element model. As shown in Figure 4.1, the element used for both the face plates and the core is the ANSYS SOLID45 element, which has six faces and eight corner nodes, with three degrees of freedom at each node: translations in the element x , y and z directions. The element has plasticity, creep, swelling, stress stiffening, large deflection, and large strain capabilities.

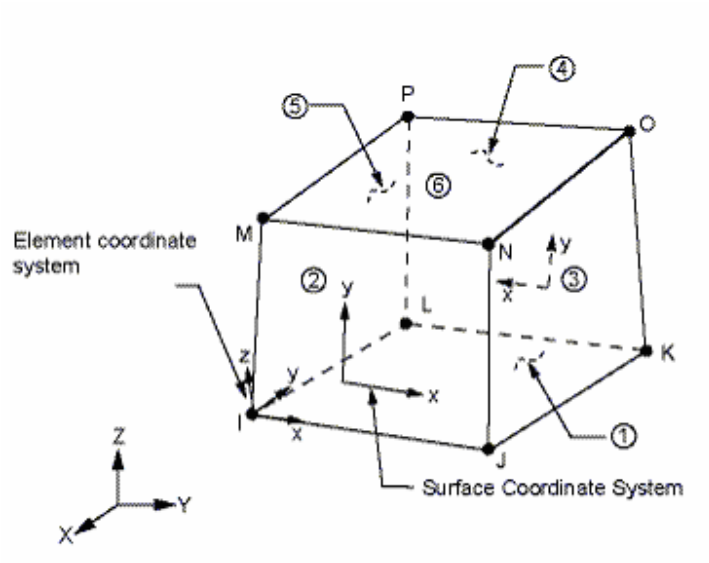


Figure 4.1 Finite element type: SOLID 45

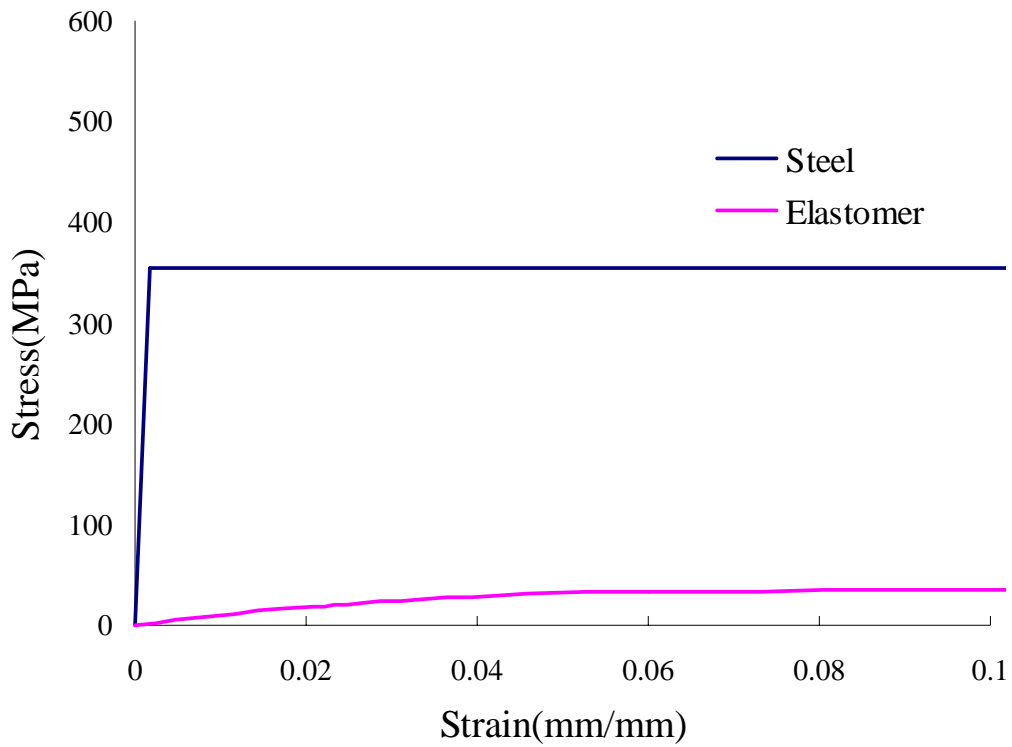


Figure 4.2 Stress versus strain curves for steel and elastomer

Figure 4.2 shows the stress versus strain curves. As shown there, an elastic-perfectly plastic constitutive model is used for the steel. The curve of the elastomer is far below that of steel, and so the two steel face plates bear most of the in-plane load.

4.1.1 Number of Elements

Figure 4.3 is the overview of the finite element model. Figure 4.4 is the profile of the finite element mesh. It shows there are two elements for a steel face plate and four elements for the elastomer core in the direction of thickness.

Each steel face plate (2 layers): $75 \times 50 \times 2 = 7,500$

Elastomer core (4 layers): $75 \times 50 \times 4 = 15,000$

Total element number: 30,000

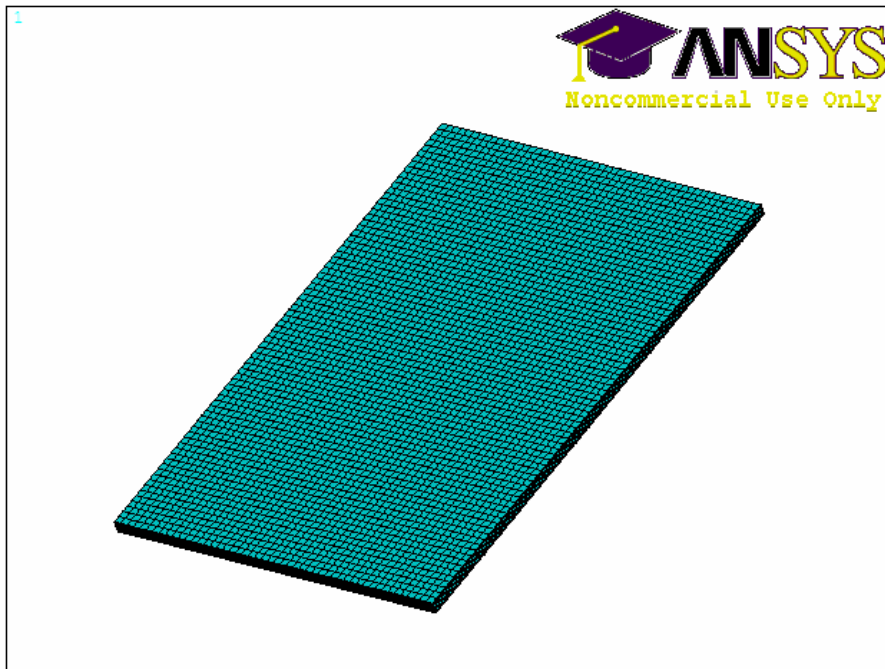


Figure 4.3 Finite element model



Figure 4.4 Profile of the sandwich panel element mesh

4.1.2 Boundary Conditions

This project deals with panels that are perfectly clamped at all four edges because in Little’s experiments the edges were clamped. The detailed boundary conditions in the ANSYS finite element model are listed in Table 4.1. (Note: coupled means an edge is free to move with all the nodes along it having the same displacement).

	Translation			Rotation about <i>x</i> , <i>y</i> , and <i>z</i> direction
	<i>x</i> -direction	<i>y</i> -direction	<i>z</i> -direction	
Left edge	Coupled	Restrained	Restrained	Restrained
Right edge	Restrained	Restrained	Restrained	Restrained
Top edge	Free	Coupled	Restrained	Restrained
Bottom edge	Free	Restrained	Restrained	Restrained

Table 4.1 Boundary conditions of the FEA model

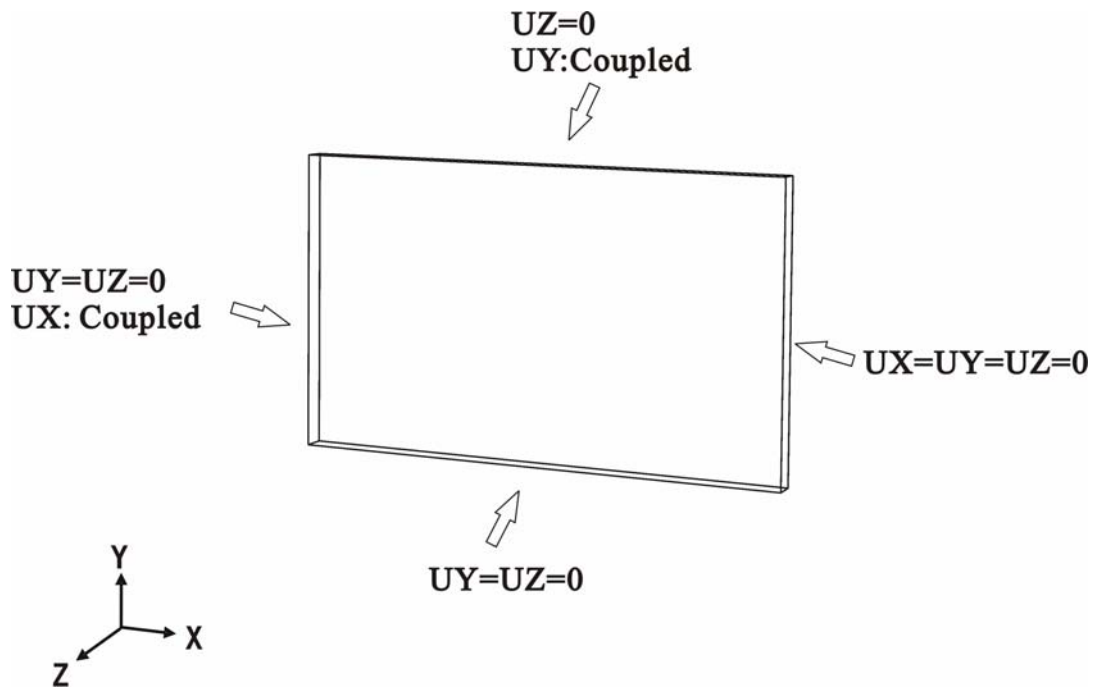


Figure 4.5 Boundary conditions of the FEA model

4.1.3 Loads

The total load is divided into two load steps. The first load step is the application of the uniform lateral pressure. The second load step is the application of a forced in-plane translation in the x -direction in order to generate the in-plane load.

4.2 Results and Comparison with Experiments

4.2.1 Definition of Failure under In-plane Compression as 0.5% Strain

When a steel plate is subjected to an increasingly large in-plane compression load, and if plate buckling is prevented, then the plate will continue to undergo in-plane deformation (shortening) indefinitely, as long as the load is further increased. As shown in Figure 4.6, the shape of the load vs. in-plane deformation curve may or may not have a peak, depending on the amount of lateral pressure. It is necessary to have some consistent definition of the “failure load”, and Little (2007) adopted the definition given in ASTM A370-05, *Standard Test Methods and Definitions for Mechanical Testing of Steel Products*, in which “failure” is defined as reaching a specified level of in-plane deflection (shortening), and the recommended level is 0.5% of the total length. In Figure 4.6 the in-plane load is non-dimensionalized by the yield stress σ_y of the steel face plates and then plotted versus deflection in the x -direction. For the experimental sandwich panel, with length 1800mm, 0.5% deflection in the x -direction is 9mm. Therefore a vertical line is plotted at 9mm. The intersection of this line with the curve of non-dimensionalized in-plane load gives the failure load for the panel.

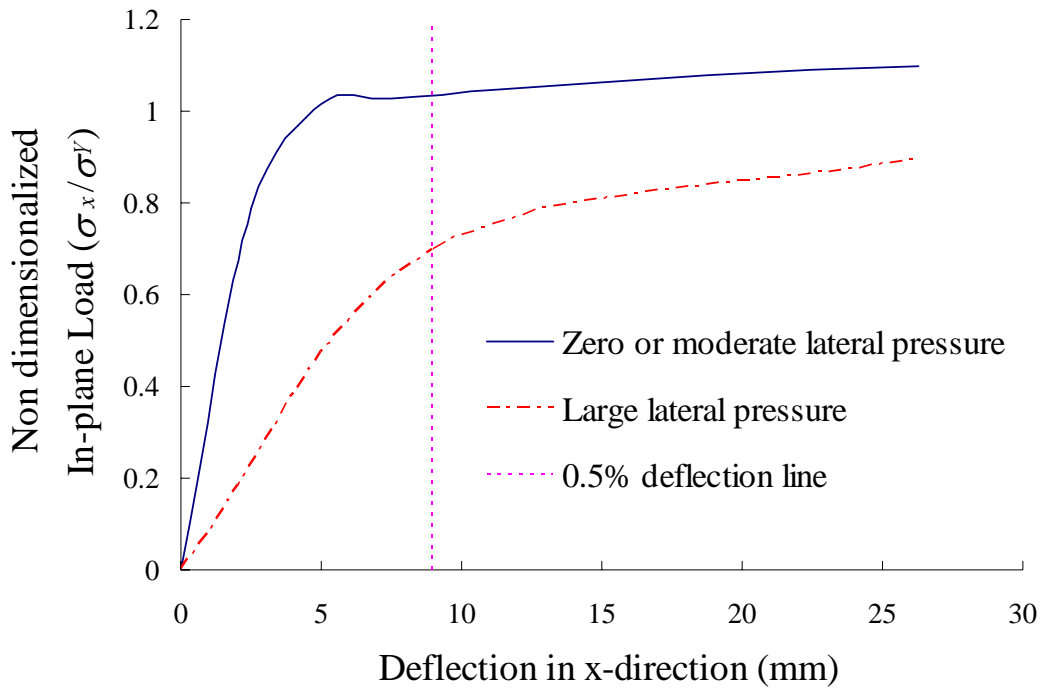


Figure 4.6 0.5% strain method

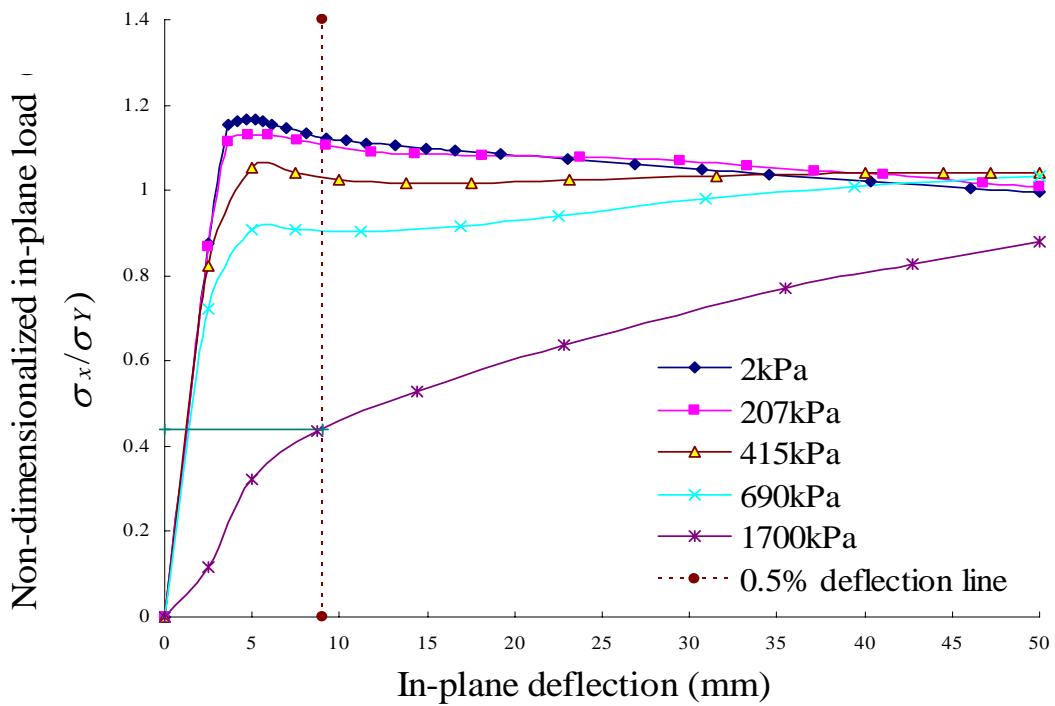


Figure 4.7 Non-dimensionalized in-plane load versus in-plane deflection

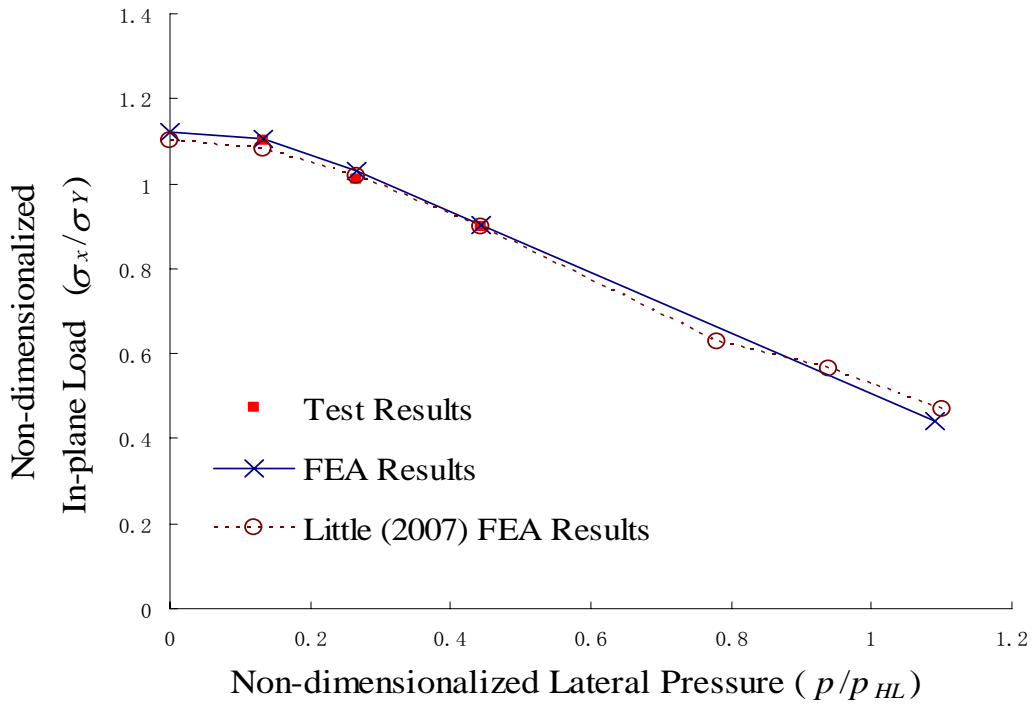


Figure 4.8 Comparison of FEA and test results

Figure 4.7 shows the five curves of non-dimensionalized in-plane load versus in-plane deflection obtained by the current finite element model for five different load cases. The figure shows that with an increase of initial lateral pressure, the average level of in-plane load decreases. The curve with lateral pressure 1700kPa always goes up, from the beginning to the end. The other four curves become flat around 9mm of in-plane deflection. With further increase of the in-plane deflection, the curves all converge to the “squash load” ($\sigma = \sigma_y$) because the modulus of the elastomer has become almost zero.

Based on the 0.5% strain criterion for failure, five failure points are read from the intersection points (e.g. 0.44 is read from the intersection point of the curve of 1700 kPa pressure and the 0.5% deflection line). The resulting interaction curve is plotted with a solid line in Figure 4.8. Little’s experimental and FEA results are also shown. Here the in-plane load is still non-dimensionalized by σ_y and the lateral pressure is non-dimensionalized by the pressure p_{HL} which is obtained by hinge line theory. The agreement is excellent and this verifies that the current finite element model is accurate.

It was noted in Section 2.2.4 that in the experimental results the non-dimensionalized in-plane compression for small lateral pressure is bigger than 1. Figure 4.8 shows that this also happens for both sets of FEA results. The reason for this was given in Section 2.2.4, and in Chapter 6 this small exceedance is removed, such that the collapse stress is equal to the yield stress.

4.2.2 Comparison of Yield Expansion Patterns under Pure Lateral Pressure

Figures 4.9 to 4.12 show expansion of the plastic zone at mid-thickness of the top and bottom face plates from the FEA for pure lateral pressure. As a comparison, Figures 4.13 to 4.16 are the plots of the plastic zone for of the semi-analytical method. Both methods show a similar expansion pattern, as follows:

1. Top face plates

Yield first occurs at the mid-length of the four edges. As pressure increases, the plastic zone spreads inward towards the center of the plate, and also sideways towards the corners. When the ultimate strength is reached, almost all the plate has yielded except for a small area at the center and the four corners.

2. Bottom face plates

Yield first occurs not only from the mid-length of the four edges, but also at the center. As pressure increases, both plastic zones become larger. The edge zone spreads inwards towards the center, and the center zone spreads outwards. When ultimate strength is reached, nearly all of the plate has yielded except for a narrow ring.

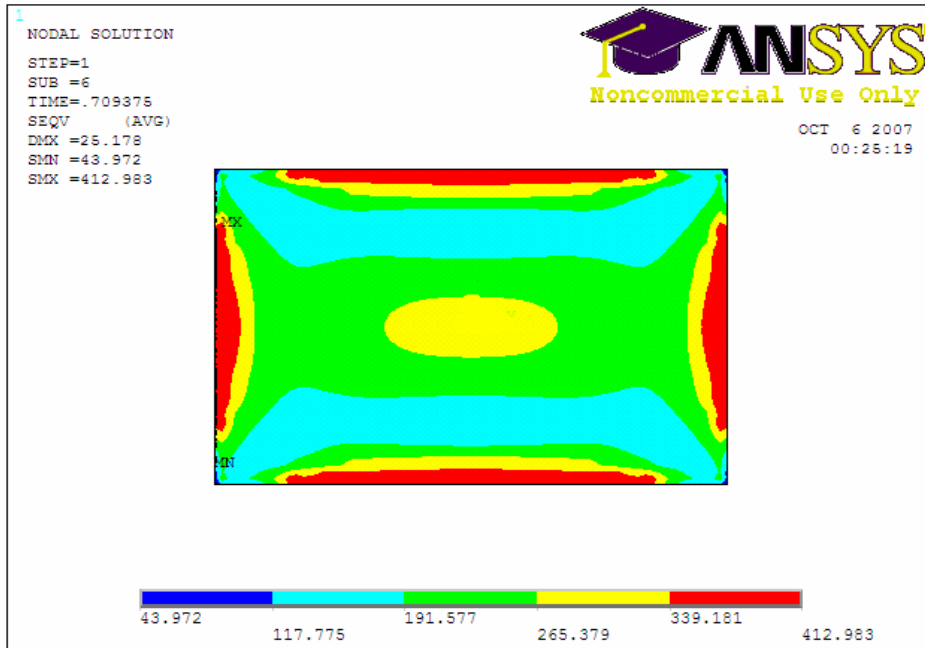


Figure 4.9 First occurrence of yield at mid-thickness of the top face plate

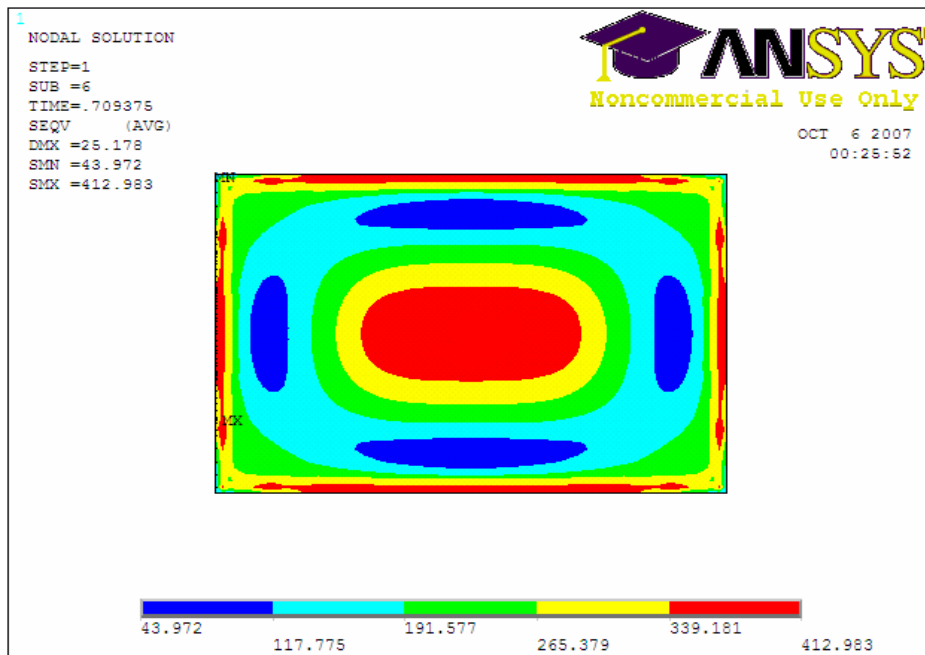


Figure 4.10 First occurrence of yield at mid-thickness of the bottom face plate

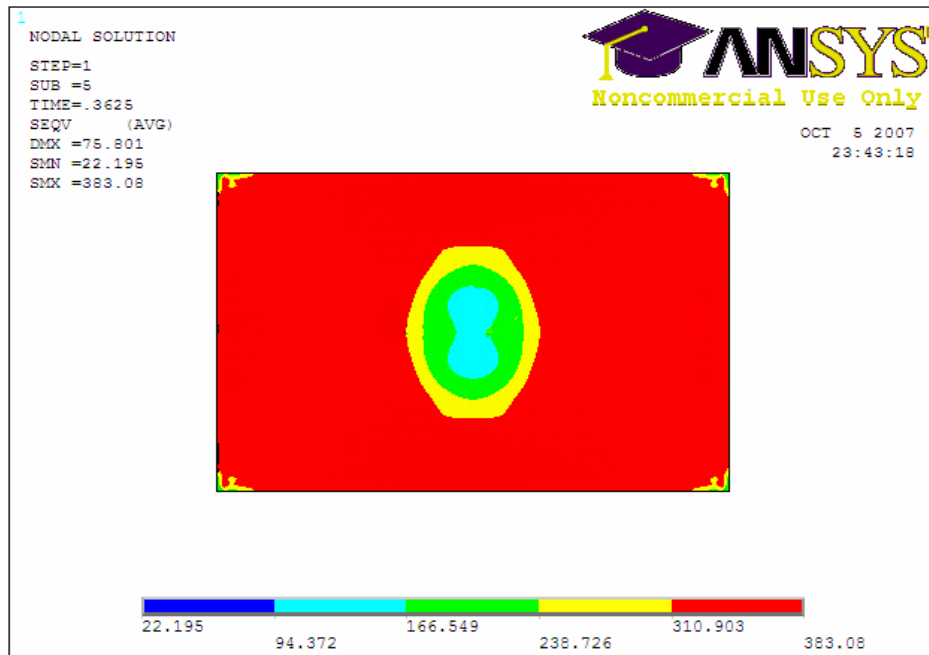


Figure 4.11 Yield pattern almost at failure at mid-thickness of the top face plate

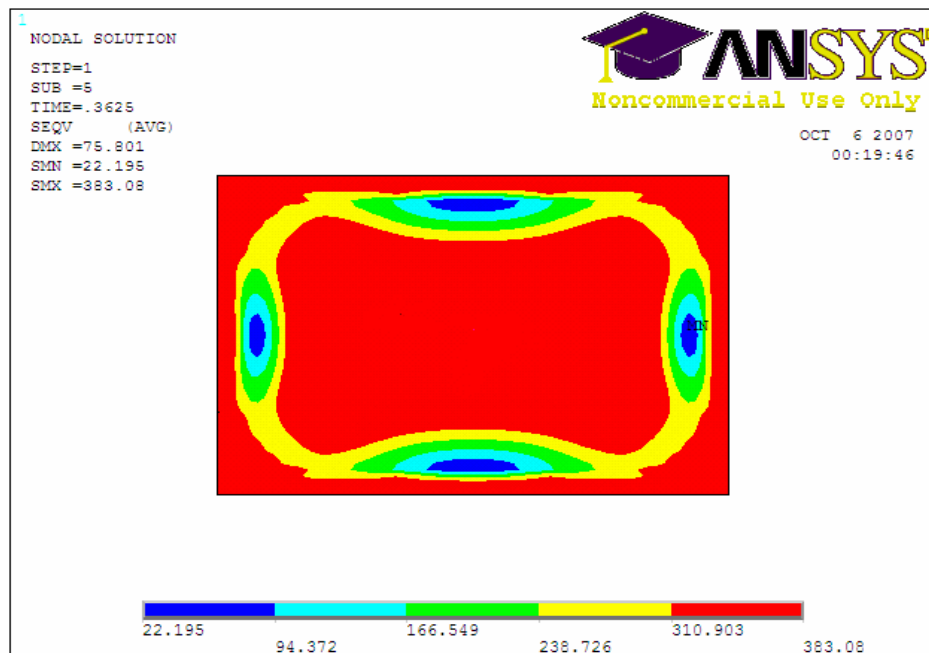


Figure 4.12 Yield pattern almost at failure at mid-thickness of the bottom face plate

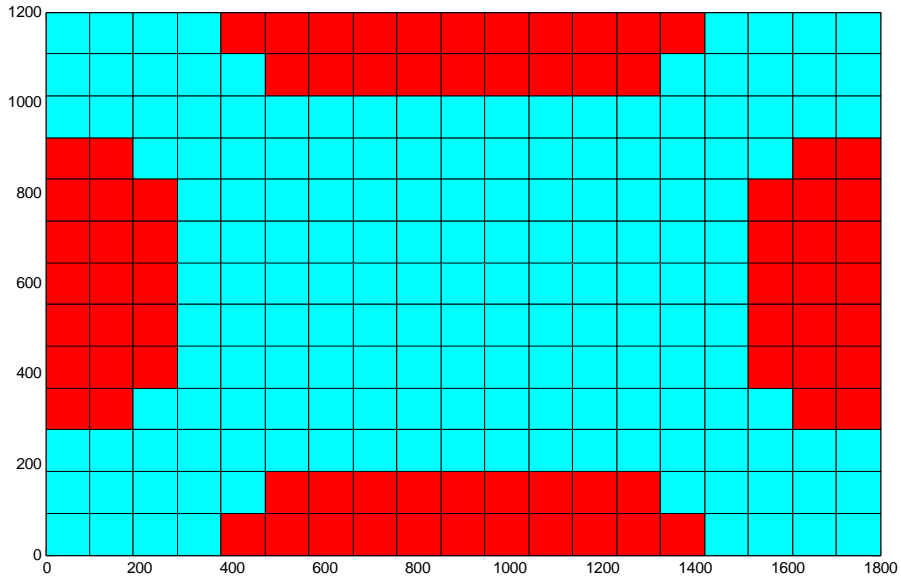


Figure 4.13 First occurrence of yield at mid-thickness of the top face plate
(Semi-analytical method)

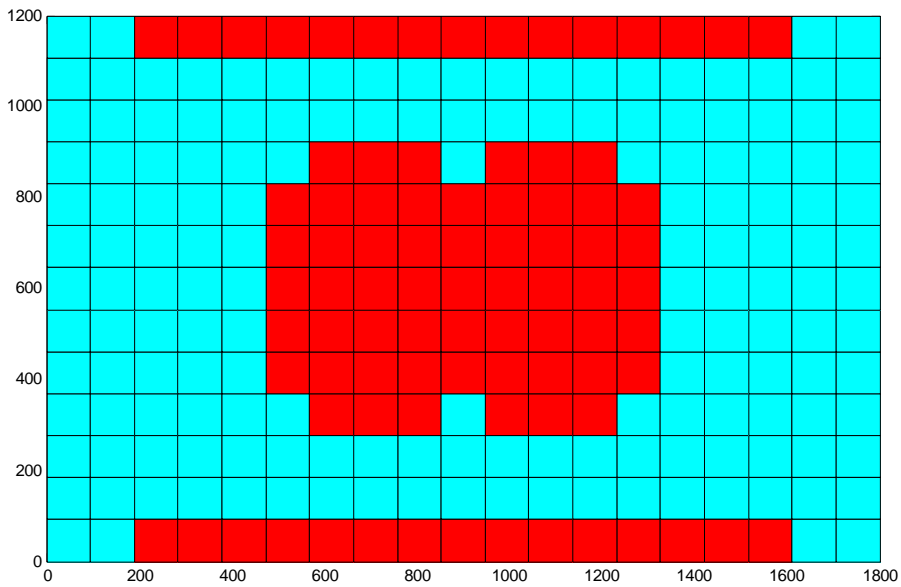


Figure 4.14 First occurrence of yield at mid-thickness of the bottom face plate
(Semi-analytical method)

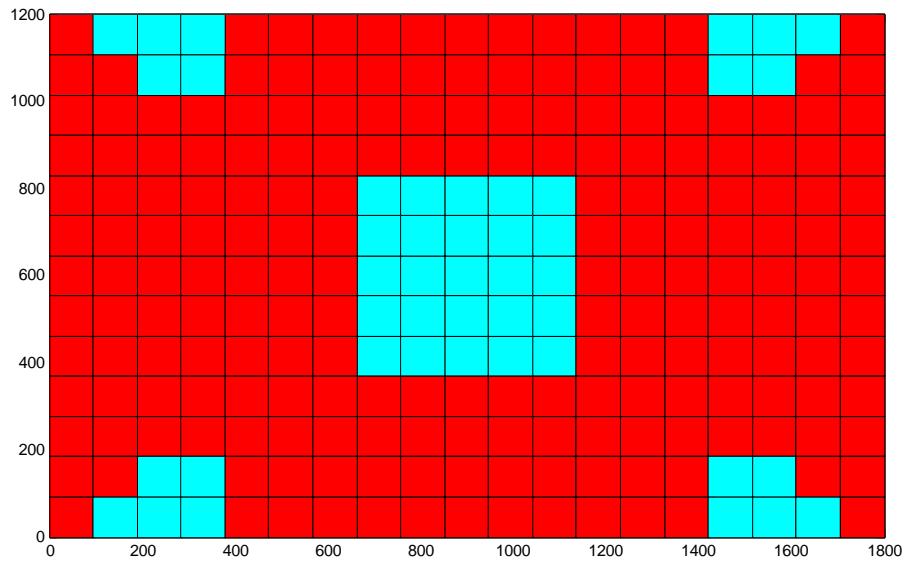


Figure 4.15 Yield pattern almost at failure at mid-thickness of the top face plate
(Semi-analytical method)

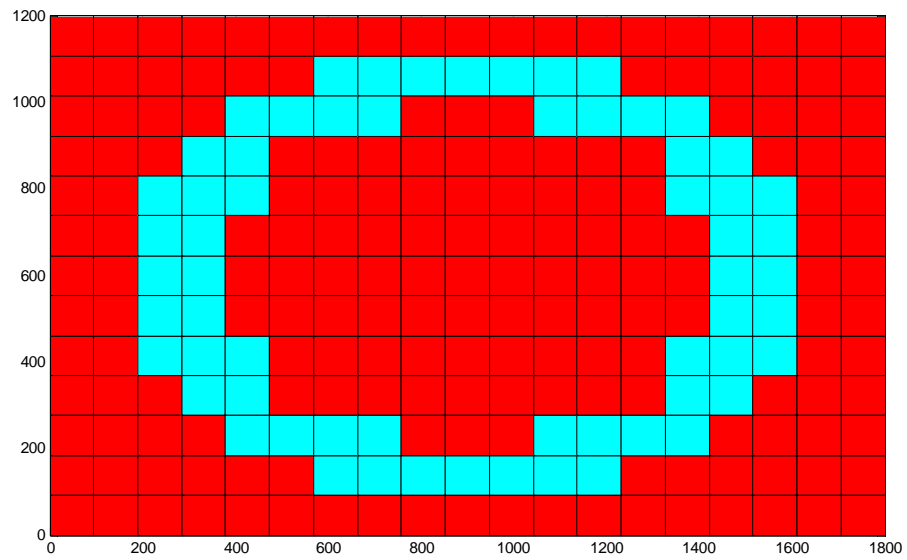


Figure 4.16 Yield pattern almost at failure at mid-thickness of the bottom face plate
(Semi-analytical method)

4.3 Definition of Failure under Pure Lateral Pressure

Figure 4.17 is a curve of non-dimensionalized lateral pressure versus lateral deflection. It shows that deflection always increases when lateral pressure becomes bigger. However, in order to plot an entire interaction curve, the failure load of pure lateral pressure without in-plane load must be obtained.

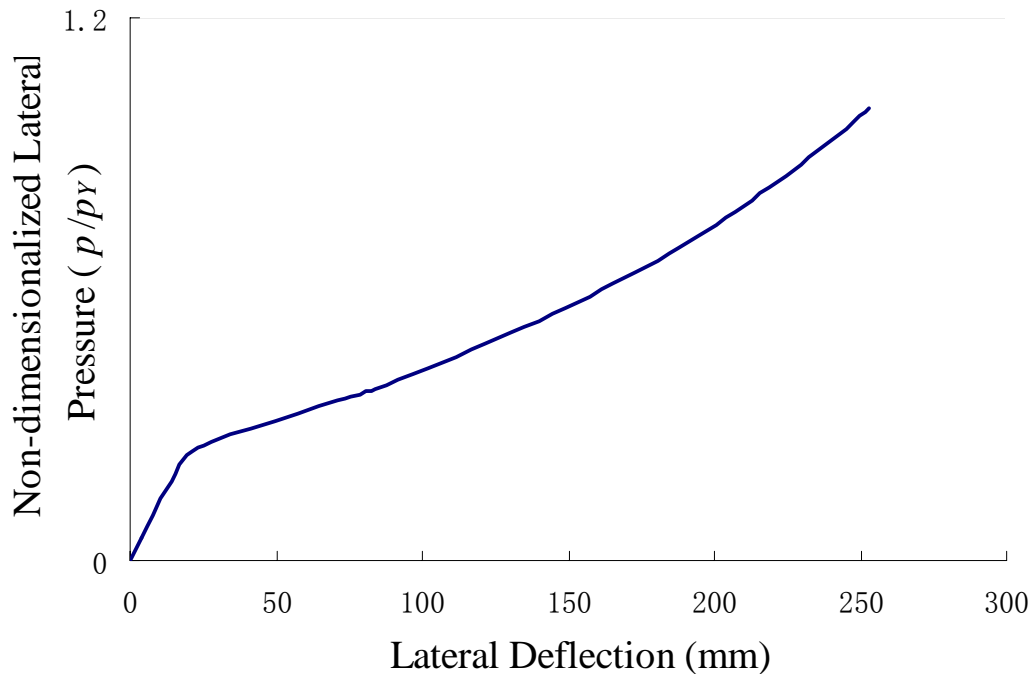


Figure 4.17 Non-dimensionalized lateral pressure versus lateral deflection

When there is in-plane compression, failure is defined as 0.5% strain based on the length of the panel. This definition cannot be used for pure lateral pressure because the dominant deformation is out-of-plane, and the in-plane deformation increases more slowly than with in-plane compression load. Therefore we must obtain a new and larger value of strain that corresponds to failure. Figure 4.18 is a plot of the plastic strain for the

same panel (i.e. Little’s experimental panel, which is considered throughout this chapter) after it has collapsed. That is, the pressure is even larger and the yielding is even more extensive than in Figures 4.11 and 4.12. Unlike yield stress, which is a constant value and extends over a large area, the maximum value of plastic strain is always concentrated at the clamped edges, where the “plastic hinges” have formed. Figure 4.18 shows that in this failure condition the largest plastic strain is about 0.16 (tensile in the face plate adjacent to the pressure and compressive in the other face plate). To be slightly conservative, the value chosen in this study is 0.15. That is, for the case of pure lateral pressure, failure of the panel is defined as corresponding to a plastic strain of 0.15, compared to 0.005 (0.5%) when there is some in-plane compression.

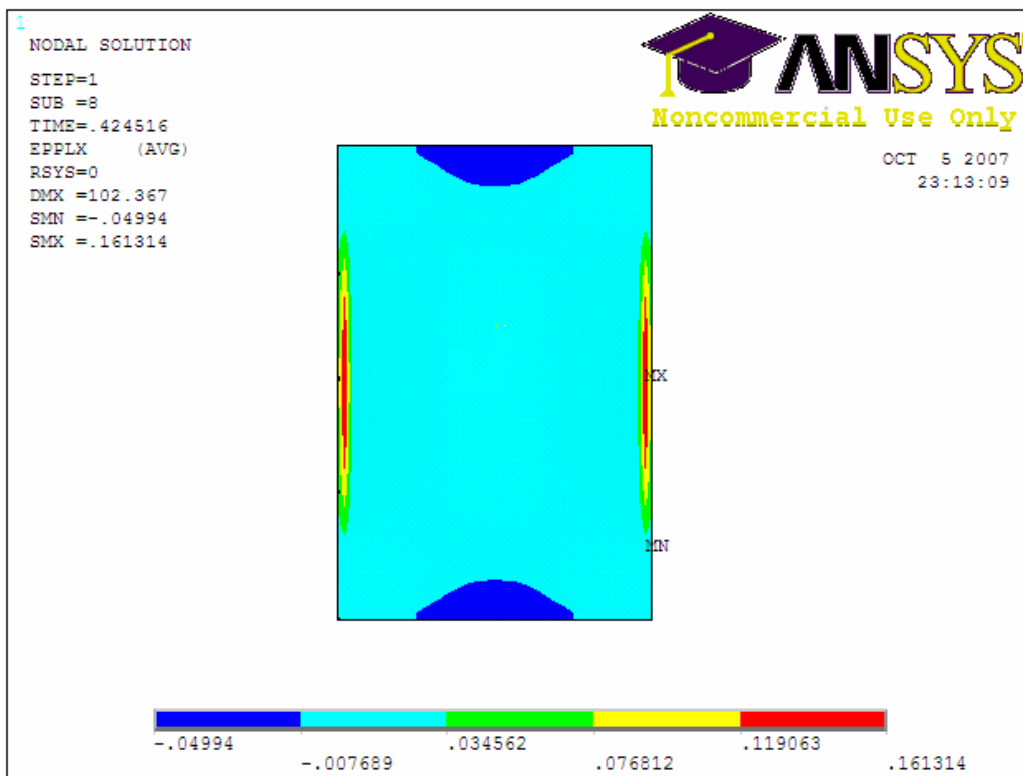


Figure 4.18 Plastic strain distribution on a sandwich panel under later pressure

4.4 Comparison of Ultimate Pressure

For the subject panel (which has the same dimensions as the test panels) the ultimate pressure from the FEA is 1.85 MPa, and from the semi-analytical method is 1.60 MPa. The hinge line pressure is $p_{HL} = 1.56$ MPa. In Figure 4.19 p_{HL} is used to obtain non-dimensional values. For completeness the FEA ultimate strength points are also plotted for the four load combinations involving in-plane compression: the three experimental combinations and the case of pure in-plane compression.

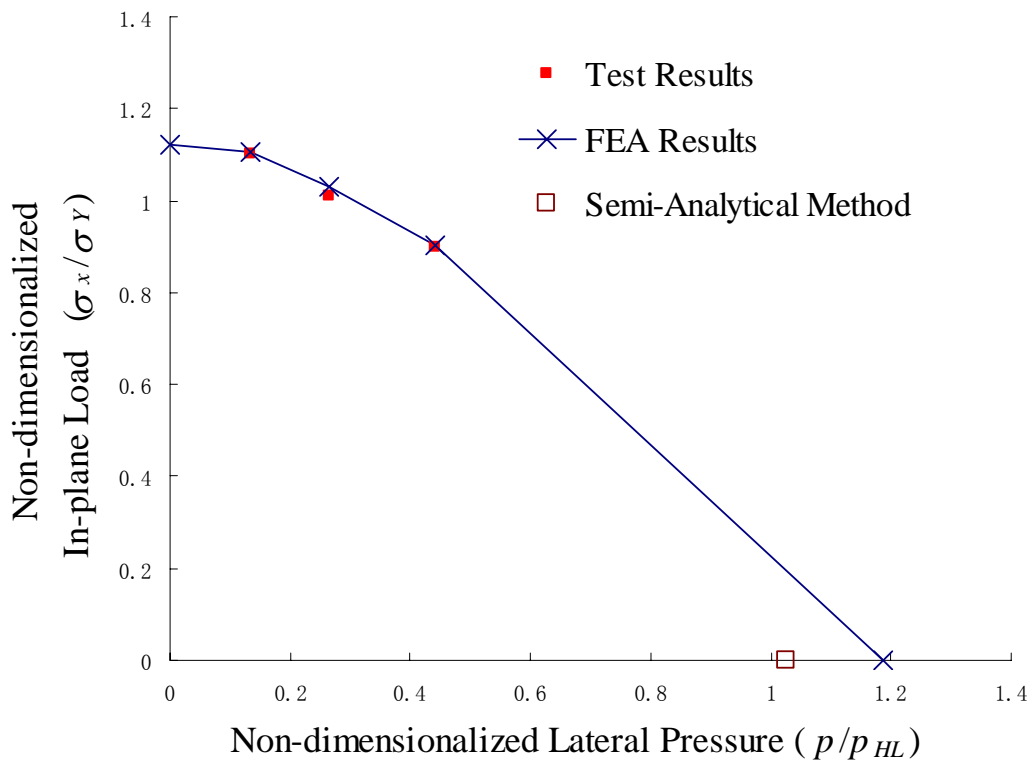


Figure 4.19 FEA interaction curve, including failure load under pure lateral pressure

Chapter 5

Correction Factor

5.1 Introduction; Overall Method

Figure 5.1 is an interaction diagram, in which the curve shows all the possible combinations of the two types of load that would interact and cause collapse of the panel. The axes are the “ultimate strength ratios”, R_σ and R_p . The numerator of each is the actual load σ_x and p , and the denominator is the collapse load if that load acted alone, denoted as $(\sigma_x)_{ult}$ and p_{ult} . For each type of load there will be a theory that ideally provides an explicit expression for the “act alone” collapse load as a function of the panel properties (α , t_c and t_f).

If this theory is correct, then for each type of load acting alone, panel collapse would correspond to the point 1 along that axis.

The goal of this study is to obtain an explicit expression for the interactive collapse of the panel as a function of its properties. This involves three separate tasks. Two of them are to obtain explicit expressions for $(\sigma_x)_{ult}$ and p_{ult} as a function of the panel properties. These will provide the denominators of the ultimate strength ratios R_σ and R_p .

The third task is to obtain an explicit expression for the interactive collapse equation $F(R_\sigma, R_p) = 1$.

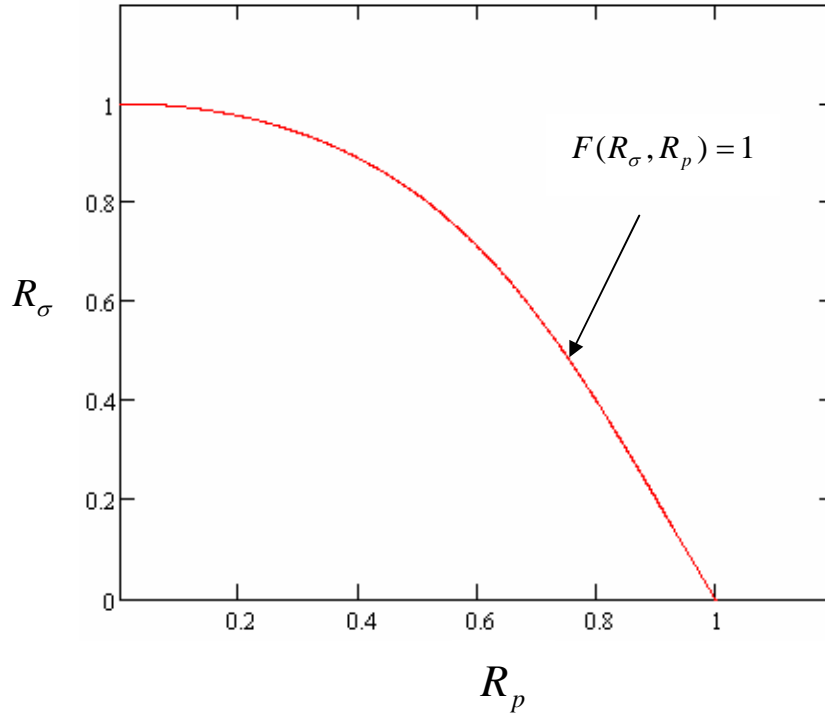


Figure 5.1 Interaction Diagram

5.1.1 Determination of $(\sigma_x)_{ult}$

The experiments of Little (2007) and the Kim and Hughes (2005) study have shown that for typical panel proportions the ultimate strength under pure in-plane compression is equal to the “squash load”: $(\sigma_x)_{ult} = \sigma_Y$. That is, the panel has such large bending rigidity that it does not buckle.

5.1.2 Determination of p_{ult}

For ordinary steel panels loaded by lateral pressure, the hinge line equation (2.9) gives a reasonably good estimate of p_{ult} . Since the face plates are steel, it is possible that the hinge line theory might give at least an approximate estimate for p_{ult} for a steel-elastomer sandwich panel. Indeed, as shown in Chapter 3, Little (2007) calculated $p_{ult,HL}$ using this theory, but in his tests the pressures were much smaller and he did not investigate the case of collapse due to pure pressure.

The next section shows that the hinge line equation is not accurate enough, and considers how it can be adapted.

5.2 Properties of FEA Models

In Chapter 4, results obtained by ANSYS were presented and compared with experimental results. The comparison shows that the finite element model successfully simulated the experiment. The next step is to calculate more cases which have different dimensions and various combinations of loads.

1. Dimensions

There are four variables in a sandwich panel:

Length a (in the x -direction, which is also the direction of the applied in-plane compressive stress σ_x)

Width b (in the y -direction)

Core thickness t_c

Face plate thickness t_f

The aspect ratio of a panel is $\alpha = a/b$, which can be any value (long or short panels). In order to cover a variety of aspect ratios, the width b is fixed to 1200 mm,

and four values of length are used: 600 mm, 1200 mm, 1800 mm, and 3600 mm. Corresponding aspect ratios are 0.5, 1, 1.5 and 3.

The in-plane load is always applied in the lengthwise (x) direction.

To have sufficient data for curve fitting, three values are given to both t_c and t_f :

t_c : 30 mm, 45 mm, 60 mm

t_f : 3 mm, 5 mm, 7 mm

With these combinations of aspect ratios and thicknesses, the final number of models to be analyzed is 36 ($4 \times 3 \times 3$).

The length, width, core thickness, face plate thickness and number of finite elements are listed for each model in Table 5.1 below.

Model Number	t_f (mm)	t_c (mm)	a (mm)	b (mm)	No. of Elements
1	3	30	600	1200	11250
2	3	45	600	1200	11250
3	3	60	600	1200	11250
4	5	30	600	1200	11250
5	5	45	600	1200	11250
6	5	60	600	1200	11250
7	7	30	600	1200	11250
8	7	45	600	1200	11250
9	7	60	600	1200	11250
10	3	30	1200	1200	22500
11	3	45	1200	1200	22500
12	3	60	1200	1200	22500
13	5	30	1200	1200	22500
14	5	45	1200	1200	22500
15	5	60	1200	1200	22500

16	7	30	1200	1200	22500
17	7	45	1200	1200	22500
18	7	60	1200	1200	22500
19	3	30	1800	1200	33750
20	3	45	1800	1200	33750
21	3	60	1800	1200	33750
22	5	30	1800	1200	33750
23	5	45	1800	1200	33750
24	5	60	1800	1200	33750
25	7	30	1800	1200	33750
26	7	45	1800	1200	33750
27	7	60	1800	1200	33750
28	3	30	3600	1200	67500
29	3	45	3600	1200	67500
30	3	60	3600	1200	67500
31	5	30	3600	1200	67500
32	5	45	3600	1200	67500
33	5	60	3600	1200	67500
34	7	30	3600	1200	67500
35	7	45	3600	1200	67500
36	7	60	3600	1200	67500

Table 5.1 General properties of 36 FEA models

5.3 Generalizing the Hinge Line Collapse Pressure Equation for a Steel-Elastomer Sandwich Panel

Figure 5.2 is an interaction diagram of the type described in Section 5.1. Based on Section 5.1.1, the value selected for $(\sigma_x)_{ult}$ is simply the yield stress for steel, σ_Y . The denominator of the other ultimate strength ratio is the collapse pressure predicted by hinge line theory, $p_{ult,HL}$. The data points are finite element results for three sandwich panels with $\alpha = 1.5$, $t_f = 5$ mm, three values of t_c (30, 45 and 60 mm) and five combinations of σ_x and p as follows:

1. Zero lateral pressure and compressive stress σ_x .
2. $0.25 p_{ult,HL}$ and compressive stress σ_x .
3. $0.5 p_{ult,HL}$ and compressive stress σ_x .
4. $0.75 p_{ult,HL}$ and compressive stress σ_x .
5. The collapse value of $p_{ult,HL}$ for zero compressive stress σ_x .

The data points have been joined by straight line segments in order to see what shape the final interaction curves need to be.

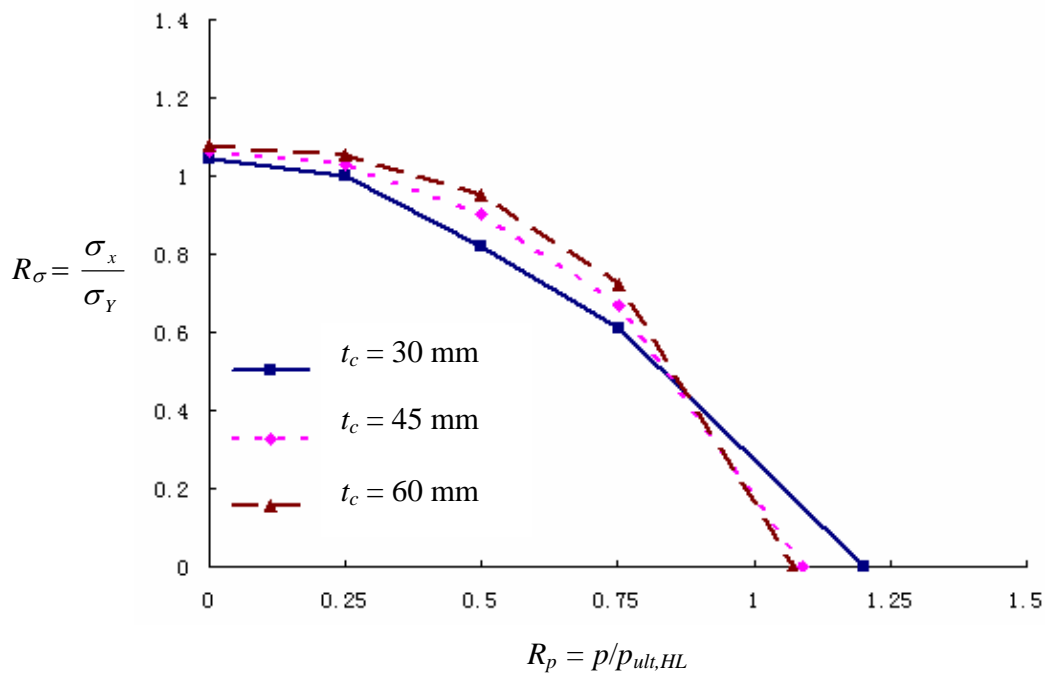


Figure 5.2 FEA Interaction Diagram ($a = 1800$ mm $b = 1200$ mm $t_f = 5$ mm)

In general the curves are similar. At the upper end point (pure in-plane compression), all three coincide at a point slightly above the “squash load” ($\sigma_x / \sigma_Y = 1$). As σ_x decreases and p increases, the curves diverge slightly. Then there is a crossover point where they reverse their relative positions. If the hinge line theory exactly accounted for the effect of t_c , all three curves would end at $p / p_{ult,HL} = 1$. Thus hinge line theory must be generalized to account for t_c , so as to give a common end point and eliminate the crossover. However, the three curves will probably still diverge between the two end points, and the interaction equation will need to be further generalized to account for t_c for the intermediate load combinations.

5.4 Modification of the Hinge Line Collapse Pressure

This section uses curve fitting of the finite element data for the “pure pressure” case to derive a correction factor f which is applied to the hinge line value $p_{ult,HL}$, in order to account for the effect of t_c , t_f and α . The corrected value of collapse pressure will be:

$$p_{ult} = p_{ult,HL} \cdot f(t_c, t_f, \alpha) \quad (5.1)$$

There are 36 values of finite element collapse pressure $p_{ult,FE}$. Table 5.2 gives the ratio $p_{ult,FE} / p_{ult,HL}$ for the 36 cases.

$t_f = 3\text{mm}$	$\alpha = 0.5$	$\alpha = 1$	$\alpha = 1.5$	$\alpha = 3$
30	1.245	1.36	1.34	1.4
45	1.2	1.25	1.22	1.305
60	1.19	1.25	1.23	1.305
$t_f = 5\text{mm}$	$\alpha = 0.5$	$\alpha = 1$	$\alpha = 1.5$	$\alpha = 3$
30	1.185	1.3	1.2	1.27
45	1.08	1.11	1.09	1.155
60	1.035	1.078	1.07	1.125
$t_f = 7\text{mm}$	$\alpha = 0.5$	$\alpha = 1$	$\alpha = 1.5$	$\alpha = 3$
30	1.185	1.32	1.22	1.26
45	1.02	1.128	1.065	1.11
60	0.95	1.04	1.02	1.07

Table 5.2 Ratios of $p_{ult,FE} / p_{ult,HL}$

Since t_c , t_f and α might have different effects on the correction factor, $f(t_c, t_f, \alpha)$ is separated into 2 parts: $g(t_c, t_f)$ and $h(\alpha)$. $g(t_c, t_f)$ depends on t_c , t_f , and $h(\alpha)$ only accounts for the effect of α . Thus:

$$f(t_c, t_f, \alpha) = g(t_c, t_f) h(\alpha) \quad (5.2)$$

In order that the correction factor f will be valid for any system of units, it is necessary to deal with dimensionless values, say \bar{t}_f and \bar{t}_c ($\alpha = a/b$ is already dimensionless). Since the plate width b is the same for all the finite element models (1200 mm), it is logical to choose b as the non-dimensionalizing denominator. However, 1200 mm is too large as a number, and so 1.2 mm has been used instead. Thus

in all the plots that illustrate the curve fitting, the values of \bar{t}_f are $3/1.2 = 2.5$, $5/1.2 = 4.17$, and $7/1.2 = 5.83$, and the values of \bar{t}_c are $30/1.2 = 25$, $45/1.2 = 37.5$, and $60/1.2 = 50$.

5.4.1 The Part of the Correction Factor Accounting for \bar{t}_c and \bar{t}_f :

$g(\bar{t}_f, \bar{t}_c)$

There are many possible choices for the form of $g(\bar{t}_f, \bar{t}_c)$: polynomials, ratios of polynomials, etc. Many forms were tried and eventually a suitable form was found. For constant \bar{t}_c the form for \bar{t}_f is:

$$g = \frac{c_1 \bar{t}_f + c_2 \bar{t}_f^3}{\bar{t}_f^3} \quad (5.3)$$

where c_1 and c_2 are constants to be determined for the three values of \bar{t}_c .

After many attempts, some suitable values of c_1 and c_2 were found and the corresponding g functions are:

$$\bar{t}_c = 25: \quad g_1 = \frac{0.49\bar{t}_f + 1.25\bar{t}_f^3}{\bar{t}_f^3} \quad (5.4)$$

$$\bar{t}_c = 37.5: \quad g_2 = \frac{1.26\bar{t}_f + 1.06\bar{t}_f^3}{\bar{t}_f^3} \quad (5.5)$$

$$\bar{t}_c = 50: \quad g_3 = \frac{2\bar{t}_f + 0.95\bar{t}_f^3}{\bar{t}_f^3} \quad (5.6)$$

These three correction factor functions are plotted with the ratios of FEA results over hinge line theory results $p_{ult,FE} / p_{ult,HL}$, in Figures 5.3 to 5.5, where α_1 , α_2 , α_3 and α_4 correspond to aspect ratios 0.5, 1, 1.5, and 3. It can be seen that the values of $p_{ult,FE} / p_{ult,HL}$ are satisfactorily fit by the three correction factor functions.

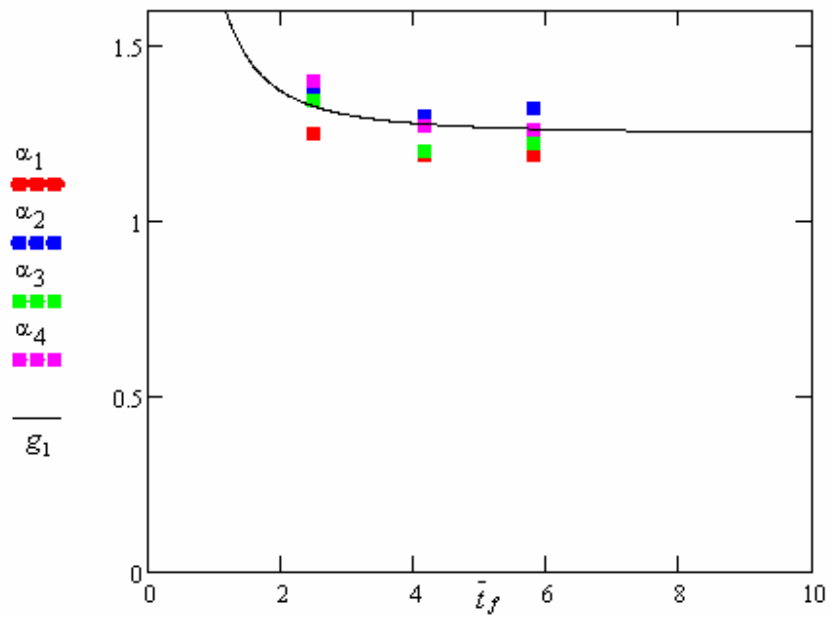


Figure 5.3 g_1 for $\bar{t}_c = 25$

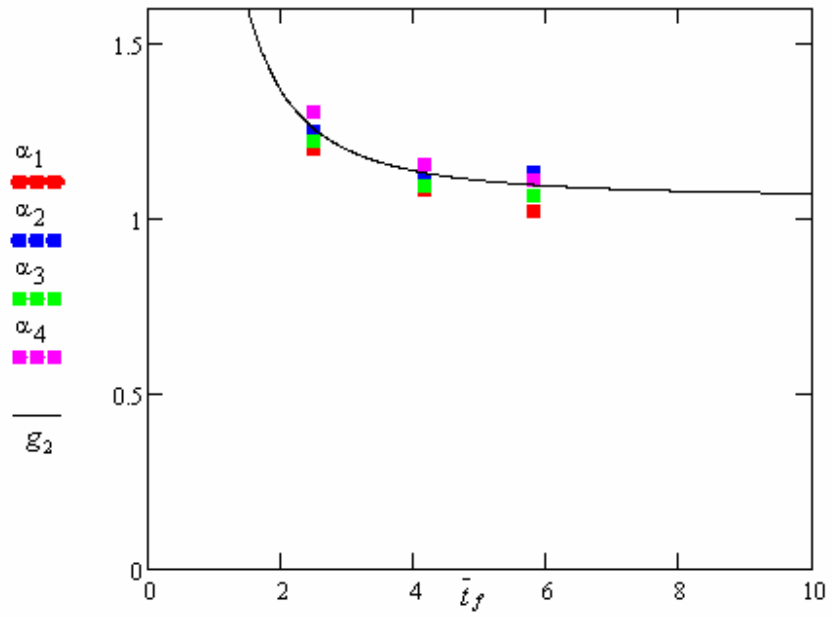


Figure 5.4 g_2 for $\bar{t}_c = 37.5$

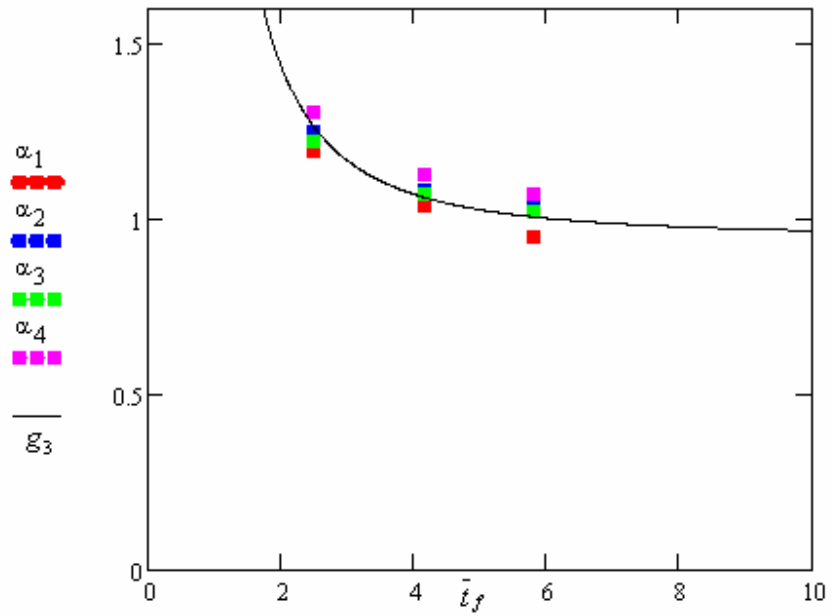


Figure 5.5 g_3 for $\bar{t}_c = 50$

The correction factor function g must allow for the effect of both \bar{t}_f and \bar{t}_c . We have already allowed for \bar{t}_f . Now we have to consider how to place \bar{t}_c into g . In Equations (5.4) to (5.6) the only difference among g_1 , g_2 and g_3 is the values of c_1 and c_2 . The corresponding values are:

$$g_1 (\bar{t}_c = 25): \quad c_1 = 0.49, \quad c_2 = 1.25$$

$$g_2 (\bar{t}_c = 37.5): \quad c_1 = 1.26, \quad c_2 = 1.06$$

$$g_3 (\bar{t}_c = 50): \quad c_1 = 2, \quad c_2 = 0.95$$

The values of c_1 and c_2 are plotted versus \bar{t}_c in Figures 5.6 and 5.7.

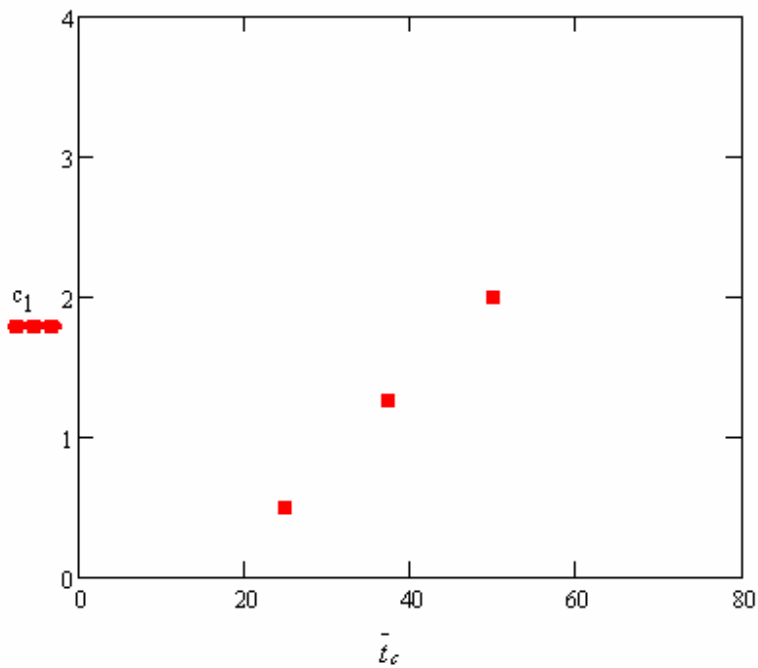
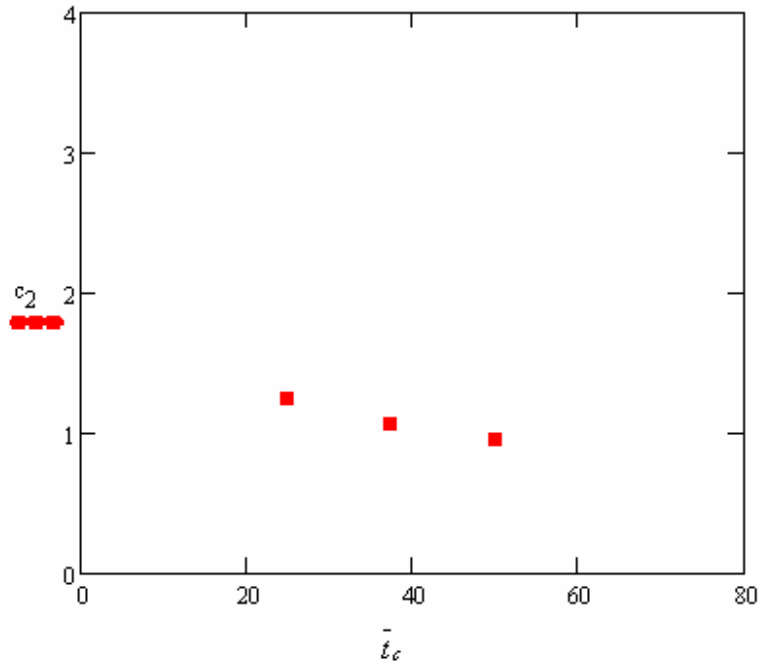


Figure 5.6 c_1 versus \bar{t}_c

Figure 5.7 c_2 versus \bar{t}_c

It can be seen from Figure 5.6 that c_1 could be approximated by a straight line, and c_2 could be fit by a curve which is a ratio of polynomials.

Equation (5.7) is the straight line for c_1 . After trying many different combinations of polynomials, Equation (5.8) was obtained for c_2 .

$$c_1(\bar{t}_c) = (0.06\bar{t}_c - 1) \quad (5.7)$$

$$c_2(\bar{t}_c) = \frac{33.6 + 0.5 \cdot \bar{t}_c}{12 + \bar{t}_c} \quad (5.8)$$

These functions of c_1 and c_2 are plotted with the data points in Figures 5.8 and 5.9, which show that the curve fitting for c_1 and c_2 is satisfactory.

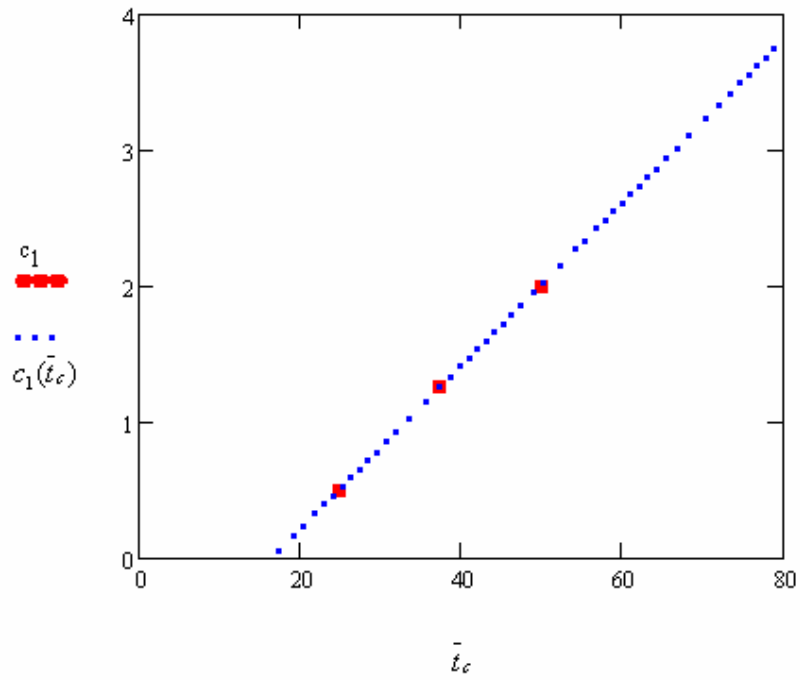


Figure 5.8 c_1 and $c_1(\bar{t}_c)$ versus \bar{t}_c

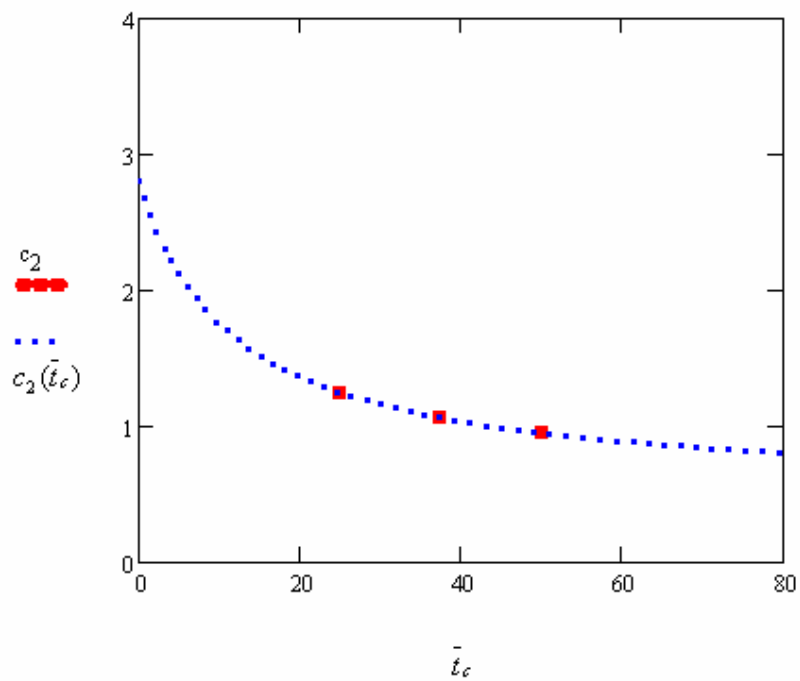


Figure 5.9 c_2 and $c_2(\bar{t}_c)$ versus \bar{t}_c

With Equations (5.7) and (5.8), Equation (5.3) is now a function of both \bar{t}_f and \bar{t}_c :

$$g(\bar{t}_f, \bar{t}_c) = \frac{(0.06\bar{t}_c - 1)\bar{t}_f + \bar{t}_f^3 \frac{33.6 + 0.5 \cdot \bar{t}_c}{12 + \bar{t}_c}}{\bar{t}_f^3} \quad (5.9)$$

Before proceeding to allow for α , we must verify that $g(\bar{t}_f, \bar{t}_c)$ allows for t_c and t_f satisfactorily. For this purpose we define a temporary value of collapse pressure:

$$P_{ult,temp} = P_{ult,HL} \cdot g(\bar{t}_f, \bar{t}_c) \quad (5.10)$$

This value $p_{ult,temp}$ can be used as the denominator to non-dimensionalize the lateral pressure of the FEA results. Figure 5.10 is a plot of the interaction diagram updated by $g(\bar{t}_f, \bar{t}_c)$.

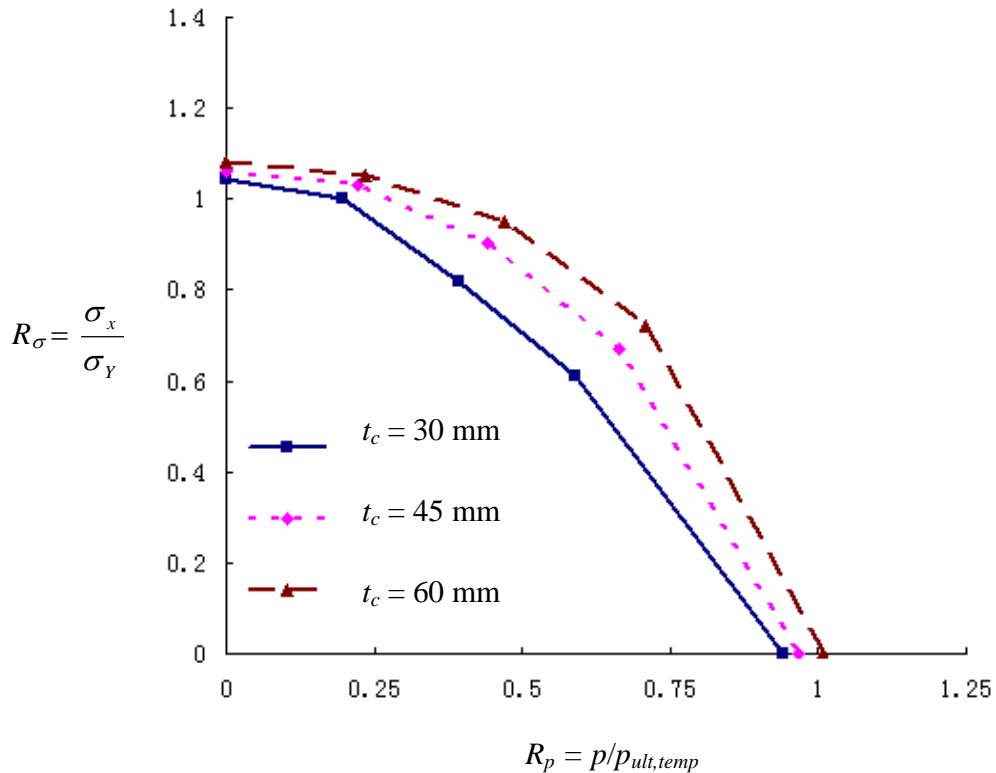


Figure 5.10 FEA Interaction Diagram ($a = 1800$ mm $b = 1200$ mm $t_f = 5$ mm)

In general the curves are similar. For the pure compressive case all three converge to a point slightly above the “squash load” ($\sigma_x / \sigma_y = 1$). As σ_x decreases and p increases, the curves diverge slightly, but the most important point is that the cross-over point in Figure 5.2 is now removed. The curves always keep their relative positions, until they end around $p / p_{ult,temp} = 1$.

The intermediate load combinations were originally located at $R_p = 0.25, 0.5$ and 0.75 . Because the denominator of R_p has been changed from $p_{ult,HL}$ to $p_{ult,temp}$, these load combinations are moved slightly.

In Fig 5.11 the correction factor is plotted along with the ratios of finite element results over hinge line theory results, $p_{ult,FE} / p_{ult,HL}$, in a 3-dimensional plot. The surface with grids is $g(\bar{t}_f, \bar{t}_c)$ and the dots are $p_{ult,FE} / p_{ult,HL}$.

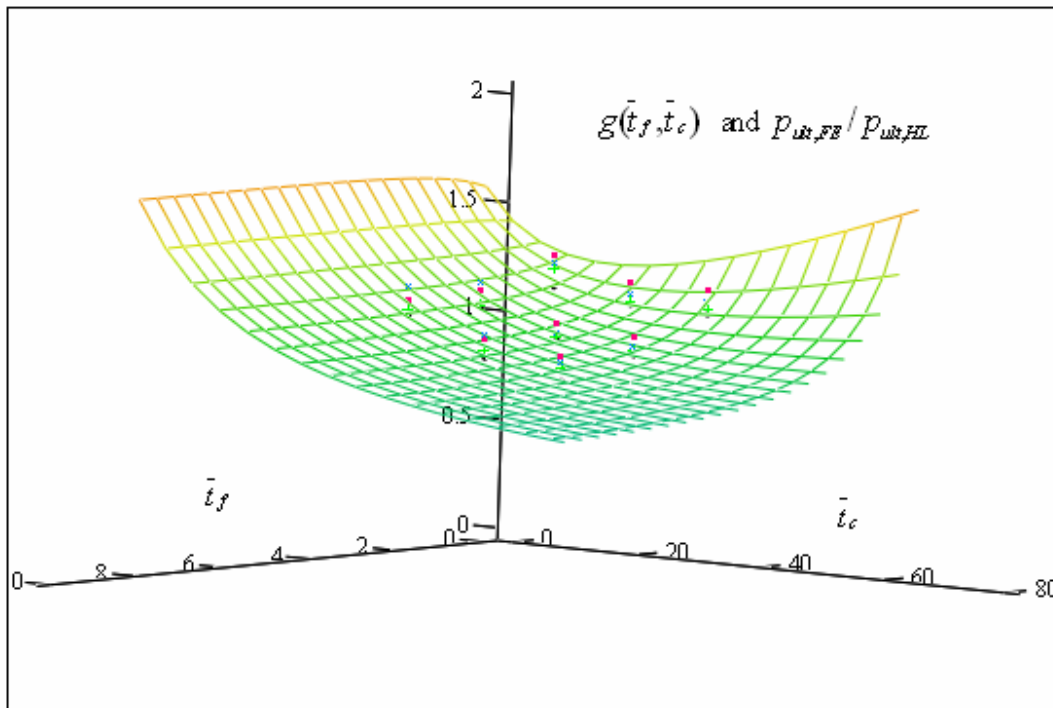


Figure 5.11 $g(\bar{t}_f, \bar{t}_c)$ and $p_{ult,FE} / p_{ult,HL}$ versus \bar{t}_f and \bar{t}_c

As shown in Figure 5.11, $g(\bar{t}_f, \bar{t}_c)$ appears to give a satisfactory fitting for the ratios of FEA results over hinge line theory results, $p_{ult,FE} / p_{ult,HL}$. It will be shown in section 5.5 that the mean error and standard deviation for the complete correction factor f are indeed satisfactory.

5.4.2 The Part of the Correction Factor Accounting for α : $h(\alpha)$

Before starting to deduce $h(\alpha)$, it is necessary to get a first view of how significant the effect of α is on collapse pressure. In Figure 5.12, four interaction curves are plotted for sandwich panels with different values of α . It should be mentioned that the value of R_p has already been updated by $g(\bar{t}_f, \bar{t}_c)$.

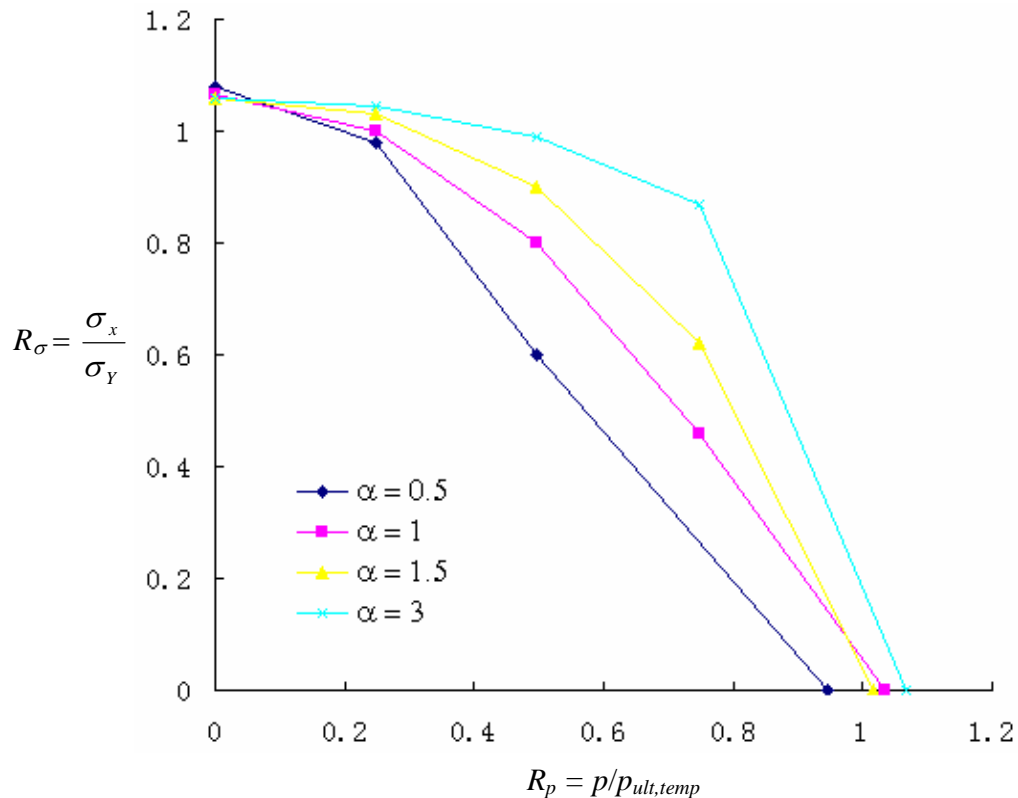


Figure 5.12 FEA Interaction Diagram ($t_f = 7$ mm $t_c = 60$ mm)

As shown in Figure 5.12, the four curves do not intersect with the x -axis at a value of 1. It is very clear that α needs to be included in the correction factor. In order to account for the effect of α , a correction factor function $h(\alpha)$ must be obtained.

The collapse pressures of all the 36 sandwich panels are non-dimensionalized by $p_{ult,temp}$ and divided into four groups p_1 , p_2 , p_3 and p_4 corresponding to different α : 0.5, 1, 1.5 and 3. These are plotted versus α in Figure 5.13.

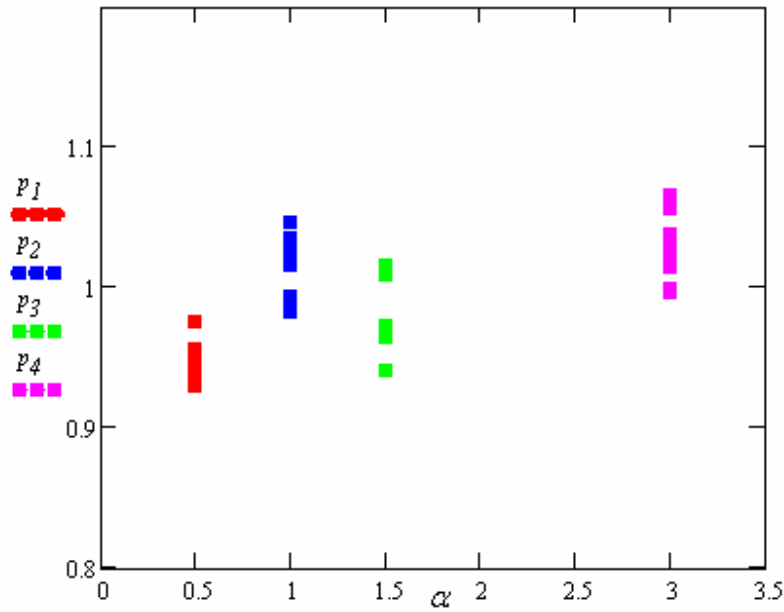


Figure 5.13 $\frac{P_{ult,FE}}{P_{ult,HL} \cdot g(t_c, t_f)}$ versus α

As seen in Figure 5.13, the difference between the four groups of values is perceptible. The values of non-dimensionalized collapse pressure for $\alpha = 0.5$ are relatively small. The values for $\alpha = 3$ are bigger than the others, and the values of $\alpha = 1$ and $\alpha = 1.5$ are in the middle.

Based on the distribution of the data, a hyperbolic tangent function is adopted:

$$h(\alpha) = 0.23 \tanh(1.5\alpha) + 0.8 \quad (5.11)$$

In Figure 5.14 the above fitting function is plotted along with the data points.

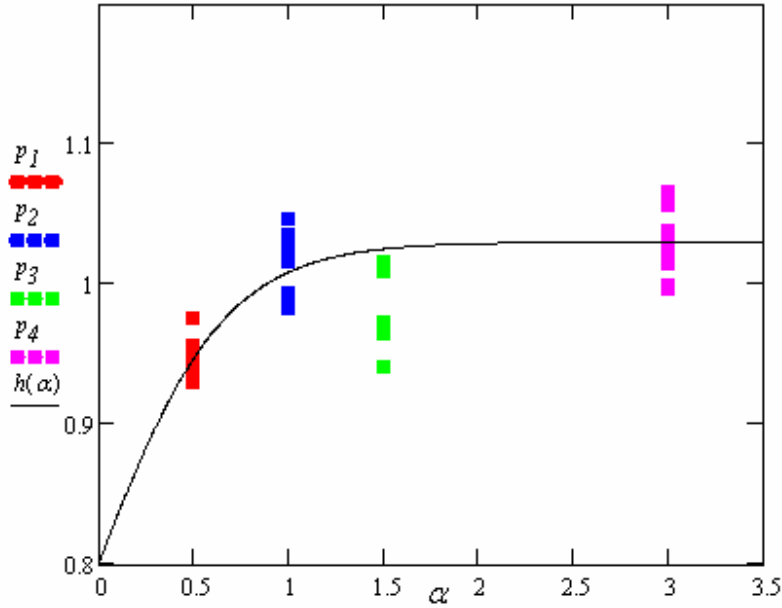


Figure 5.14 $\frac{P_{ult,FE}}{P_{ult,HL} \cdot g(\bar{t}_c, \bar{t}_f)}$ and $h(\alpha)$ versus α

As shown in Figure 5.14, the values for $\alpha = 1.5$ are below the fitting function, but overall the function gives a satisfactory fit.

Since function $h(\alpha)$ has now been obtained, the complete correction factor is:

$$f(\bar{t}_c, \bar{t}_f, \alpha) = g(\bar{t}_f, \bar{t}_c) \cdot h(\alpha) = \left[\frac{(0.06\bar{t}_c - 1)\bar{t}_f + \bar{t}_f^3 \frac{33.6 + 0.5 \cdot \bar{t}_c}{12 + \bar{t}_c}}{\bar{t}_f^3} \right] \times [0.23 \tanh(1.5\alpha) + 0.8] \quad (5.12)$$

With the combination of Equation (2.9) and Equation (5.12), the collapse lateral pressure load p_{ult} in Equation (5.1) is now a product of three terms:

$$p_{ult} = p_{HL} \times \left[\frac{(0.06\bar{t}_c - 1)\bar{t}_f + \bar{t}_f^3 \frac{33.6 + 0.5 \cdot \bar{t}_c}{12 + \bar{t}_c}}{\bar{t}_f^3} \right] \times [0.23 \tanh(1.5\alpha) + 0.8] \quad (5.13)$$

5.5 Verification of the Correction Factor

To verify the correction factor, the relative errors $e = \frac{P_{ult,FE} - P_{ult}}{P_{ult,FE}}$ are calculated.

Since there are 36 analyzed sandwich panels, the number of values of e is also 36. The value range of e is divided into 13 bands. Within each band the number of errors is divided by the total number and plotted in Figure 5.15.

It can be seen from Figure 5.15 that the mean value of all the errors is close to zero and larger error values have low frequency of occurrence. The average value of e is -0.007, and the standard deviation is 0.03. These statistical results confirm that the correction factor gives an ultimate pressure which agrees well with the FEA results.

We can now use the correction factor to modify the original hinge line theory. The corrected values of p_{ult} in Equation (5.13) are used as the reference values to non-dimensionalize the lateral pressure, and Figure 5.12 is replotted in Figure 5.16. It can be seen that now all four curves intersect the R_p axis close to 1.

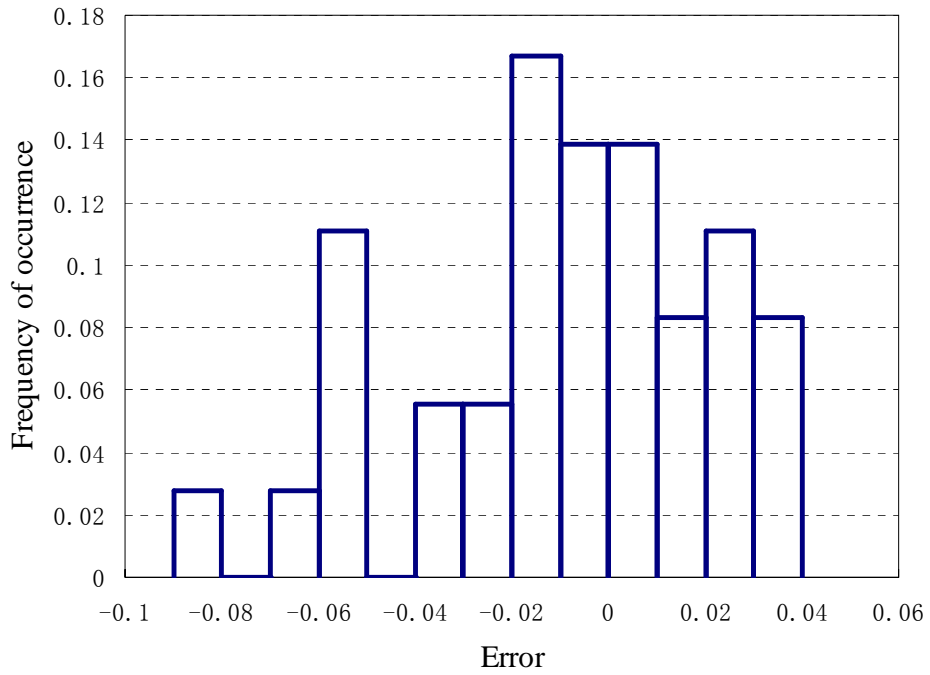


Figure 5.15 Distribution of the error of the correction factor

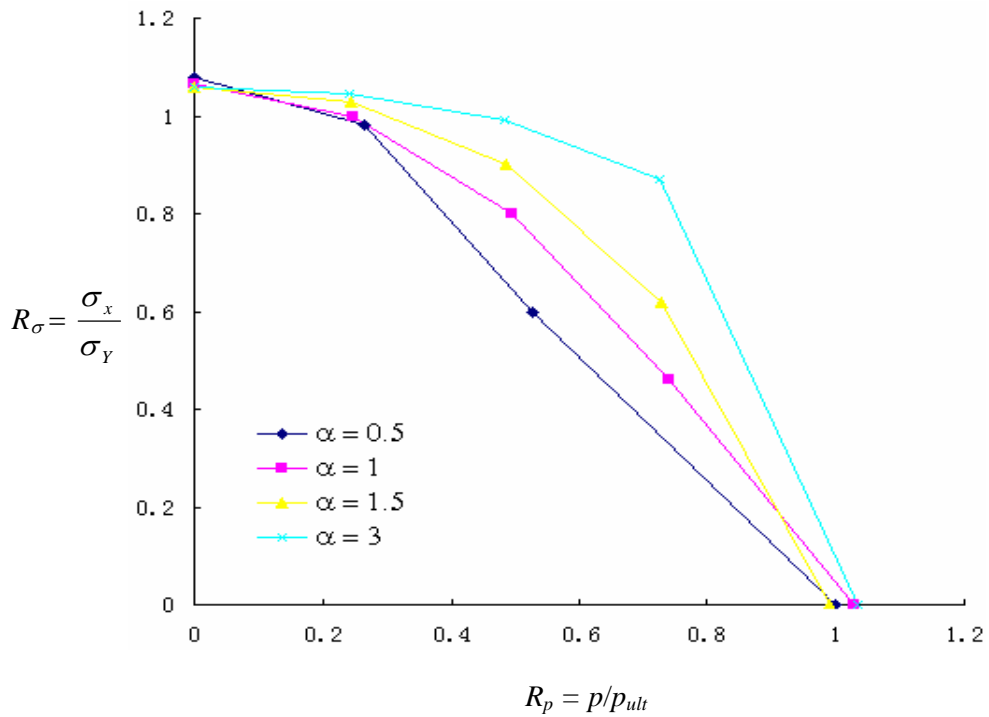


Figure 5.16 Updated FEA Interaction Diagram ($t_f = 7$ mm $t_c = 60$ mm)

Chapter 6

Method for Obtaining an Explicit Equation for the Interactive Collapse of a Steel-Elastomer Sandwich Panel

In Chapter 5, the results of finite element analyses are used to obtain a correction factor that is applied to the hinge line collapse pressure $p_{ult,HL}$ to make the interaction curves converge at $R_p = 1$. The next step is to find a method to calculate the interactive ultimate strength of a sandwich panel for various combinations of load.

One of the best ways of dealing with this complicated situation is to make use of interaction formulas in which the variables are the ratios of each load to its ultimate strength. If just one type of load acted, a value of unity for that load ratio would correspond to collapse. As shown in Figure 5.1, for a combination of in-plane and lateral load, collapse occurs when the interactive collapse function satisfies $F(R_\sigma, R_p) = 1$. The purpose of this Chapter is to derive this function, thus giving an explicit formula for calculating the ultimate strength of sandwich panels.

6.1 Samples of Interactive Ultimate Strength Data Points

There are four dimensions for a sandwich panel: length a , width b , face plates thickness t_f , and core thickness t_c . The aspect ratio $\alpha = a/b$ accounts for the effect of both a and b . As seen from Figure 6.1, the sandwich panels with different t_f have similar interaction curves. Therefore t_f only influences p_{ult} which is the denominator of R_p and is given by Equation (5.13). However Figure 6.2 shows that for different t_c the shapes of the interaction curves are different. Figure 6.3 illustrates interaction curve shapes for sandwich panels with different α . For sandwich panels with small α such as 0.5, the interaction curve is almost straight from coordinate (0,1) to (1,0). When the aspect ratio is increased, the outward bulge of the interaction curve steadily increases. For aspect ratio 3, the interaction curve has a distinct knee at mid-length. From these observations, only two variables, t_c and α , need to be included in the desired formula.

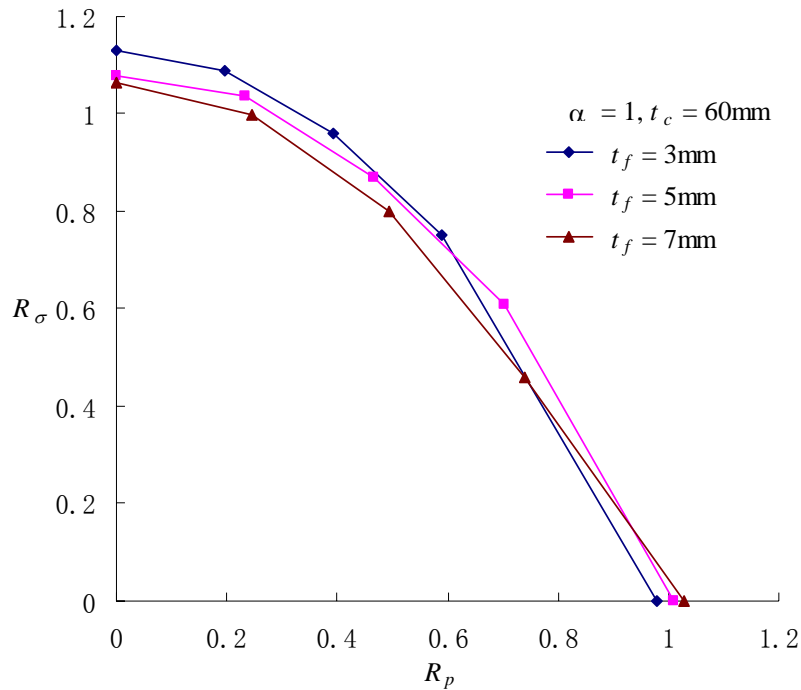


Figure 6.1 Interaction curves of sandwich panels with different face plate thickness

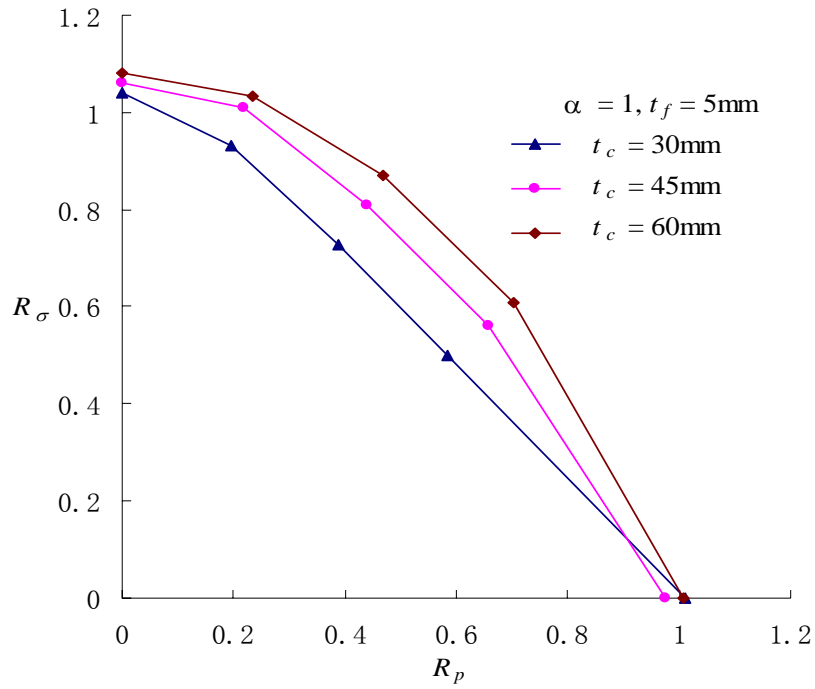


Figure 6.2 Interaction curves of sandwich panels with different core thickness

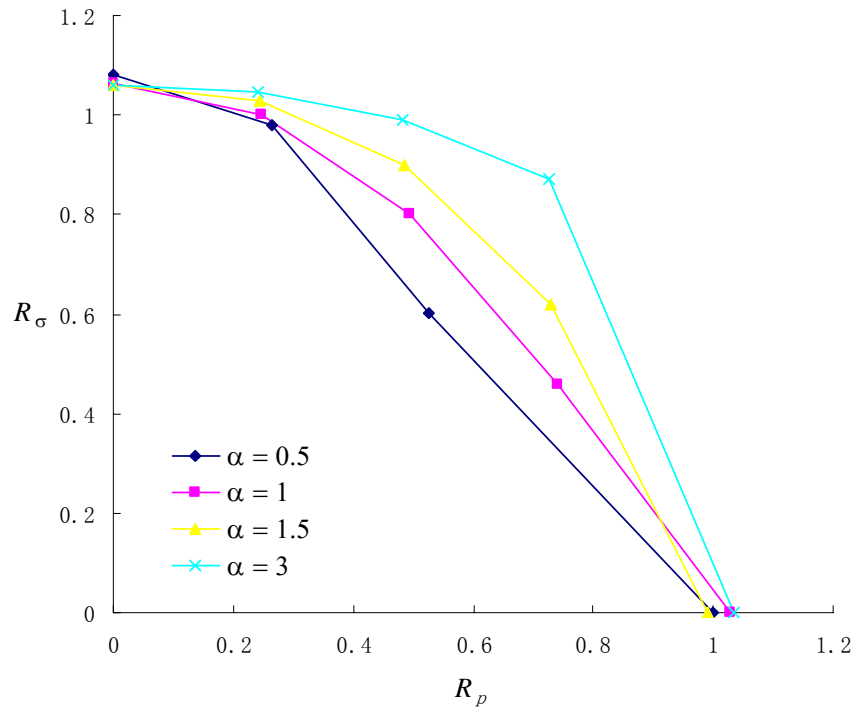


Figure 6.3 Interaction curves of sandwich panels with different aspect ratios

6.2 Finding an Interaction Equation

In spite of the differences of the curves, there is one common feature for all of them. The slope of the intersection with R_σ axis must be zero for all sandwich panels. This characteristic is due to the natural symmetry of the pressure load. No matter whether the lateral pressure is applied on the upper face plate or the lower face plate, the in-plane compression causing collapse would be the same.

In contrast, at the (1,0) position there is no such symmetry, and hence the curves do not intersect the R_p axis at 90° .

A general form of the interaction equation which has this desired shape is:

$$X^2 - CX^2Y^m + Y^n = 1 \quad (6.1)$$

where X and Y respectively stand for R_p and R_σ . The coefficient C is dependent on t_c and α , and would be changed in order to generate required curve shapes. The exponents of the both X terms in Equation (6.1) are fixed at 2 because of the need for zero slope at (0,1).

In order to show that the linear variation of X must be avoided, the following equation

$$X^2 - CXY + Y = 1 \quad (6.2)$$

is plotted in Figure 6.4. As can be seen, the curves generated by this function do not have the characteristic of symmetry about the R_σ -axis.

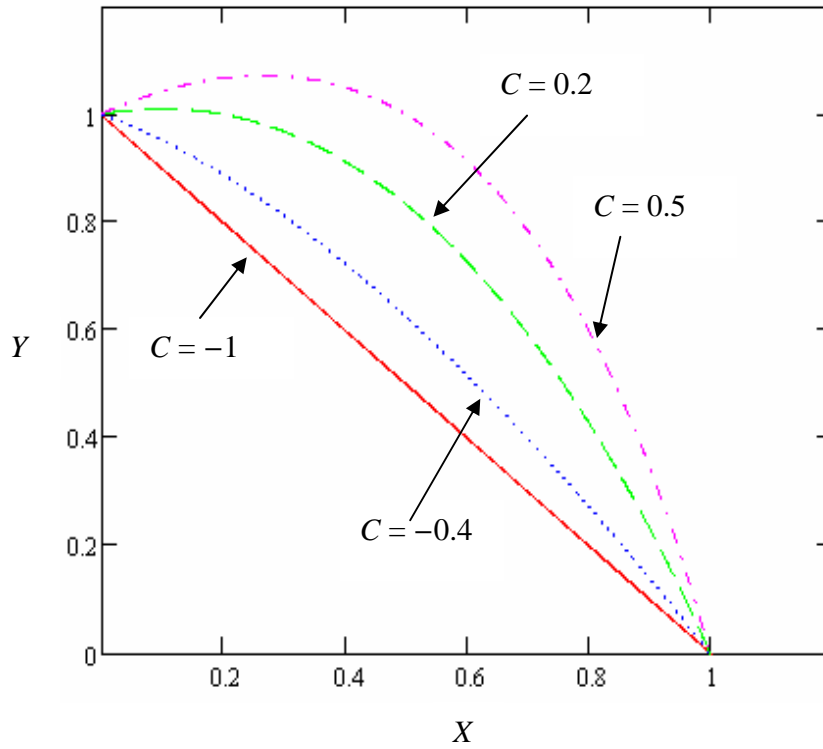


Figure 6.4 Curve shapes of Equation (6.2) $X^2 - CXY + Y = 1$

Next we need to obtain the exponents m and n . Four combinations of m and n are substituted in Equation (6.1):

$$m = 1, n = 1 \quad X^2 - CX^2Y + Y = 1 \quad (6.3)$$

$$m = 1, n = 2 \quad X^2 - CX^2Y + Y^2 = 1 \quad (6.4)$$

$$m = 2, n = 1 \quad X^2 - CX^2Y^2 + Y = 1 \quad (6.5)$$

$$m = 2, n = 2 \quad X^2 - CX^2Y^2 + Y^2 = 1 \quad (6.6)$$

The four equations are respectively plotted in Figures 6.5, 6.6, 6.7 and 6.8.

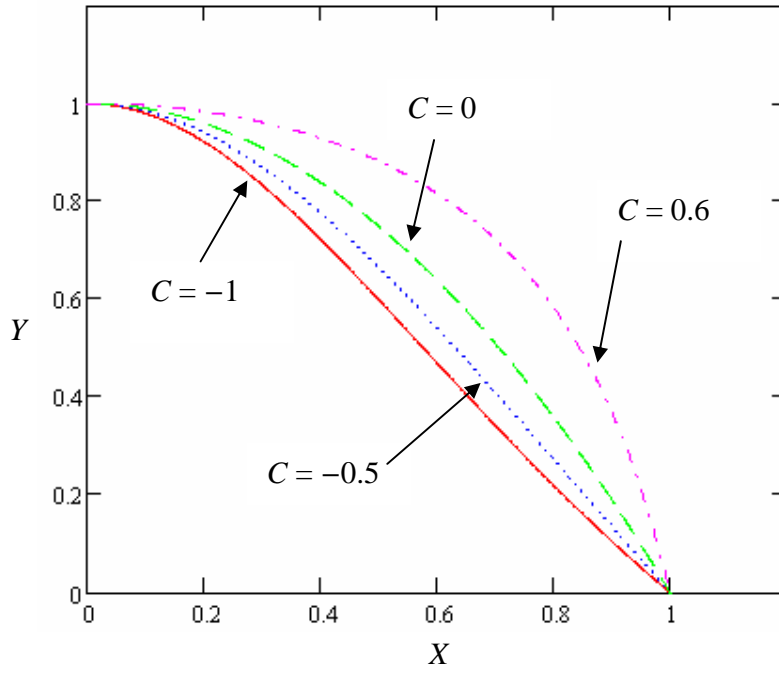


Figure 6.5 Curve shapes of Equation (6.3) $X^2 - CX^2Y + Y = 1$

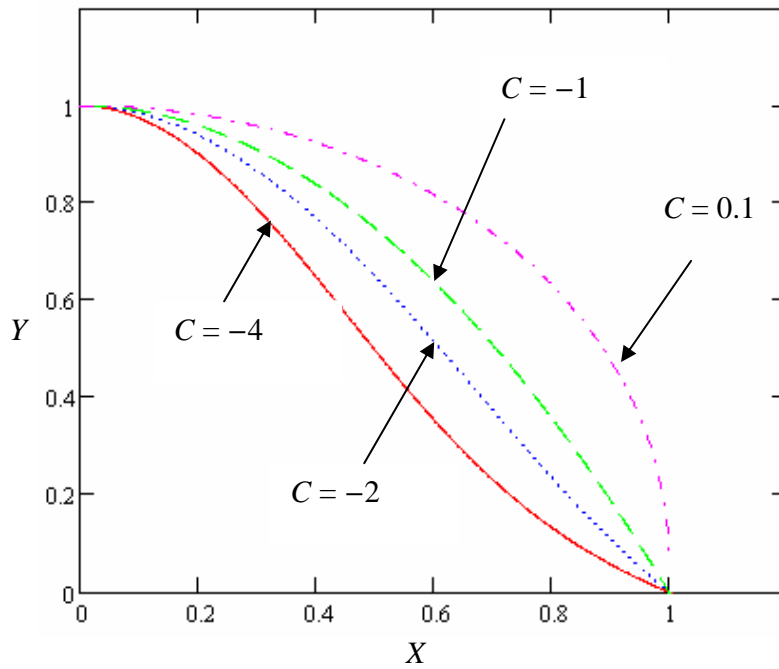


Figure 6.6 Curve shapes of Equation (6.4) $X^2 - CX^2Y + Y^2 = 1$

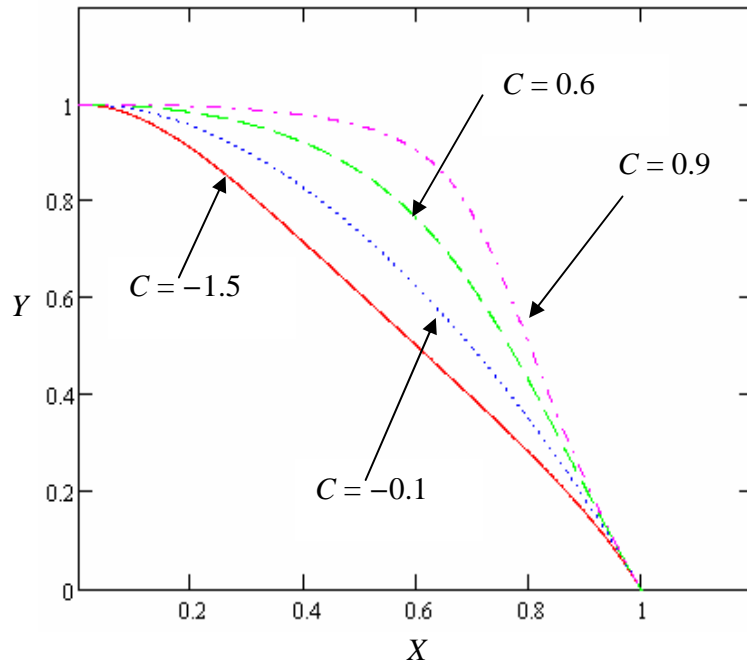


Figure 6.7 Curve shapes of Equation (6.5) $X^2 - CX^2Y^2 + Y = 1$

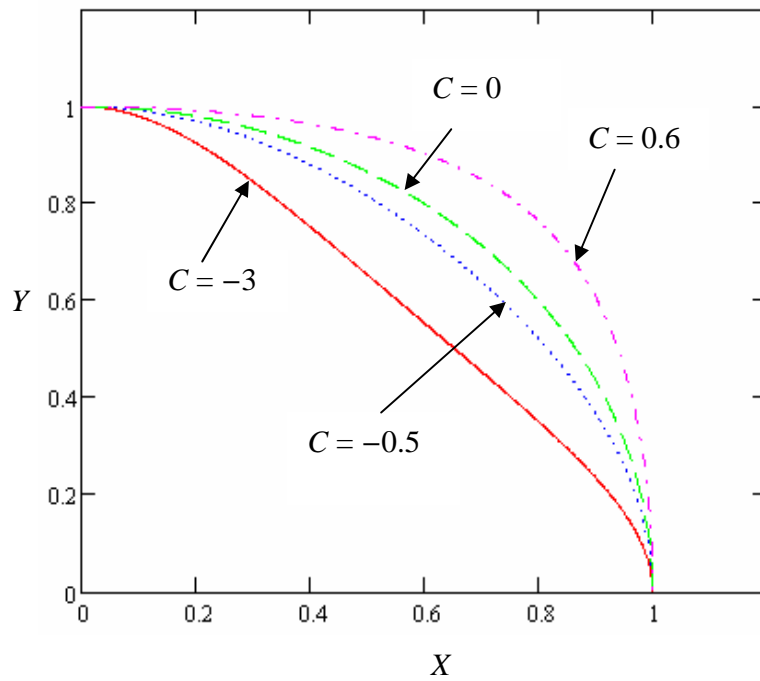


Figure 6.8 Curve shapes of Equation (6.6) $X^2 - CX^2Y^2 + Y^2 = 1$

As illustrated in Figures 6.5, 6.6 and 6.8, Equations (6.3), (6.4) and (6.6) can produce different curve shapes but they cannot produce a knee for large α . Only Equation (6.5) can generate a large outward bulge, as shown for $C = 0.9$. Therefore Equation (6.5) $X^2 - CX^2Y^2 + Y = 1$ is chosen as the interaction formula.

The next step is to adjust the variable C to generate curves to fit the FEA results. Before that, a correction needs to be made to the FEA results. As noted in Sections 2.2.4 and 4.2.1, for the case of pure in-plane compression the collapse stress (both experimental and finite element) exceeded the yield stress by 5-10% because in both cases the elastomer core is carrying this portion of the load. This is not the purpose of the core, and designers would be reluctant to include this small extraneous “extra strength” in their design calculations.

Therefore the FEA results are treated in three ways according to the proportion of in-plane load:

1. Pure in-plane compression: R_σ is set to 1 which makes the pure in-plane load case collapse stress equal to the yield stress.
2. Pure lateral pressure: Results are kept the same because there is no in-plane load.
3. Combined load: R_p is still the same and R_σ is proportionally reduced. The extra strength of the pure in-plane load case is defined as $R_{\sigma,extra}$. This value is scaled down smoothly in proportion to the ratio of the two load types. The scaled value is $\sin[\arctan(R_\sigma / R_p)] * R_{\sigma,extra}$ and this value is subtracted from the original in-plane strength.

Finally the corrected results are fit by Equation (6.5). As shown in the plots of Figures 6.9 to 6.20, values of C have been chosen such that the formula $X^2 - CX^2Y^2 + Y = 1$ gives a good fit to the FEA results.

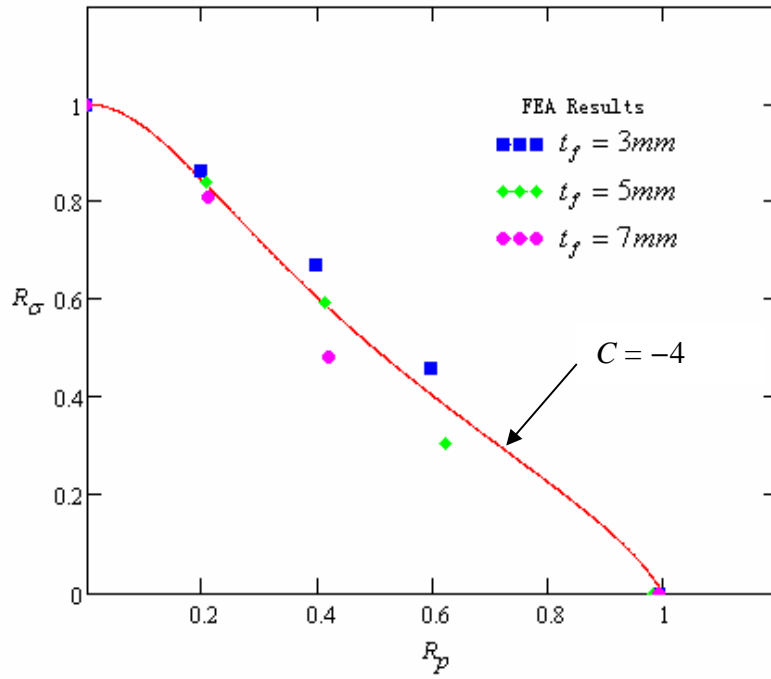


Figure 6.9 Interaction Diagram of sandwich panels with $t_c = 30mm$, $\alpha = 0.5$

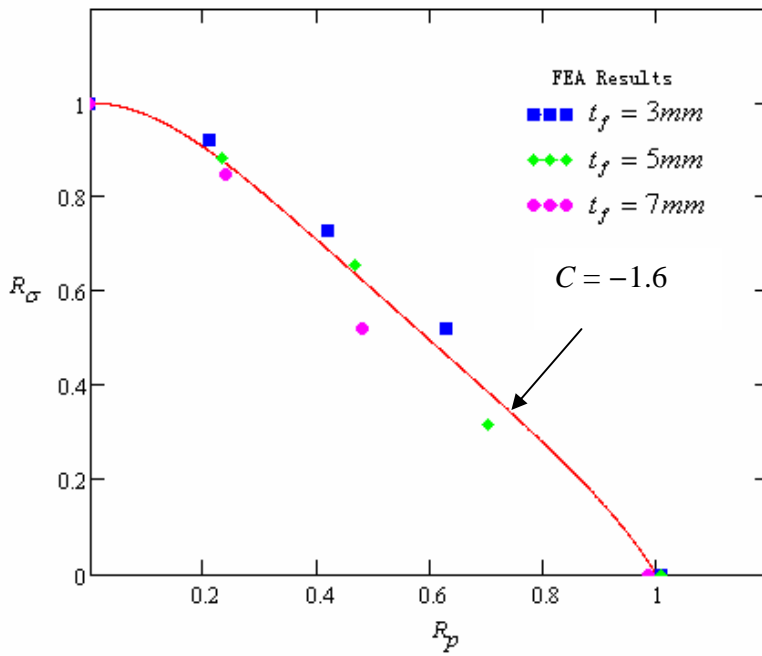


Figure 6.10 Interaction Diagram of sandwich panels with $t_c = 45mm$, $\alpha = 0.5$

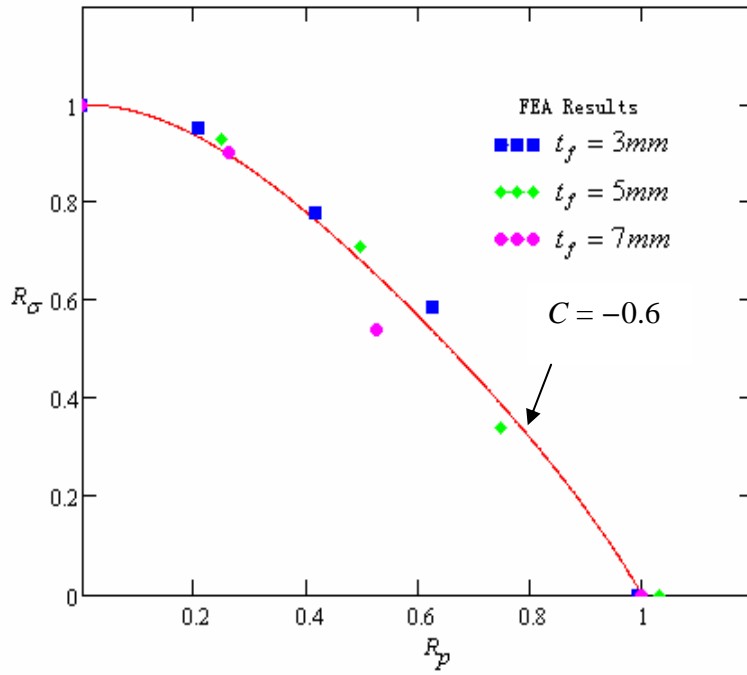


Figure 6.11 Interaction Diagram of sandwich panels with $t_c = 60mm$, $\alpha = 0.5$

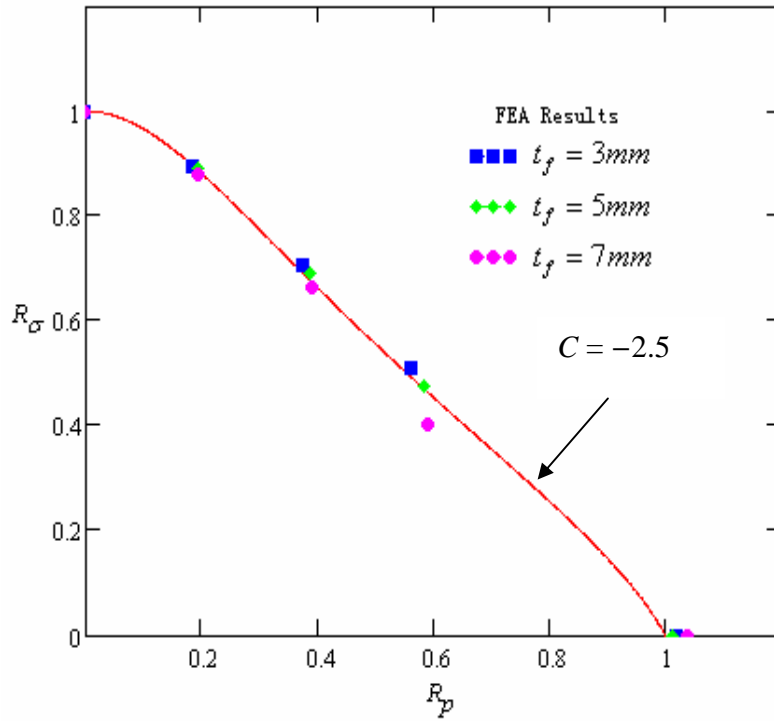


Figure 6.12 Interaction Diagram of sandwich panels with $t_c = 30mm$, $\alpha = 1$

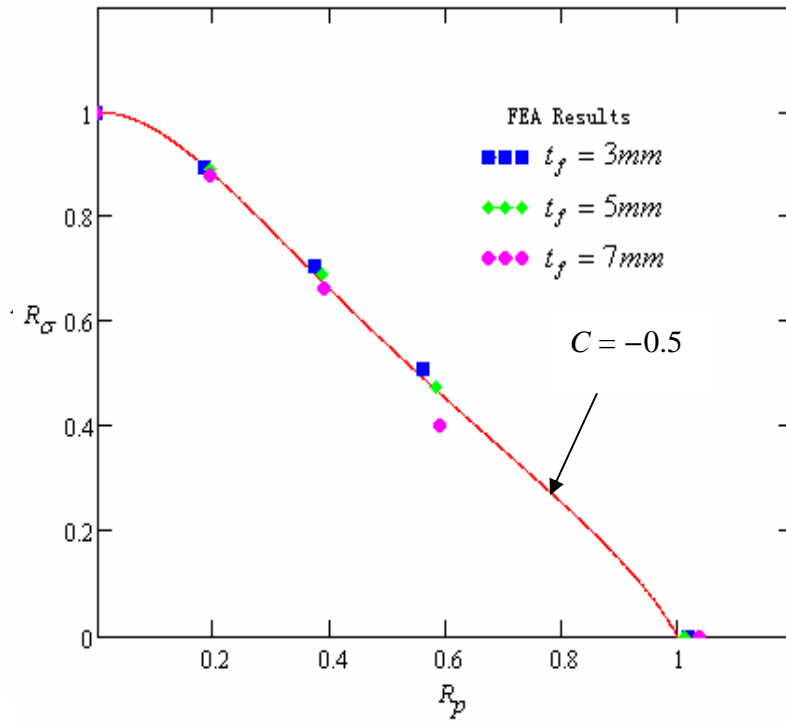


Figure 6.13 Interaction Diagram of sandwich panels with $t_c = 45mm$, $\alpha = 1$

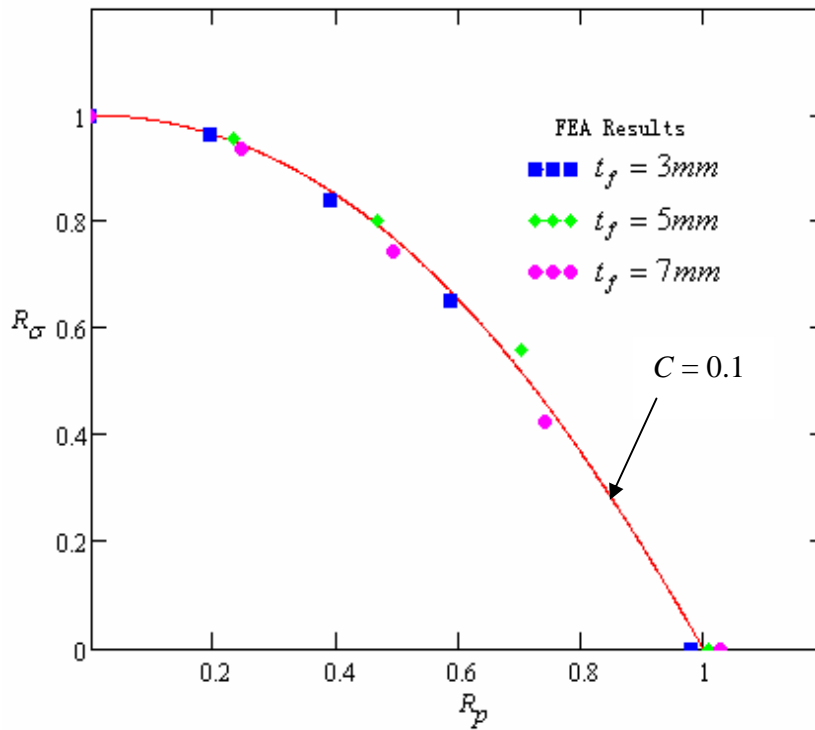


Figure 6.14 Interaction Diagram of sandwich panels with $t_c = 60mm$, $\alpha = 1$

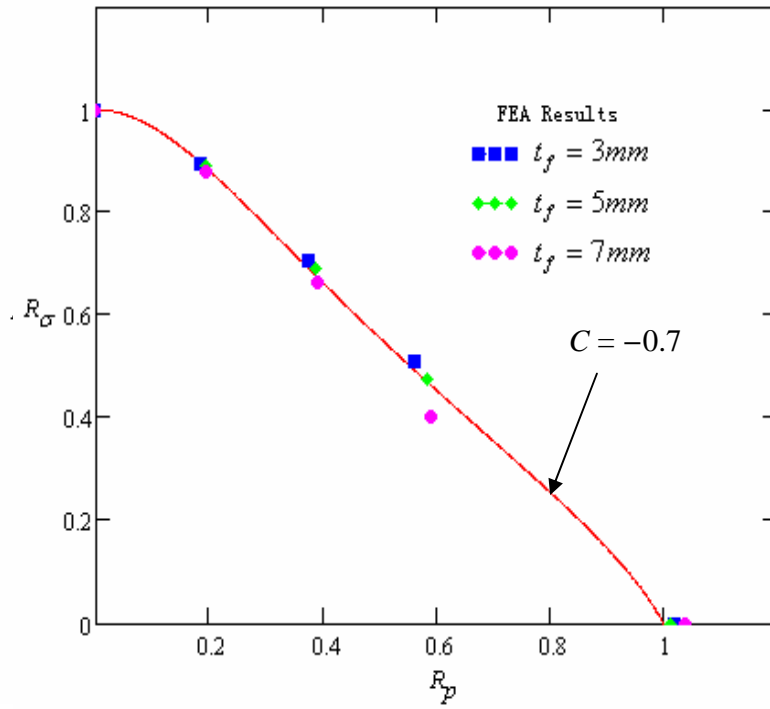


Figure 6.15 Interaction Diagram of sandwich panels with $t_c = 30mm$, $\alpha = 1.5$

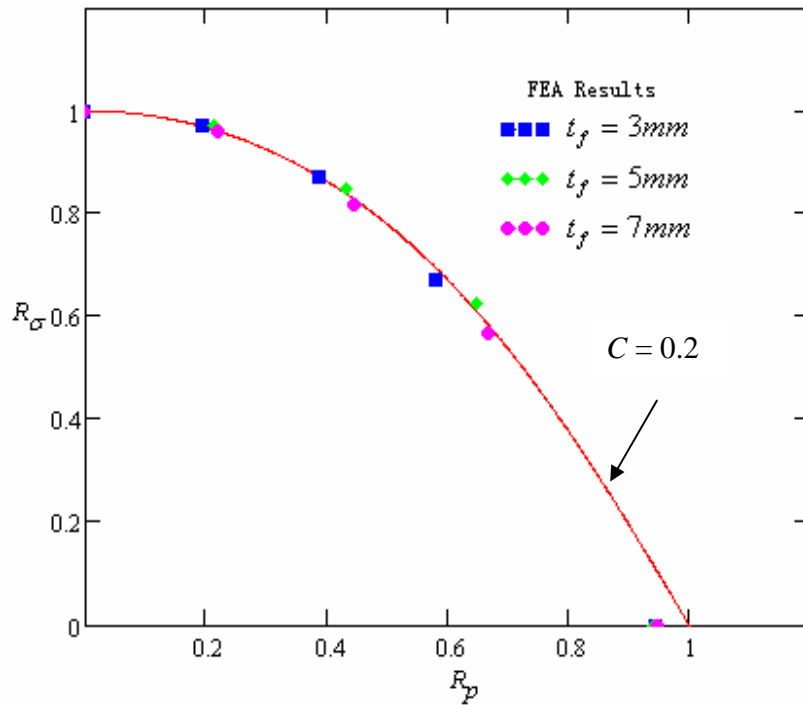


Figure 6.16 Interaction Diagram of sandwich panels with $t_c = 45mm$, $\alpha = 1.5$

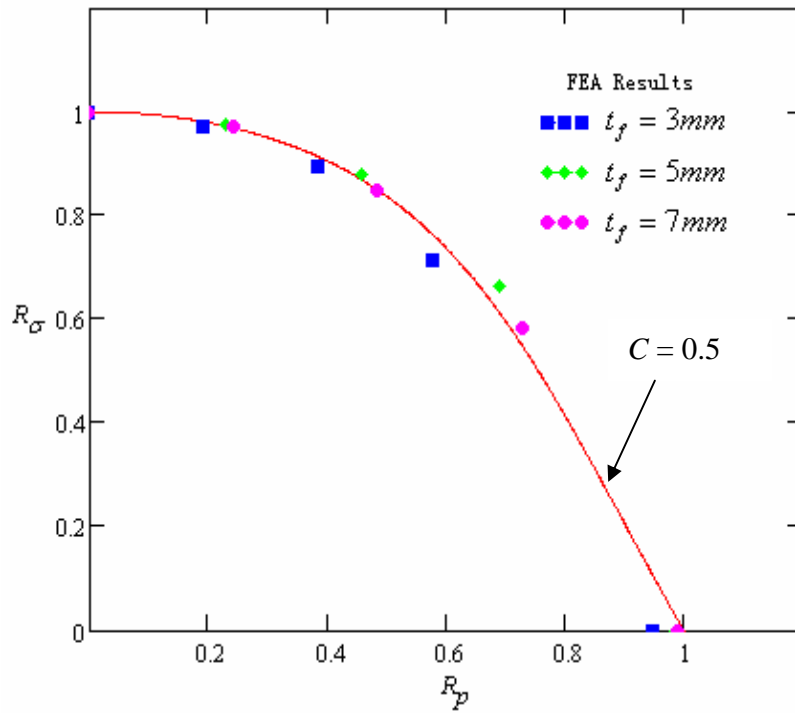


Figure 6.17 Interaction Diagram of sandwich panels with $t_c = 60mm$, $\alpha = 1.5$

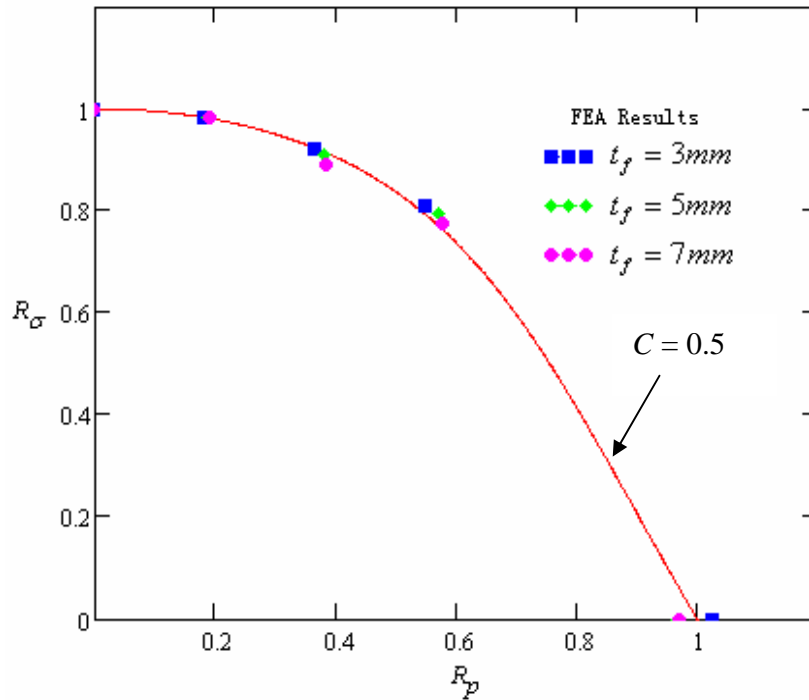


Figure 6.18 Interaction Diagram of sandwich panels with $t_c = 30mm$, $\alpha = 3$

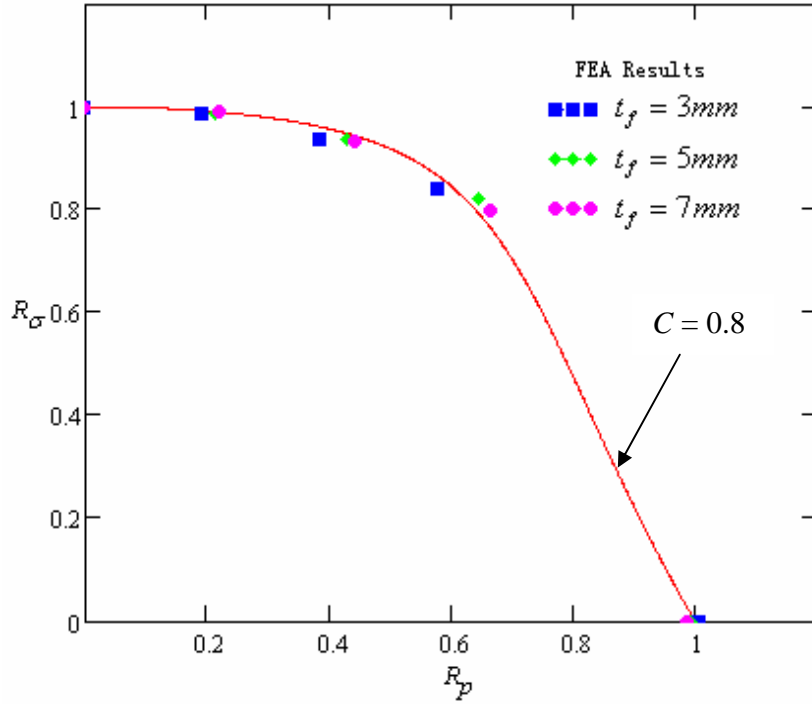


Figure 6.19 Interaction Diagram of sandwich panels with $t_c = 45mm$, $\alpha = 3$

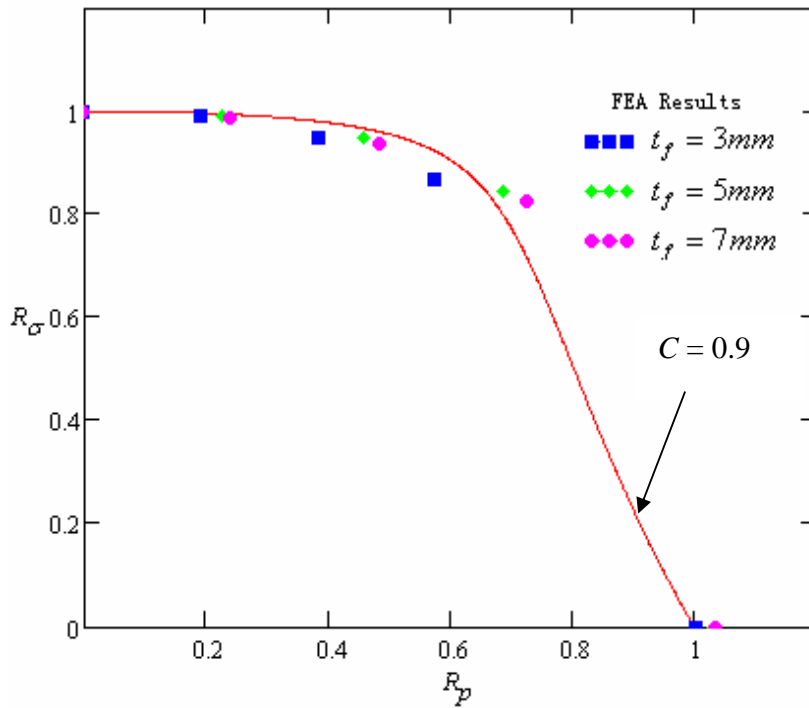


Figure 6.20 Interaction Diagram of sandwich panels with $t_c = 60mm$, $\alpha = 3$

6.3 Obtaining an Expression for the Coefficient C

	$\bar{t}_c=25$	$\bar{t}_c=37.5$	$\bar{t}_c=50$
$\alpha = 0.5$	-4	-1.6	-0.6
$\alpha = 1$	-2.5	-0.5	0.1
$\alpha = 1.5$	-0.7	0.2	0.5
$\alpha = 3$	0.5	0.8	0.9

Table 6.1 Values of C for different sandwich panels

The various values of coefficient C for different sandwich panels are listed in Table 6.1. As in Chapter 5, the core thickness is normalized by 0.1% of b , the sandwich panel width.

As discussed in section 6.1, there are only two variables for C . One is the core thickness \bar{t}_c and the other is the aspect ratio α .

1. Allowing for core thickness

Since there are four aspect ratios, four corresponding expressions for $C_{\alpha i}(\bar{t}_c)$ ($i = 1, 4$) have been obtained by trying various ratios of polynomials and choosing the simplest expressions which gave a satisfactory fit to the FEA data.

$$\alpha = 0.5: \quad C_{\alpha 1}(\bar{t}_c) = \frac{-4000 + \bar{t}_c^2}{\bar{t}_c^2} \quad (6.7)$$

$$\alpha = 1: \quad C_{\alpha 2}(\bar{t}_c) = \frac{-2000 + \bar{t}_c^2}{\bar{t}_c^2} \quad (6.8)$$

$$\alpha = 1.5: C_{\alpha 3}(\bar{t}_c) = \frac{-1100 + \bar{t}_c^2}{\bar{t}_c^2} \quad (6.9)$$

$$\alpha = 3: C_{\alpha 4}(\bar{t}_c) = \frac{-315 + \bar{t}_c^2}{\bar{t}_c^2} \quad (6.10)$$

The four functions are plotted with the FEA data in Figures 6.21 to 6.24. As can be seen, the functions give a good fit to the FEA data. As the core becomes thicker, its influence diminishes and C tends towards 1.

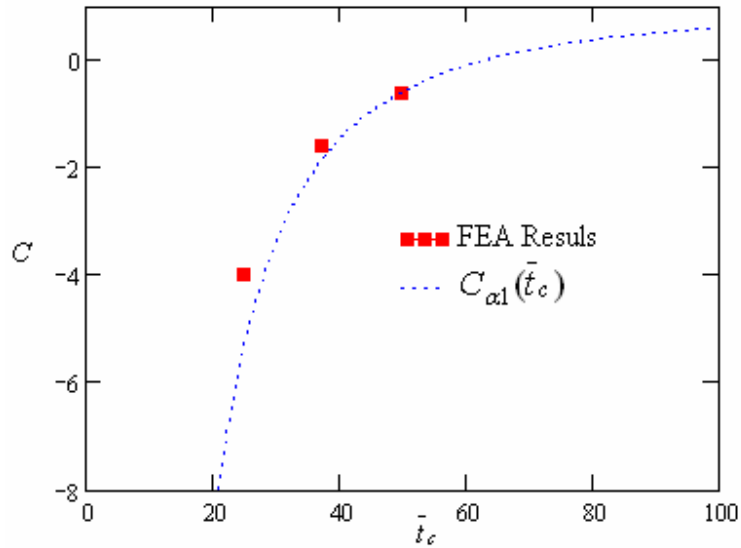


Figure 6.21 C versus \bar{t}_c for $\alpha = 0.5$

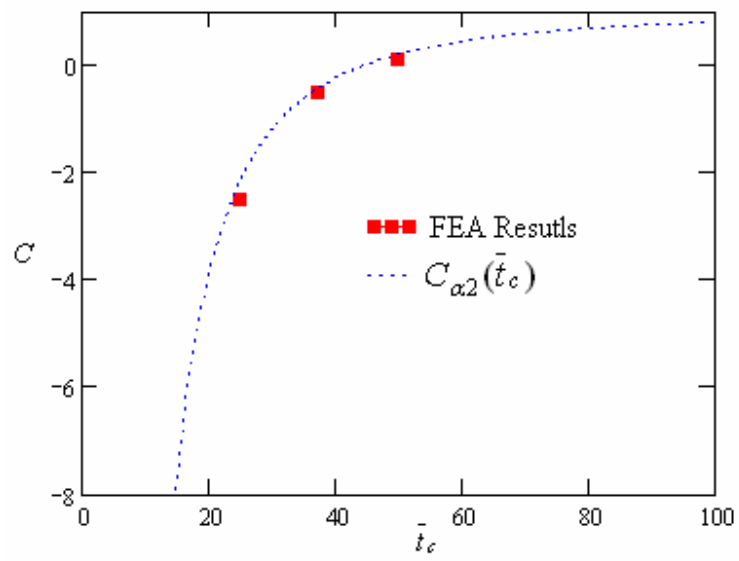


Figure 6.22 C versus \bar{t}_c for $\alpha = 1$

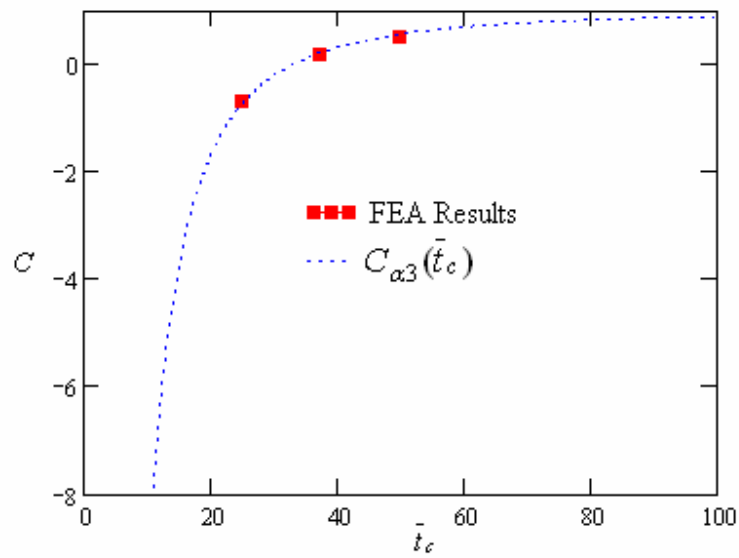


Figure 6.23 C versus \bar{t}_c for $\alpha = 1.5$

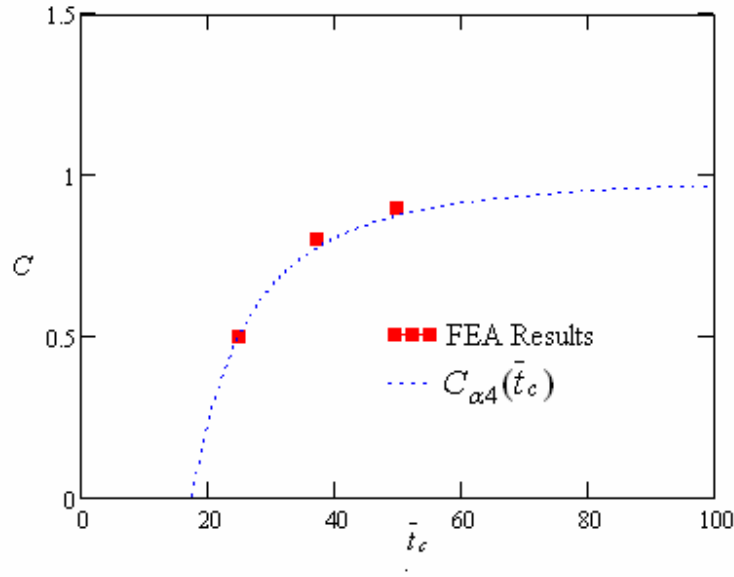


Figure 6.24 C versus \bar{t}_c for $\alpha = 3$

2. Allowing for aspect ratio

Since there are three core thicknesses, three corresponding expressions for $C_{i_c}(\alpha)$ ($i = 1, 3$) have been obtained by trying various ratios of polynomials and choosing the simplest expressions which gave a satisfactory fit to the FEA data.

$$\bar{t}_c = 25: \quad C_{i_c1}(\alpha) = \frac{-4.2 + \alpha^2}{0.5 + \alpha^2} \quad (6.11)$$

$$\bar{t}_c = 37.5: \quad C_{i_c2}(\alpha) = \frac{-1.6 + \alpha^2}{0.5 + \alpha^2} \quad (6.12)$$

$$\bar{t}_c = 50: \quad C_{i_c3}(\alpha) = \frac{-0.7 + \alpha^2}{0.5 + \alpha^2} \quad (6.13)$$

The three functions are plotted with the FEA data in Figures 6.25 to 6.27. As can be seen, the functions give a good fit to the FEA data. As the aspect ratio increases, its influence diminishes and C tends towards 1.

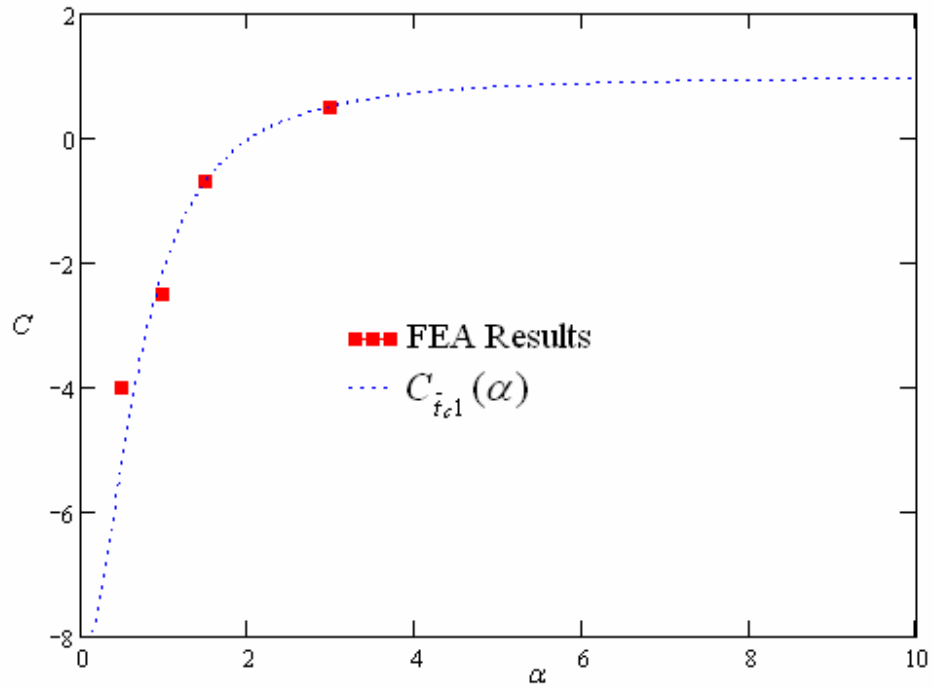


Figure 6.25 C versus α for $\bar{t}_c = 25$

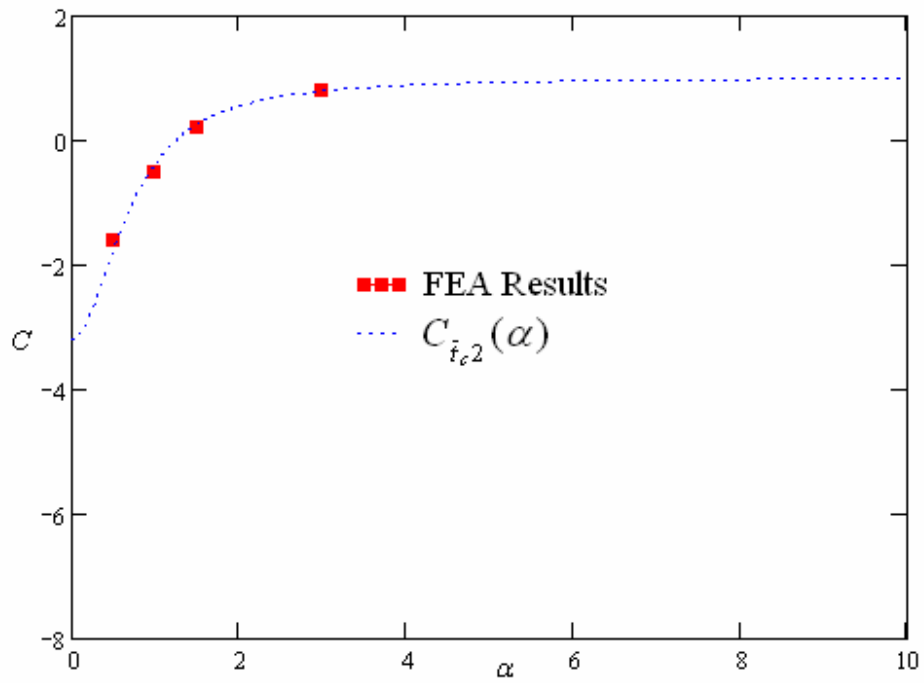


Figure 6.26 C versus α for $\bar{t}_c = 37.5$

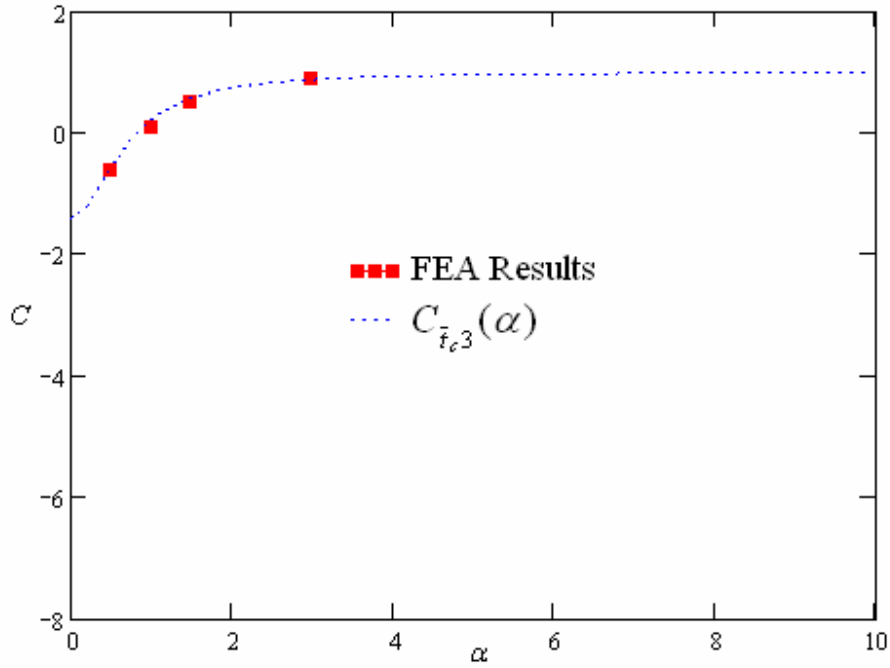


Figure 6.27 C versus α for $\bar{t}_c = 50$

Based on the two obtained functions $C_\alpha(\bar{t}_c)$ and $C_{\bar{t}_c}(\alpha)$, the final form of function $C(\alpha, \bar{t}_c)$ is:

$$C(\alpha, \bar{t}_c) = 1 - \frac{3000}{(0.5 + \alpha^2)\bar{t}_c^2} \quad (6.14)$$

$C(\alpha, \bar{t}_c)$ is plotted in Figure 6.28 along with the values in Table 6.1. From the 3D plot below, it can be seen that $C(\alpha, \bar{t}_c)$ fits with the values in Table 6.1 satisfactorily.

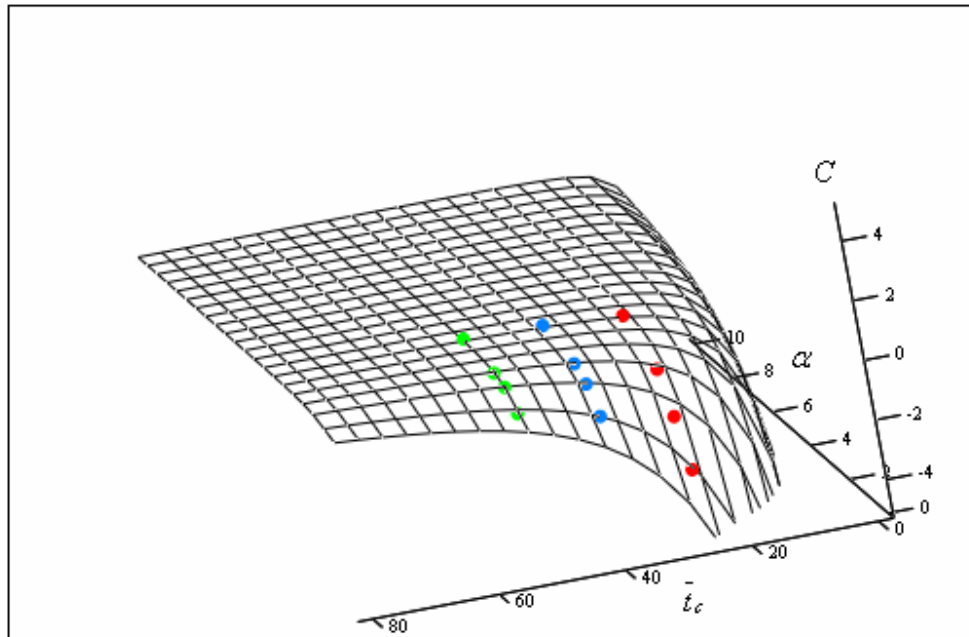


Figure 6.28 C versus α and normalized \bar{t}_c

Now that the function $C(\alpha, \bar{t}_c)$ has been obtained, the C values can then be calculated by inputting values of α and \bar{t}_c , and the desired interaction curves can be generated.

Figure 6.29 is the plot of the interaction surface for all values of R_σ , R_p and C . If a load combination point is under the surface, the sandwich panel would not collapse. If a load combination point is on or above the surface, the ultimate strength is reached.

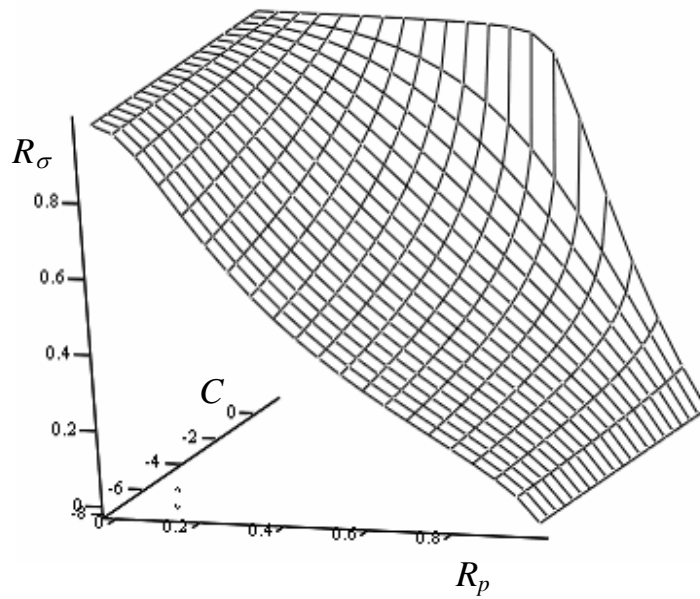


Figure 6.29 Interaction surface

Thus the final interaction equation is given by Equation (6.5) with X and Y replaced by R_p and R_σ :

$$R_p^2 - C(\alpha, \bar{t}_c) R_p^2 R_\sigma^2 + R_\sigma = 1 \quad (6.15)$$

in which $C(\alpha, \bar{t}_c)$ is given by Equation (6.14). The denominator of R_p is p_{ult} , given by Equation (5.13).

6.4 Verification

In order to verify the interaction formula, the errors between the FEA results and the values obtained by the formula are defined as:

For the 36 Pressure-only points:

$$e = (R_p)_{FE} - R_p(\bar{t}_f, \bar{t}_c, \alpha) \quad (6.16.a)$$

The other 141 points:

$$e = (R_\sigma)_{FE} - R_\sigma(\bar{t}_f, \bar{t}_c, \alpha) \quad (6.16.b)$$

The bias (average value) and the standard deviation of all the errors are calculated. The value range of e is divided into 24 bands. The relative frequency of occurrence of errors in each band are calculated and plotted in Figure 6.30. The resulting overall bias is -0.003, and the standard deviation is 0.029. Based on this bias and standard deviation, the standard normal distribution is plotted in Figure 6.31.

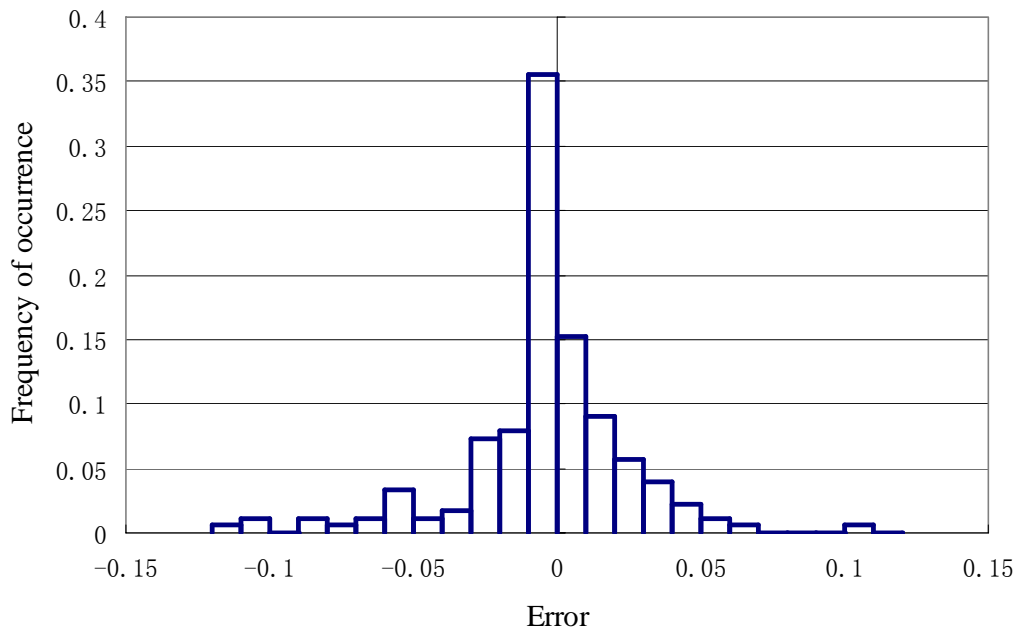


Figure 6.30 Probabilities of the errors of the interaction formula

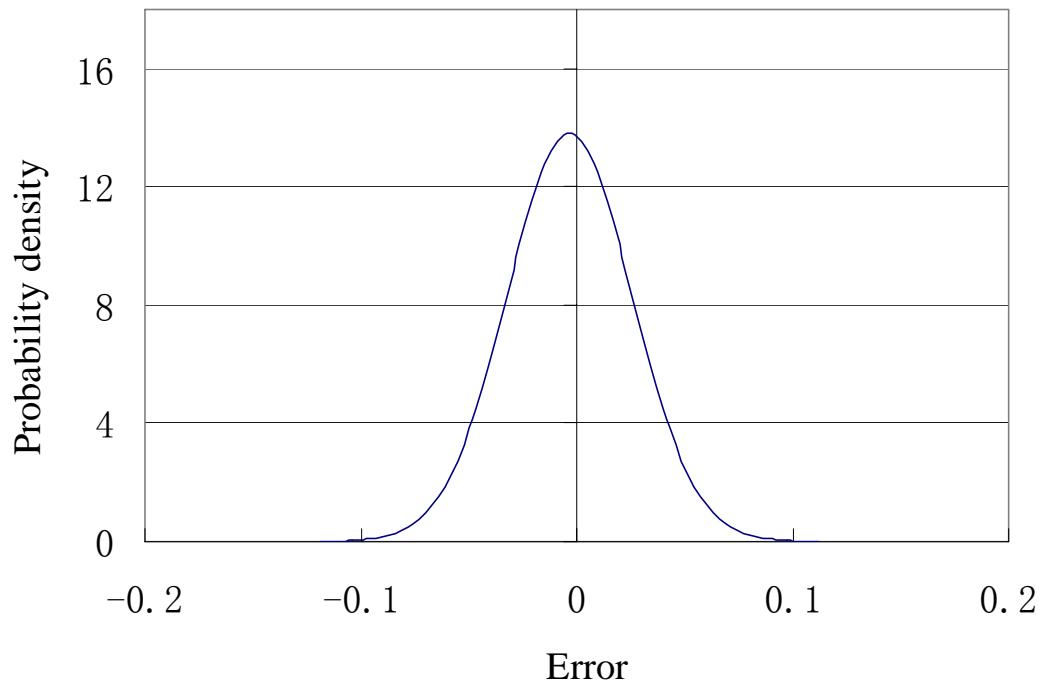


Figure 6.31 Standard normal distribution of the errors of the interaction formula

It is clear that most errors are among the range from -0.03 to 0.03, and the average value is very close to zero. Since the standard deviation is 0.029 and the radius of the interactive collapse curve is never very far from 1 (see Figure 6.7), the standard deviation corresponds to a percentage error of only 3%. Therefore the interaction formula is not only simple but also has the accuracy required for the design of steel-elastomer sandwich panels of standard proportions.

The FEA data points covered the range of standard proportions of t_f/b , t_c/b and α . The interaction equation can be used within the following limits:

$$0.002 < t_f/b < 0.006$$

$$0.020 < t_c/b < 0.060$$

$$0.5 < \alpha < \infty$$

We then can employ the interaction formula to calculate R_σ or R_p by inputting one of them to obtain the other one. Once the values of R_σ and R_p are acquired, the real value of ultimate strength can be obtained by multiplying R_σ by σ_Y and R_p by p_{ult} , which is given by Equation (5.13).

6.5 Some Observations about the Interaction Formula

The interaction formula is Equation (6.5): $X^2 - CX^2Y^2 + Y = 1$. As can be seen from Figure 6.7, when C is increased from -1.5 to 0.9, a knee emerges around the center of the interaction curve and becomes bigger and bigger.

Since the largest value of C in Table 6.1 is 0.9, Equation (6.14) was chosen such that C is always less than 1. In this Section, C is separately set to be bigger than 1 and equal to 1, and the properties of the corresponding curves are investigated.

1. $C > 1$

If Equation (6.5) is solved for Y , the following equation is obtained:

$$Y = \frac{1 - \sqrt{1 + 4C(X^2 - 1)X^2}}{2CX^2} \quad (6.17)$$

If $C > 1$, $1 + 4C(X^2 - 1)X^2$ would be smaller than zero within some range of X , therefore Y would be complex within this range of X . Figure 6.32 is the plot of Equation (6.17) for $C = 1.01$. As can be seen, the curve consists of two separate parts because there are some values of X for which Y is a complex number. Therefore C cannot be larger than 1.

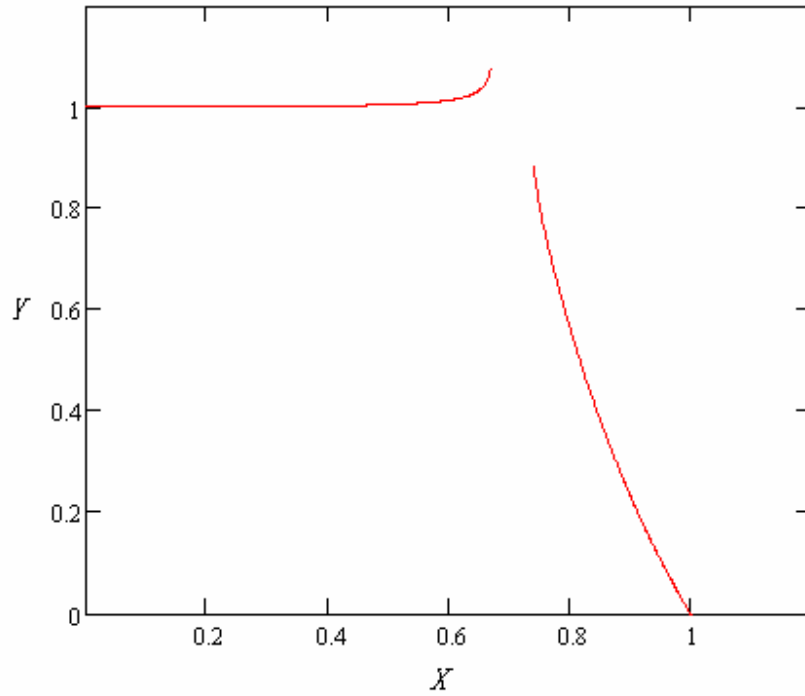


Figure 6.32 Curve shapes of function $X^2 - CX^2Y^2 + Y = 1$ when $C = 1.01$

2. $C = 1$

When C in Equation (6.17) is set to 1, the equation becomes:

$$Y = \frac{1 - \sqrt{(2X^2 - 1)^2}}{2X^2} \quad (6.18)$$

As plotted in Figure 6.33, there are two possibilities for Equation (6.18):

$$\text{If } X > \frac{\sqrt{2}}{2}, Y = \frac{1}{X^2} - 1 \quad (6.19)$$

$$\text{If } X \leq \frac{\sqrt{2}}{2}, Y = 1 \quad (6.20)$$

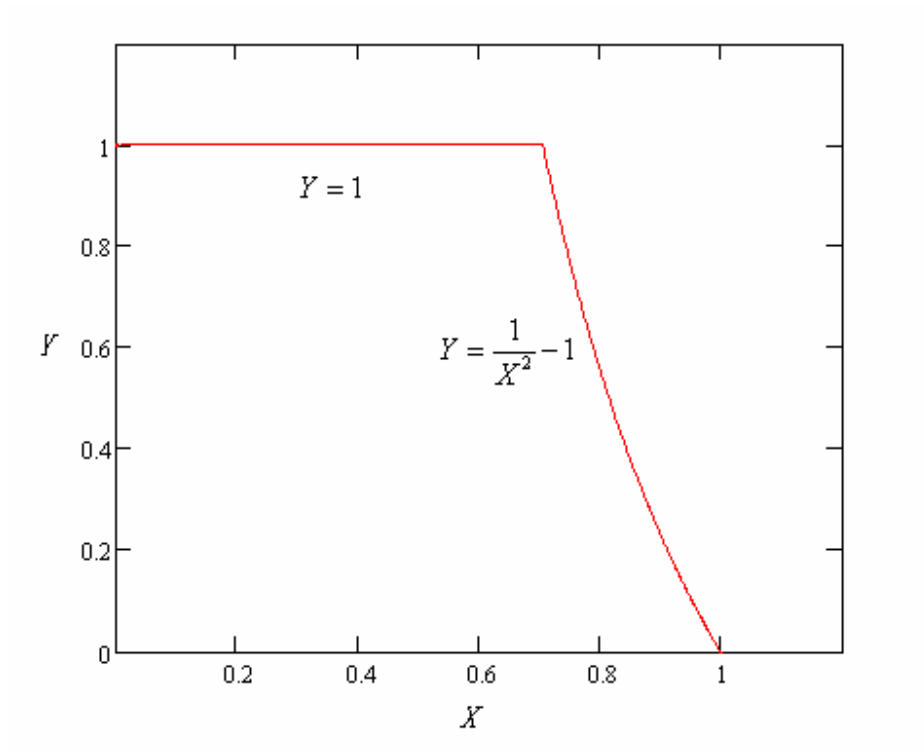


Figure 6.33 Curve shapes of function $X^2 - CX^2Y^2 + Y = 1$ when $C = 1$

Chapter 7

Summary and Conclusions

1. Hinge line theory can only calculate ultimate strength for pure lateral pressure load. For metal-faced and elastomer-cored sandwich panels, the actual ultimate strength is different, and so the hinge line equation needs to be generalized to allow for the sandwich properties.

2. By using the Galerkin method and extending the semi-analytical method to clamped sandwich panels, the governing equations of sandwich panels derived by Librescu et al. (1997) have been solved. For the load case of pure lateral pressure, the results of ultimate strength obtained by the semi-analytical method are similar to those obtained by hinge line theory. For the experimental panel, the semi-analytical method gave a collapse pressure of 1.6 MPa compared to 1.85 MPa from the FEA. Unfortunately, the semi-analytical method requires too much computation. Therefore the hinge line theory is used as the starting point for the pressure-only case.

3. Little (2007) presents full-scale test results for three clamped sandwich panels involving three combinations of in-plane compression and lateral pressure. All three test results closely matched the results from the finite element model that was used in this study, thus verifying the accuracy of the latter. Little (2007) also made a similar finite element model, and his results also matched the test data.

4. The verified finite element model was then used to obtain the results for a large set of sandwich panels with various dimensions and load combinations. Altogether $3 \times 3 \times 4 \times 5 \approx 180$ FEA data points were calculated for interactive collapse. For pure pressure there are $3 \times 3 \times 4 = 36$ data points. These data points were used to derive a correction factor for the hinge line formula in order to account for sandwich properties t_f , t_c and α . To verify the correction factor, the relative errors between the corrected hinge line theory and FEA results were calculated. The bias of the relative errors is -0.007, and the standard deviation is 0.03, which confirms that the generalized hinge line formula gives accurate values of ultimate strength of sandwich panels under pure lateral pressure.

5. Except for the pressure-only FEA data points, the other $3 \times 3 \times 4 \times 4 \approx 144$ FEA data points were corrected so as not to count the small in-plane load carried by the elastomer core. Based on the corrected FEA data points, a general expression was developed for an interaction equation. The resulting equation has a bias of -0.003 and a standard deviation of 0.029. Since the radius of the interaction curve is close to 1, this standard deviation is of the order of 3%, which shows that the ultimate strength values given by the interaction equation are very close to the FEA results. The interaction equation is so simple that the ultimate strength of clamped sandwich panels under combined in-plane compression and lateral pressure can be easily calculated as a function of t_f , t_c and α . The data points covered the range of standard proportions of t_f/b , t_c/b and α , and the interaction equation can be used within the following limits:

$$0.002 < t_f/b < 0.006$$

$$0.020 < t_c/b < 0.060$$

$$0.5 < \alpha < \infty$$

REFERENCES

- Alexandrov, A.I., Briuker, L.E., Kurshin, L.M. and Prusakov, A.P. (1960). Research on Three-Layered Panels, Oboronghiz, Moscow
- ASTM A370-05 (2005). Standard Test Method and Definitions for Mechanical Testing of Steel Products, American Standard for Testing and Materials, 100 Barr Harbour Drive, West Conshohocken, Pa.
- Drucker, D.C. (1958). Plastic Design Methods, Advantages and Limitations, Transactions of SNAME, Vol. 65, pp 172-196.
- Fletcher, C.A.J. (1984). Computational Galerkin Methods, Springer Verlag, New York.
- Hause, T., Librescu, L. and Camarda, C.J. (1998). Postbuckling of Anisotropic Flat and Double-curved sandwich Panels under Complex Loading Condition, International Journal of Solids and Structures, Vol. 35, No. 23, pp. 3007-3027.
- Heder M. (1991). Buckling of Sandwich Panels with Different Boundary Conditions, A Comparison between FE-Analysis and Analytical Solutions, Composite Structures, Vol. 19, No. 4, pp 313-332.
- Hughes, O.F. (1988). Ship Structural Design; A Rationally-Based, Computer-Aided Optimization Approach, SNAME, New Jersey.
- Kim, B.J. and Hughes, O.F. (2005). Analytical solution for the ultimate strength of metal-faced elastomer-cored sandwich panels under in-plane edge compression and lateral pressure, Journal of Sandwich Structures and Materials, Vol. 7, No. 5, pp. 363-394.
- Librescu, L., Hause, T. and Camarda, C.J. (1997). Geometrically Nonlinear Theory of Initially Imperfect Sandwich Plates and Shells Incorporating Non-Classical Effects, AIAA Journal, Vol. 35, No. 8, pp. 1392-1403.
- Little, J. (2007). Sandwich Plate System Panels under In-plane and Uniform Lateral Pressure, Master's Thesis, University of Alberta, Department of Civil and Environmental Engineering, Edmonton, Alberta, Canada.

- Lloyd's Register of Shipping (2000). SPS for Shipbuilding, Marine Bulletin, Special Report, Lloyd's Register Marine Business, 71 Fenchurch St., London, September 2000.
- Padhi, G.S., Shenoi, R.A., Moy, S.S.J. and Hawkins, G.L. (1998). Progressive failure and ultimate collapse of laminated composite plates in bending, *Composite Structures*, Vol. 40, No. 3-4, pp. 277-291.
- Paik, J.K., Thayamballi, A.K., Lee, S.K. and Kang, S.J. (2001) A semi-analytical method for the elastic-plastic large deflection analysis of welded steel or aluminum plating under combined in-plane and lateral pressure loads, *Thin-Walled Structures*, Vol. 39, No. 2, pp 125-152.
- Plantema, F.J. (1966). *Sandwich Construction; The Bending and Buckling of Sandwich Beams, Plates, and Shells*, John Wiley & Sons, Inc., London.
- Reissner, E. (1948). Finite Deflections of Sandwich Plates, *Journal of the Aeronautical Sciences*, Vol. 15, No. 7, pp. 435-440.
- Sobotka, Z. (1989). *Theory of Plasticity and Limit Design of Plates*, Elsevier, New York.
- Szilar, R. (1974). *Theory and Analysis of Plates; Classical and Numerical Methods*, Prentice-Hall, Inc., New Jersey.
- Save, M.A., Massonnet, C.E. and Saxce, G.D. (1997). *Plastic Limit Analysis of Plates, Shells and Disks*, Elsevier, Amsterdam.
- Welch, D. (2005). *The Sandwich Plate System*, Presentation at Glasgow College of Nautical Studies, Glasgow, January 2005.

Vita

Feng Zhou was born on December 29, 1979 in Zhuzhou, Hunan Province, China. In September 1997, he began his undergraduate study in the College of Traffic Science and Engineering of Huazhong University of Science and Technology, Wuhan, China, majoring in Naval Architecture and Ocean Engineering. He received his Bachelor's degree in Engineering in June 2001 and continued to study in the same institute. He received his Master's degree in Naval Architecture and Ocean Engineering in June 2004. Feng Zhou came to Virginia Tech in the fall of 2004 and entered the graduate program in the Department of Aerospace and Ocean Engineering. This dissertation completes his PhD degree in Aerospace Engineering from Virginia Tech.